


May 2019

# Molecular Mechanisms Mediating Morphogenesis of the Basal Epithelial Tissue Fold During Midbrain-hindbrain Boundary Formation in Zebrafish

Mike Roger Visetsouk  
*University of Wisconsin-Milwaukee*

Follow this and additional works at: <https://dc.uwm.edu/etd>

 Part of the [Cell Biology Commons](#), and the [Developmental Biology Commons](#)

---

## Recommended Citation

Visetsouk, Mike Roger, "Molecular Mechanisms Mediating Morphogenesis of the Basal Epithelial Tissue Fold During Midbrain-hindbrain Boundary Formation in Zebrafish" (2019). *Theses and Dissertations*. 2136.  
<https://dc.uwm.edu/etd/2136>

This Dissertation is brought to you for free and open access by UWM Digital Commons. It has been accepted for inclusion in Theses and Dissertations by an authorized administrator of UWM Digital Commons. For more information, please contact [open-access@uwm.edu](mailto:open-access@uwm.edu).

MOLECULAR MECHANISMS MEDIATING MORPHOGENESIS OF THE BASAL  
EPITHELIAL TISSUE FOLD DURING MIDBRAIN-HINDBRAIN BOUNDARY  
FORMATION IN ZEBRAFISH

by

Mike Roger Visetsouk

A Dissertation Submitted in  
Partial Fulfillment of the  
Requirements for the Degree of

Doctor of Philosophy  
in Biological Sciences

at

The University of Wisconsin-Milwaukee

May 2019



## ABSTRACT

### MOLECULAR MECHANISMS MEDIATING MORPHOGENESIS OF THE BASAL EPITHELIAL TISSUE FOLD DURING MIDBRAIN-HINDBRAIN BOUNDARY FORMATION IN ZEBRAFISH

by

Mike Roger Visetsouk

The University of Wisconsin-Milwaukee, 2019  
Under the Supervision of Jennifer H. Gutzman, PhD

The formation of a fully functional organism requires the morphogenesis of cell and tissue structures during development. It is important to understand the mechanisms that mediate morphogenesis, since cell and tissue structures are crucial to physiological function. Here, we studied basal epithelial tissue folding as a model to determine the mechanisms of morphogenesis. We investigated a highly conserved basal tissue fold known as the midbrain-hindbrain boundary (MHB) using zebrafish. MHB formation relies on cell shape changes in a single-cell layered epithelial structure called the neural tube. The molecular mechanisms that mediate cell shaping during basal tissue folding are not well understood. Our studies revealed that calcium and Wnt5b, known morphogens in development, mediate MHB tissue folding. We found that calcium, via *Calmodulin 1a*, regulates cell length at the deepest point of the MHB fold through myosin light chain kinase and actomyosin. Furthermore, we demonstrated that cells at the deepest MHB fold point decrease in cell width and increase in cell depth, generating anisotropic cell shape. Wnt5b modulates this MHB anisotropic cell shape. However, basally at the MHB, Wnt5b regulates microtubule stability, potentially through JNK, to mediate anisotropic cell shape. Together, these studies are important for the future development

of preventative and therapeutic approaches to structural birth defects and for the future of tissue engineering in regenerative medicine.

© Copyright by Mike Roger Visetsouk, 2019  
All Rights Reserved

To my friends and family, especially my parents, sister, and partner,  
for which none of this work would be possible without their unconditional love and  
support

# TABLE OF CONTENTS

<b>Chapter 1</b> .....	<b>1</b>
<b>Introduction</b> .....	<b>1</b>
<b>1.1 Development</b> .....	<b>1</b>
<b>1.2 Morphogenesis</b> .....	<b>2</b>
<b>1.3 Epithelium</b> .....	<b>3</b>
<b>1.4 Epithelial tissue morphogenesis</b> .....	<b>4</b>
1.4.1 Epithelial tissue shapes .....	5
1.4.2 Cell shapes during epithelial tissue morphogenesis .....	7
<b>1.5 Molecular mechanisms for coordinating epithelial morphogenesis</b> .....	<b>8</b>
1.5.1 The role of the cytoskeleton and associated proteins in epithelial cell shape .....	9
1.5.2 The role of protein localization in cell shape .....	13
<b>1.6 Basal epithelial tissue folding:</b> .....	<b>14</b>
1.6.1 Model of basal epithelial tissue folding: MHB formation .....	14
1.6.2 Shape changes at the MHB basal tissue fold in zebrafish .....	15
1.6.3 Mechanisms controlling MHB basal tissue folding .....	16
<b>1.7 Thesis statement</b> .....	<b>26</b>
<b>Chapter 2</b> .....	<b>28</b>
<b>Calcium signals drive apical-basal cell length during basal epithelial tissue folding</b> .....	<b>28</b>
<b>2.1 Abstract</b> .....	<b>28</b>
<b>2.2 Introduction</b> .....	<b>29</b>
<b>2.3 Materials and methods</b> .....	<b>30</b>
2.3.1 Zebrafish husbandry and maintenance.....	30
2.3.2 Live imaging of calcium transients and analysis.....	30
2.3.3 Pharmacological manipulations .....	31
2.3.4 Live confocal imaging and cell shape analysis.....	32
2.3.5 Calmodulin 1a rescue construct.....	33
<b>2.3.6 Antisense morpholino oligonucleotide and mRNA injections</b> .....	<b>33</b>
2.3.7 In situ hybridization .....	34
2.3.8 Analysis of apoptosis.....	34
2.3.9 Immunohistochemistry .....	35
2.3.10 MHB microdissection .....	35
2.3.11 Reverse transcription – PCR (RT-PCR) .....	36
2.3.12 Western blot analysis with MHB specific tissue.....	37
2.3.13 Statistical analyses .....	37
<b>2.4 Results</b> .....	<b>38</b>
2.4.1 Ca <sup>2+</sup> mediates apical-basal cell length at the MHBC during basal tissue folding. ....	38
2.4.2 Calcium signals to non-muscle myosin II to mediate cell shape at the MHB.....	40
2.4.3 Calmodulin and MLCK regulate MHBC cell shape during basal tissue folding .....	42
<b>2.5 Discussion</b> .....	<b>63</b>
<b>2.6 Contributions</b> .....	<b>65</b>

<b>Chapter 3.....</b>	<b>67</b>
<b><i>Differential regulation of microtubules drive basal anisotropic cell shape during basal epithelial tissue folding.....</i></b>	<b>67</b>
<b>3.1 Abstract .....</b>	<b>67</b>
<b>3.2 Introduction .....</b>	<b>68</b>
<b>3.3 Materials and methods .....</b>	<b>69</b>
3.3.1 Zebrafish husbandry, maintenance, and strains .....	69
3.3.2 Antisense morpholino oligonucleotide and mRNA injections.....	70
3.3.3 Live confocal imaging and cell shape analysis.....	70
3.3.4 Western blot and two-dimension SDS PAGE analysis .....	73
3.3.5 Microtubule imaging and analysis .....	74
3.3.6 MRLC-GFP imaging and analysis .....	76
3.3.7 Immunohistochemistry .....	76
3.3.8 Pharmacological manipulations .....	79
3.3.9 Statistical analyses .....	79
<b>3.4 Results .....</b>	<b>80</b>
3.4.1 Three-dimensional neuroepithelial cell shape analysis reveals anisotropic cell shape. ....	80
3.4.2 Basal anisotropic cell shape is significantly enhanced between 18 ss and 24 ss. ....	81
3.4.3 Wnt5b is required for anisotropic cell shape both apically and basally at the MHBC. ....	83
3.4.4 Wnt5b regulates tubulin during MHB morphogenesis. ....	84
3.4.5 Wnt5b regulates microtubule dynamics during early MHB morphogenesis. ....	87
3.4.6 Microtubule polymerization is required for basal, but not apical, anisotropic cell shape in MHBC cells at 24 ss. ....	88
3.4.7 Microtubule filament stability is required for Wnt5b-mediated basal anisotropic cell shape. ....	89
3.4.8 JNK is regulated by Wnt5b and mediates microtubule dynamics at the MHBC. ....	90
3.4.9 JNK is required for basal anisotropic MHBC cell shape.....	91
3.4.10 Microtubule filament stability is required for JNK-mediated basal anisotropic cell shape. ....	92
<b>3.5 Discussion .....</b>	<b>121</b>
<b>3.6 Contributions .....</b>	<b>125</b>
<b>Chapter 4.....</b>	<b>126</b>
<b><i>General Discussion.....</i></b>	<b>126</b>
<b>4.1 Summary of key findings and future directions. ....</b>	<b>126</b>
<b>4.2 Mechanisms employed to control specific aspects of cell shape. ....</b>	<b>132</b>
4.2.1 The role of molecular cues and molecular context in determining cell shape .....	132
4.2.2 Cytoskeletal networks in defining cell shape .....	135
4.2.3 Intracellular protein localization in determining shape .....	137
<b>4.3 Differential cell shapes determine tissue structure.....</b>	<b>139</b>
4.3.1 Apical versus basal tissue structures.....	139
4.3.2 Radial versus axial tissue structures.....	140
4.3.3 Tissue bends versus tissue folds .....	141
<b>4.4 Concluding remarks.....</b>	<b>143</b>
<b>References.....</b>	<b>144</b>

**APPENDIX A: Z-series processing of live confocal images to project data in the X-Z plane and to quantify anisotropic cell shape at the MHBC..... 157**

**APPENDIX B: Z-series processing of live confocal images to project data in the X-Z plane and to quantify anisotropic cell shape in cells outside of MHBC. .... 159**

**APPENDIX C: Differential Two-Dimensional SDS-PAGE and Mass Spectrometry Pipeline. .... 160**

**APPENDIX D: Quantification of microtubules using live imaging of EMTB-GFP and  $\beta$ -tubulin immunohistochemistry. .... 161**

**APPENDIX E: Quantification of NMII using MRLC-GFP and actin using phalloidin staining.. 163**

**APPENDIX F: Quantification of  $\beta$ -catenin immunohistochemistry. .... 164**

**Curriculum Vitae..... 165**

## LIST OF FIGURES

<b>Figure 1.</b> Model of a single-cell layered epithelial tissue.....	19
<b>Figure 2.</b> Model of some possible epithelial tissue shapes.....	20
<b>Figure 3.</b> Model of some possible epithelial cell shape changes.....	21
<b>Figure 4.</b> Model of the zebrafish MHB.....	22
<b>Figure 5.</b> Timeline of MHB formation in zebrafish.....	22
<b>Figure 6.</b> Illustration of cell shape changes in the zebrafish MHB.....	23
<b>Figure 7.</b> Model of MHBC cell shape mediators required for basal epithelial tissue folding.....	24
<b>MOVIE 1.</b> Calcium transients at the MHB.....	46
<b>Figure 8.</b> Calcium transients are enriched in the MHB at 18 ss.....	47
<b>Figure 9.</b> Calcium transients promote decreases in cell length at the MHBC.....	48
<b>Figure 10.</b> Calcium regulates cell length at the MHBC.....	49
<b>Figure 11.</b> Pharmacological manipulations change intracellular $Ca^{2+}$ levels and do not increase apoptosis or affect N-cadherin localization in the MHB.....	50
<b>Figure 12.</b> Calcium regulates MHB basal tissue folding.....	51
<b>Figure 13.</b> Confirmation of MHB tissue dissection.....	52
<b>Figure 14.</b> Calcium signals to NMII at the MHB to modulate MHBC cell length.....	54
<b>Figure 15.</b> Calcium regulates MHB basal tissue folding, but not cell width, through NMII.....	56
<b>Figure 16.</b> Calcium inhibition rescues NMII over-activation at the MHBC.....	57
<b>Figure 17.</b> Calcium does not affect NMII-mediated cell width during MHB basal tissue folding.....	58



<b>Figure 18.</b> <i>Calmodulin 1a</i> is expressed at the MHBC before and at the onset of MHB morphogenesis.....	59
<b>Figure 19.</b> Confirmation of <i>calmodulin1a</i> morpholino-mediated knockdown.....	59
<b>Figure 20.</b> <i>Calmodulin 1a</i> and MLCK mediate cell length at the MHBC.....	60
<b>Figure 21.</b> Quantification of MHBC angle and MHB cell width.....	61
<b>Figure 22.</b> <i>Calmodulin 1a</i> mediates pMRLC levels at the MHB during basal tissue folding.....	62
<b>Figure 23.</b> Neuroepithelial cell shape analysis reveals anisotropic shape that is enhanced basally during morphogenesis.....	94
<b>Figure 24.</b> <i>Wnt5b</i> is required for anisotropic cell shape both apically and basally at the MHBC.....	96
<b>Figure 25.</b> <i>wnt5b</i> morpholino knockdown phenocopies <i>wnt5b pipetail<sup>(ti265)</sup></i> mutants, including defects in anisotropic cell shape at the MHBC.....	97
<b>Figure 26.</b> <i>wnt5b</i> knockdown does not affect apical or basal MHBC cell area, MHB cell proliferation, or anisotropic cell shape outside of the MHBC during early morphogenesis.....	98
<b>Figure 27.</b> Differential two-dimensional SDS-PAGE and mass spectrometry reveal <i>Wnt5b</i> may be important for tubulin protein levels at the MHB.....	100
<b>Figure 28.</b> <i>Wnt5b</i> regulates tubulin protein levels at the MHB.....	102
<b>Figure 29.</b> <i>wnt5b</i> knockdown does not affect apical or basal localization of myosin regulatory light chain (MRLC) or actin at the MHBC.....	104
<b>Movie 2.</b> Control MO EB3-GFP Raw Data Timelapse.....	105
<b>Movie 3.</b> Control MO EB3-GFP Tracks Timelapse.....	105

<b>Movie 4.</b> <i>wnt5b</i> MO EB3-GFP Raw Data Timelapse.....	106
<b>Movie 5.</b> <i>wnt5b</i> MO EB3-GFP Tracks Timelapse.....	106
<b>Figure 30.</b> Wnt5b regulates microtubule dynamics at the MHB.....	107
<b>Figure 31.</b> Colchicine treatment affects microtubule dynamics at the MHBC.....	108
<b>Figure 32.</b> Microtubule polymerization is required for basal anisotropic cell shape at the MHBC.....	109
<b>Figure 33.</b> Colchicine treatment does not affect basal MHBC cell area.....	110
<b>Figure 34.</b> Colchicine treatment does not affect cell shape outside the MHBC.....	111
<b>Figure 35.</b> Microtubule filament stability is required for Wnt5b-mediated basal anisotropic cell shape.....	112
<b>Figure 36.</b> JNK is regulated by <i>wnt5b</i> .....	113
<b>Figure 37.</b> <i>wnt5b</i> knockdown affects basal but not apical localization of $\beta$ -catenin....	114
<b>Movie 6.</b> DMSO EB3-GFP Raw Data Timelapse.....	114
<b>Movie 7.</b> DMSO EB3-GFP Tracks Timelapse.....	115
<b>Movie 8.</b> SP600125 EB3-GFP Raw Data Timelapse.....	115
<b>Movie 9.</b> SP600125 EB3-GFP Tracks Timelapse.....	116
<b>Figure 38.</b> JNK mediates microtubule dynamics at the MHBC.....	116
<b>Figure 39.</b> JNK is required for basal anisotropic MHBC cell shape.....	117
<b>Figure 40.</b> JNK inhibition does not affect anisotropic cell shape outside the MHBC...	118
<b>Figure 41.</b> Microtubule filament stability is required for JNK-mediated basal anisotropic cell shape.....	119
<b>Figure 42.</b> Proposed mechanism for differential regulation of apical and basal anisotropic cell shape in MHBC cells.....	120

## LIST OF ABBREVIATIONS

2-APB	2-aminoethoxydiphenyl borate
AJ	Adherens junction
ANOVA	Analysis of variance
ARP2/3	Actin related protein 2/3
Bleb	blebbistatin
BMP	bone morphogenetic protein
BSA	bovine serum albumin
C. elegans	Caenorhabditis elegans
Ca <sup>2+</sup>	calcium
Calm1a	calmodulin 1a
Cdc42	Cell division cycle 42
CRISPR	clustered regularly interspaced short palindromic repeats
DMSO	Dimethyl sulfoxide
Drosophila	Drosophila melanogaster
EB3	end-binding protein 3
EDTA	ethylenediaminetetraacetic acid
EF1 $\alpha$	elongation factor 1 alpha
EMTB-GFP	ensconsin microtubule binding protein -Green fluorescent protein
F-actin	filamentous-actin
GFP	Green Fluorescent Protein
GSK3 $\beta$	glycogen synthase kinase 3 beta

Hpf	hours post fertilization
HSD	honest significant difference
JNK	Jun N-Terminal Kinase
MAP	microtubule associated protein
MCAK	mitotic centromere-associated kinesin
Memcherry	membrane cherry
MemGFP	membrane green fluorescent protein
MHB	Midbrain-hindbrain boundary
MHBC	Midbrain-hindbrain boundary constriction
$\mu$ l	microliter
MLCK	myosin light chain kinase
$\mu$ m	micron
MO	morpholino
MRLC	myosin regulatory light chain
Mypt1	myosin phosphatase 1
NIS	Nikon Imaging System
nl	nanoliter
NMII	non-muscle myosin II
NMIIA	non-muscle myosin IIA
NMIIB	non-muscle myosin IIB
PBS	phosphate buffered saline
PBT	phosphate buffered saline with Tween-20
PCP	planar cell polarity

PFA	paraformaldehyde
pg	picogram
PH3	phosphorylated histone 3
pJNK	phosphorylated jun N-terminal Kinase
pMLC2	phosphorylated myosin light chain 2
pMRLC	phosphorylated myosin regulatory light chain
Ppt	pipetail
Prim-6	primordium-6
RFP	Red Fluorescent Protein
Rho-GAP	Rho-GTPase activating protein
Rho-GEF	Rho-Guanine nucleotide exchange factor
ROCK	Rho-associated protein kinase
ROI	region of interest
RT-PCR	reverse transcriptase-polymerase chain reaction
SDS-PAGE	sodium dodecyl sulfate-polyacrylamide gel electrophoresis
ss	somite stage
TBST	Tris buffered saline with Tween-20
Thaps	thapsigargin
TJ	Tight junction
Xenopus	Xenopus laevis
XMAP215	Xenopus microtubule associated protein 215

## ACKNOWLEDGEMENTS

I would first and foremost like to thank Dr. Jennifer Gutzman, for which her invaluable guidance, advice, and support has made all aspects of this work possible and for which I will be eternally grateful for. I would like to thank the Gutzman lab members for their contributions, critical comments and discussion of the data and manuscript. Thank you to Dr. Ava Udvardia, University of Wisconsin-Milwaukee Department of Biological Sciences, and to members of the Biological Approaches to Developmental Diseases and Systems Solutions Collaborative Research Team, University of Wisconsin-Milwaukee, for helpful comments and discussion of this work. Thank you to Elizabeth Falat for assistance in making the *calmodulin 1a* rescue construct and data quantification. Thank you to Thomas Stancato from the Gutzman lab for assistance with  $\beta$ -tubulin and  $\beta$ -catenin immunostaining. I thank Dr. Caren Norden from the Max Planck Institute of Molecular Cell Biology and Genetics for kindly providing the EB3-GFP, EMTB-GFP, and MRLC-GFP plasmid constructs used in these studies. Thank you to Dr. Diane Slusarski, University of Iowa, for the *pipetail<sup>ti265</sup>* mutants. I would also like to acknowledge Dr. Andrea Rau from the French National Institute for Agricultural Research, INRA (Jouy en Josas, France) and the University of Wisconsin-Milwaukee School of Public Health for assistance with statistical analyses. I thank Dr. Ionel Popa, University of Wisconsin-Milwaukee Physics Department and Dr. Daad Saffarini, University of Wisconsin-Milwaukee Biological Science Department, for use of equipment. I would like to acknowledge Dr. Philipp Keller and Yinan Wan from the HHMI Janelia Research Campus for kindly providing the previously unpublished pCS2+GCaMP6s-eGFP construct. I would like to thank Dr. Erez Raz from the Institute

of Cell Biology at the University of Munster for providing us with the zebrafish MLCK expression construct. This work was supported by UWM Research Growth Initiative to J.H.G. and a UWM AOP fellowship to M.R.V.

# Chapter 1

## Introduction

### ***1.1 Development***

Development is a culmination of all the biological processes utilized to transform a single-cell zygote into a complex multi-cellular organism. Developmental studies have revealed the following essential processes that drive the formation of an organism: 1) controlled cell proliferation and apoptosis, 2) cell differentiation, 3) spatial and temporal organization, migration, and patterning of cells into distinctive tissues, regions, and polarized body axes, and 4) the creation of structure and form of the whole organism and its constituent organs, tissues, and cells, commonly referred to as morphogenesis.

The importance for understanding development is evident by the striking frequency of birth defects, occurring in as many as 1 in every 33 (or 3%) live births in the US (Hoyert et al., 2006). Additionally, some structural birth defects such as anencephaly and spina bifida where the brain and spinal cord are not formed properly can lead to various degrees of neurological impairment or post-natal fatalities (Avagliano et al., 2018). Our global understanding of development will shape our ability to uncover different disease etiologies and improve treatment modalities. This dissertation work will focus on morphogenesis.



## **1.2 Morphogenesis**

Morphogenesis refers to the creation of form at the scale of the whole organism or at the level of its constituent parts including organs, tissues, and the cells that comprise them all. Ultimately, morphogenesis of a whole organism is coordinated at the level of the constituent cells and tissues by changes in cell and tissue shape and changes in intrinsic mechanical force. To understand the underlying mechanisms of morphogenesis, it is crucial to look at the level of the cells and tissues.

Additionally, understanding morphogenesis is important because the shape of cells, tissues, and organs can be necessary for eliciting specific physiological functions, and is consistent with the shape-function paradigm in biology. For example, vision relies on specific shape and organization of cell and tissue structures in the eye (Bovolenta and Martinez-Morales, 2018) and the morphogenesis of a structure known as the midbrain-hindbrain boundary (MHB) is important for delineating the formation of the midbrain from the hindbrain during brain development (Gibbs et al., 2017).

Understanding the process of morphogenesis will allow us to determine potential approaches to treat or mitigate the occurrence of some diseases like coloboma, where the eye is misshapen (Bovolenta and Martinez-Morales, 2018), or Joubert syndrome in which development of midbrain and hindbrain structures are perturbed (Basson and Wingate, 2013; Parisi and Glass, 1993). Here, we will concentrate on the mechanisms of morphogenesis for a specific tissue type called an epithelium.

### **1.3 Epithelium**

There are four main types of tissues: connective, muscle, nervous, and epithelial. Most organs are composed of multiple tissue types; however, many distinctive physiological processes are carried out by epithelial tissues. Epithelial tissues typically line a surface or a cavity, known as a lumen. Examples of this include the gut, kidney, lung, and secretory organs like salivary, sebaceous, or pancreatic glands. A variety of different structural features of epithelia are important for the functions of these organs. One of these features is the ability of epithelial tissues to establish and define a physical boundary that can compartmentalize and provide directionality for different physiological processes. For instance, epithelial tissues can secrete enzymes, metabolic waste products, or fluids into the lumen of a duct or tubule system or they can absorb molecules like amino acids and glucose from the luminal side of a tubule system such as the nephron or the small intestines (Cheeseman, 1992; Rinschen et al., 2018; Thompson, 1969; Walton et al., 2016).

The hallmark features of epithelial tissues include the following: polarity of cells along a directional axis known as the apical-basal axis, the presence of different intercellular junctions polarized along the apical-basal axis, and adherence of the basal side of epithelial cells to a network of extracellular matrix.

The shape of an epithelium is an important facet of tissue function. For example, in the small intestines, tissue folds are required for increasing the available surface area lining the lumen where nutrients can be absorbed and delivered into the blood stream (Walton et al., 2016). Additionally, the shape and orientation of the nephron loops in the

kidney are important for establishing the countercurrent multiplier system for concentrating the urine filtrate (Gottschalk and Mylle, 1959).

During development, some tissues composed of precursor stem cells are transiently epithelial prior to differentiation. This transient tissue coordinates the organization of an adult organ structure. An example of this is the cerebral cortex of the brain, in which a transient epithelial structure known as the neuroepithelium orients the migration of cells fated to become neurons or glial cells, into the six cortical layers of the developing cortex (Romero et al., 2018). This process lends credence to the idea that epithelial tissues are not only important for physiological functionality, but also in developing functional organ structure. Therefore, it is important that we understand how epithelial tissue shapes are generated in order to understand organ and tissue functions and pathologies.

#### **1.4 Epithelial tissue morphogenesis**

Epithelial cell and tissue shape are not congruent in all dimensions and in fact are typically different along particular directions. For instance, during early brain development, brain precursor stem cells, called neuroepithelial cells, are longer in one direction, while narrower in the orthogonal direction (Gutzman et al., 2015). Cell shape can also be non-congruent from different planes. As an example, during *Xenopus* gastrulation, cells that are involuting generate a bottle shape with one surface of the cell smaller compared to the surface of the cell at the opposite end (Lee and Harland, 2007). Therefore, in order to characterize and study epithelial morphogenesis, it is essential that we provide directional context for describing the orientation of cells and

tissues. We refer to the following conventional anatomical axes to characterize the orientation of a cell and tissue: the apical-basal axis (Y-axis), the anterior-posterior axis (X-axis), or the medial-lateral axis (Z-axis) (Figure 1). Depending on the orientation of the tissue in the embryo, the Z-axis may refer to the dorsal-ventral axis. At the level of the whole organism, the axes are used to describe the establishment of anterior-posterior polarity where anterior regions development structures that include the head and posterior regions that include the tail. At the level of the cell, different molecules can be asymmetrically localized and can elicit polarization of cell and tissue shape along the anatomical axes. These include molecules like claudins that are differentially localized apically and form tight junctions between epithelial cells (Baumholtz et al., 2017). In epithelial cells, proteins of the focal adhesion complex are typically localized basally (Burrige and Chrzanowska-Wodnicka, 1996). Using the conventional anatomical axes will provide a context for studying and describing cell and tissue shapes during the process of epithelial morphogenesis.

#### 1.4.1 Epithelial tissue shapes

In general, epithelial tissues can be represented as a three-dimensional sheet of cells with apical-basal polarity established along the Y-axis (Figure 1). The epithelial sheet can form various shapes, of which we will describe a subset of possible structures (Figure 2) during tissue morphogenesis. To help define these shapes, we will use some new terminology. The apical or the basal edges of a tissue could move closer together to form a gradual tissue curve or a sharp tissue hinge (Figure 2A-B).

*Radial Dome:* An epithelial sheet of tissue may curve radially (Figure 2C) towards the apical surface and form an apical tissue dome, for example, during lens placode invagination (Muccioli et al., 2016). A basal tissue dome, on the other hand, will form when the tissues curve basally (Figure 2C), as found during optic cup formation (Bryan et al., 2016; Sidhaye and Norden, 2017) and bud formation in hydra (Holz et al., 2017).

*Radial Cone:* Epithelial tissues may form a radial hinge, or cone shape, either apically or basally (Figure 2D). Apical cones are found during initial salivary gland development in *Drosophila* (Sanchez-Corrales et al., 2018). To date, a basal cone has not yet been described *in vivo* (Figure 2D).

*Axial Bend:* If the tissue sheet curves along one axis (axial), the tissue will form a bend (Figure 2E). Apical tissue bends have been described during neural tube formation in chick (Nishimura et al., 2012). However, an example of a basal tissue bend has not yet been characterized during development.

*Axial Fold:* A tissue fold is generated if a hinge forms along one axis of the tissue (Figure 2F). Apical tissue folding occurs during ventral furrow formation in *Drosophila* (Heer et al., 2017; Martin et al., 2009) and during neural tube formation in *Xenopus* (Poznanski et al., 1997; Schroeder, 1970; Vijayraghavan and Davidson, 2017). It is possible that neural tubes form from both tissue bends and tissue folds, based on potential differences in size and mechanical strain of a neuroepithelium, either along different regions of an embryo or across species. We have previously identified basal tissue folding during midbrain-hindbrain boundary (MHB) formation. Based on morphological data and observations, we further hypothesize that basal tissue folds generate villi in the gut (Ng et al., 2005; Shyer et al., 2013).

It is important to note that the simple tissue shapes described in Figure 2 are just a few different examples of the shapes that epithelial tissues may generate. Tissue shapes can vary widely. We hypothesize that different regions of a tissue may form a variety of structures or repetition of the same structure.

#### 1.4.2 Cell shapes during epithelial tissue morphogenesis

Spatially coordinated cell shape changes are a crucial driving force for epithelial morphogenesis. Using the conventional anatomical axes, we can describe the types of cell shape changes that occur during tissue shaping (Figures 1 and 3).

*Apical or Basal Cell Shapes:* On the apical or basal side of a cell, the cell surface can shrink (apical constriction) or expand (apical expansion) (Figure 3A). The cell surface may change to have equal dimensions in all directions, resulting in isotropic cell shape or change to have unequal dimensions in different directions, resulting in anisotropic cell shape (Figure 3B). Apical cell shaping is important for neural tube formation in chick, where cells throughout the neural plate generate anisotropic cell shape in the medial-lateral direction (Nishimura et al., 2012). In *Xenopus*, specific cells at the midline of the neural plate apically constrict and form a tissue hinge point during neural tube closure (Poznanski et al., 1997; Schroeder, 1970; Vijayraghavan and Davidson, 2017). Apical constriction contributes to ventral furrow formation in early *Drosophila* development (Heer et al., 2017; Martin et al., 2009) and during lens placode invagination (Lang et al., 2014; Plageman et al., 2011; Plageman et al., 2010). Apical expansion (Figure 3A) has been described during MHB formation in zebrafish; however, it has only been characterized along the anterior-posterior direction in basal tissue

folding (Gutzman et al., 2008). Therefore, it is unknown if this cell shape occurs isotropically or anisotropically. We hypothesize that apical expansion is required for generating a sharp basal tissue fold during MHB morphogenesis. Basal expansion has not yet been described *in vivo*. Basal constriction was reported during optic cup and MHB morphogenesis (Gutzman et al., 2018; Gutzman et al., 2008; Sidhaye and Norden, 2017). However, anisotropic basal cell shape has not been previously reported and the mechanism for how it forms remains to be elucidated.

*Cell Length, width and depth:* Epithelial cells can change in length, width, and depth in the Y-, X-, and Z- dimensions, respectively (Figure 3C). Cells elongate during neural induction (Davidson and Keller, 1999; Schroeder, 1970; Suzuki et al., 2012) and optic cup morphogenesis (Bryan et al., 2016). Cells at the MHB hinge point shorten, while cells throughout the MHB narrow during MHB formation (Gutzman et al., 2015). This dissertation will reveal that cells at the MHBC become deeper. Collectively, all of these different cell shapes can be spatially organized to generate tissue form.

### ***1.5 Molecular mechanisms for coordinating epithelial morphogenesis***

Different shapes in specific regions of the cell can be produced by instructional signaling cues. One example of this includes the ubiquitous signal, calcium. During neural tube closure, calcium plays a role in apical constriction (Christodoulou and Skourides, 2015; Suzuki et al., 2017), while in the context of the *Drosophila* egg chamber, it mediates basal tissue contraction (He et al., 2010). Additionally, the secreted extracellular signaling molecule and known morphogen, Wnt, has been shown to be important for both apical and basal constriction. During *Xenopus* and *C. elegans*

gastrulation, and during shaping of the mammalian lung epithelium, the Wnt signal is critical for apical constriction (Choi and Sokol, 2009; Fumoto et al., 2017; Lee et al., 2006) but during MHB morphogenesis in the zebrafish, it plays an integral role in allowing cells to constrict basally at the MHBC (Gutzman et al., 2018). Instructional cues, such as calcium in the context of neurulation and egg chamber elongation, are known to provide signals to the cytoskeleton to modulate cell shapes (Christodoulou and Skourides, 2015; He et al., 2010; Suzuki et al., 2017) and thus the mechanisms for regulating the cytoskeleton have long been the focus of many morphogenetic studies.

### 1.5.1 The role of the cytoskeleton and associated proteins in epithelial cell shape

The cytoskeleton is an extensively studied regulator of epithelial cell and tissue shape. Although the cytoskeleton is ubiquitous, it can be modulated by various mechanisms to control cell and tissue shaping behaviors. Regulation of cytoskeletal protein abundance, modifications, or modulation of cytoskeleton binding proteins can fine-tune cytoskeletal function during development and morphogenesis.

*Actomyosin:* The actin cytoskeleton and associated proteins are a widely studied network in morphogenesis. Actin is composed of filaments assembled from  $\beta$ -actin protein monomers. The actin cytoskeleton can localize both apically and basally in epithelial cells during cell shaping, as shown in the following examples. Apically, actomyosin mediates apical constriction during *Xenopus* gastrulation, neural tube closure in vertebrates and ventral furrow formation in *Drosophila* (Martin et al., 2009;



Vasquez et al., 2014)(Heer et al., 2017; Lee and Harland, 2007; Martin et al., 2009; Nishimura et al., 2012; Plageman et al., 2011). Basally, actin is important for *Drosophila* egg chamber elongation and invagination of the retinal neuroepithelium (He et al., 2010; Sidhaye and Norden, 2017).

Contraction of cell shape can be mediated through the actin cytoskeleton by the cross-linking of actin motor proteins known as myosins. Non-muscle myosin II (NMII) proteins are ubiquitously expressed and have been well studied for the role of mediating contraction during cell shaping (Munjal and Lecuit, 2014). Non-muscle myosin II proteins contain a globular head domain and a coiled-coil tail domain (Munjal and Lecuit, 2014). Movement of the myosin protein along the actin filament is ATPase driven and is the force-generating mechanism for contractility of the actin filaments (Munjal and Lecuit, 2014). If the network of actin and myosin are linked to the cell membrane, the contraction of the actomyosin network can result in contraction of the cell membrane and constriction of the cell shape (Munjal and Lecuit, 2014).

The actomyosin network can be modulated via several different mechanisms. One means for regulating actomyosin contractility is through regulating the phosphorylation state of NMII. For instance, phosphorylation of the myosin regulatory light chain protein (MRLC), which binds to the neck region of the non-muscle myosin II protein, results in activation (Munjal and Lecuit, 2014). The phosphorylation state of MRLC can be modulated by kinases such as myosin light chain kinase (MLCK) and Rho-associated protein kinase (ROCK) or phosphatases like myosin phosphatase (Munjal and Lecuit, 2014). ROCK activity can be modulated by Rho protein which, in turn, can be activated by guanosine nucleotide exchange factors like Rho-GEF or

deactivated by GTPase activating proteins like Rho-GAP (Munjal and Lecuit, 2014; Van Aelst and Symons, 2002). In addition to the regulation of myosin function, actin dynamics, which includes nucleation, polymerization or depolymerization, and remodeling activity, can be modulated by other members of the Rho family of small G proteins including Rac1 and Cdc42, which utilize actin binding proteins, cofilin, formins, and the Arp2/3 complex (Hanna and El-Sibai, 2013; Van Aelst and Symons, 2002). Both myosin-mediated contractility and actin polymerization will be important features for the fine-tuned control of cell and tissue morphogenesis.

*Microtubules and associated proteins:* Microtubules are composed of 13 laterally interacting protofilaments assembled from dimers of alpha- and beta-tubulin (Etienne-Manneville, 2010). Polymerization and depolymerization activity of microtubules (microtubule dynamics) are important mediators of morphogenesis (Burnside, 1971; Cearns et al., 2016; Jayachandran et al., 2016; Messier, 1969; Singh et al., 2018), but the role for microtubules in cell shaping have not been extensively investigated. Microtubules regulate cell elongation in the neuroepithelium (Burnside, 1971; Cearns et al., 2016; Jayachandran et al., 2016; Messier, 1969). It functions in regulating apical constriction of eye disc and salivary gland epithelium in the fly (Booth et al., 2014; Fernandes et al., 2014), and in bottle cells during *Xenopus* gastrulation (Choi and Sokol, 2009; Lee and Harland, 2007). However, microtubules were not found to regulate cell elongation in bottle cells during gastrulation, as they do in cells undergoing neurulation (Lee and Harland, 2007).

Regulating microtubule dynamics is possible through several mechanisms. One mechanism is through modulating the accessibility of microtubule filament dimers, which

can be carried out by the protein Stathmin (Etienne-Manneville, 2010). Microtubule filaments can acquire direct post-translational modifications that affect microtubule stability and polymerization dynamics, including acetylation and detyrosination (Etienne-Manneville, 2010). Microtubule associated proteins such as XMAP215 and End binding protein 1 (EB1) can stabilize microtubule filaments or can destabilize microtubules for faster catabolism, as is accomplished by the protein, MCAK (Etienne-Manneville, 2010). Microtubule filament severing enzymes like katanin are, likewise, critical for modulating microtubule-mediated processes (Quarumby and Lohret, 1999). Similar to the actin cytoskeleton, microtubule filaments can be differentially oriented and localized within the cell to accomplish specific cell tasks including the transport of cargo, intracellularly. Transport of cargo to specific target regions of the cell is important for cell functions such as transducing signals across the cell body, polarization of proteins, or membrane protein trafficking (Rogers and Gelfand, 2000; Sheetz, 1996).

Directionally controlled transport of molecules may be important for cell shaping. The microtubule motor proteins, kinesin and dynein, can travel along the length of the filament along only one direction. Microtubule filaments are polarized with  $\alpha$ -tubulin at the minus end and  $\beta$ -tubulin at the plus end of the microtubule dimer (Etienne-Manneville, 2010). Kinesin travels toward the plus end of the microtubule filament and dynein travels toward the minus end. The difference in directional motility allows for specific regulation of cargo transport, if microtubules are organized within the cell. Although microtubules are not known to function by producing mechanical contractile force as the actomyosin cytoskeleton, microtubule filaments have high tensile strength and have been demonstrated to function as a protrusive force for stabilizing cell

structures during morphogenesis (Singh et al., 2018). Therefore, microtubule filaments can be oriented and localized along specific direction to control cell shapes.

Both the actomyosin and microtubule cytoskeleton have diverse mechanisms for regulation, allowing for fine-tuned cell shaping. Controlling localization and orientation of the cytoskeleton could provide a mechanical basis for where and how cell shape changes take place.

### 1.5.2 The role of protein localization in cell shape

Asymmetric localization of proteins may be a driving force for generating shapes within a specific region of the cell. For instance, cell shape may depend on different cell adhesion complexes and linking molecules that can bind, localize, and spatially orient the cytoskeleton to specific regions of the cell membrane (Baumholtz et al., 2017; Nishimura et al., 2012; Plageman et al., 2011). Apical cell adhesion complexes include tight junctions (TJ), which consist of molecules from the occludins and claudins family, and adherens junctions (AJ), which consist of cadherin proteins. Basal adhesion complexes, which attach cells to the basement membrane, include the focal adhesion complex and are made up of proteins such as  $\beta$ -integrin, vinculin, and focal adhesion kinase (Burrige and Chrzanowska-Wodnicka, 1996; Hynes, 2002).

The ability of cell adhesion molecules to regulate cell shape could be through directing the orientation of actomyosin contractions or cell membrane protrusive forces via microtubule filament orientation. For example, adherens junction molecules and other associated molecules including N-cadherin, Nectin-2, Shroom-3, and Celsr1, have

been shown to position actomyosin and NMII modulating proteins such as RhoGEF and ROCK apically for apical constriction during neural tube closure and lens placode invagination (Morita et al., 2010; Nishimura et al., 2012; Plageman et al., 2010)(Morita et al., 2010; Nishimura et al., 2012; Plageman et al., 2010). Focal adhesion complex molecules including Focal Adhesion Kinase and  $\beta$ -integrins can be localized basally (Bogdanovic et al., 2012; Gutzman et al., 2018; Martinez-Morales et al., 2009; Nicolas-Perez et al., 2016). We hypothesize that basal focal adhesions are important for localizing the actin cytoskeleton basally for MHB morphogenesis, but further studies are needed to confirm this. Although apical and basal cell shapes have been associated to specific localization of protein complexes to either the apical or basal cell regions, it is unclear how they might mediate cell length, width, and depth.

## **1.6 Basal epithelial tissue folding:**

### **1.6.1 Model of basal epithelial tissue folding: MHB formation**

Although a myriad of studies has elucidated the mechanisms for controlling apical tissue folding, far less has been investigated in the mechanism coordinating basal epithelial tissue folding and will subsequently be the focus of this dissertation. One of the earliest identified basal tissue folds is found in the developing neural tube and is known as the midbrain-hindbrain boundary (MHB). As the name suggests, the MHB delineates formation of the midbrain from the hindbrain (Gibbs et al., 2017; Lowery et al., 2009). We specifically use the MHB of the embryonic zebrafish, *Danio rerio*, as a model to study basal tissue folding (Figure 4). Formation of the MHB in zebrafish occurs within the first 24 hours post fertilization (hpf) (Figure 5), allowing for a rapid timeline of

investigation relative to the mammalian mouse model in which MHB formation occurs at stage E14 or approximately 14 days post fertilization (Lowery and Sive, 2009).

Zebrafish embryos also develop *ex-utero*, are transparent, and the neural tube is readily accessible for imaging, live, at single-cell resolution using confocal microscopy. Many *in vivo* and *in vitro* methods for investigating cellular shape, subcellular protein localization and protein dynamics after genetic and pharmacological manipulations are also possible using the zebrafish model. Based on these collective features, we decided to use the zebrafish MHB model for investigating the molecular mechanisms of basal epithelial tissue folding.

### 1.6.2 Shape changes at the MHB basal tissue fold in zebrafish

MHB formation in the zebrafish proceeds as follows: formation is initiated at 18 somite stage (ss) or about 18 hpf, after the neural tube has formed (Figure 5A). Neural tube inflation with embryonic cerebral-spinal fluid occurs concurrently with MHB formation, beginning first in the hindbrain ventricle, followed by in the midbrain ventricle (Figure 5C-D) (Lowery and Sive, 2005). The neural tube consists of a single-cell layered pseudostratified epithelium (Figure 6A) in which a series of cell shape changes are required for the MHB to fold (Figure 6B-E). Cells at the point of deepest constriction of the MHB, at the hinge point, termed the MHB constriction (MHBC) shorten in apical-basal length and become narrower in the anterior-posterior direction by 24 ss (Figure 6B-C) (Gutzman et al., 2015). By primordium-6 stage (prim-6) or about 24 hpf, cells at the MHBC constrict along the basal surface (Figure 6D) and expand (Figure 6E) along the apical surface, leading to a wedged cell shape and an acute angle along the basal

side of the tissue at the MHBC hinge point (Gutzman et al., 2018; Gutzman et al., 2008). This tissue folding subsequently generates a constriction in the neural tube and clearly delineates the presumptive midbrain region from the presumptive hindbrain region (Gutzman et al., 2008; Lowery et al., 2009).

### 1.6.3 Mechanisms controlling MHB basal tissue folding

Early investigation of brain formation revealed that the contractile state of the neuroepithelia is important for tissue shape, as shown through demonstrating the role of the non-muscle myosin II protein regulator, myosin phosphatase, in mediating morphogenesis (Gutzman and Sive, 2010). We investigated if myosin played a role during MHB morphogenesis and determined that non-muscle myosin II proteins (NMII) were important for cell shortening and narrowing at the MHB (Figure 7A-B). In fact, two different isoforms of the NMII protein were discovered to differentially modulate independent aspects of MHB cell shape within the same cellular context. Specifically, we found that apical-basal MHBC cell length is regulated by non-muscle myosin IIA (NMIIA) (Figure 7A) while anterior-posterior MHB cell width was found to be regulated by non-muscle myosin IIB (NMIIB) (Figure 7B) (Gutzman et al., 2015). However, the molecular pathways that differentially activate and regulate the NMII proteins during basal tissue folding are still unknown.

To help identify regulators of the NMII proteins, we were interested in finding signaling molecules that are expressed specifically at the MHB and that are known to regulate actomyosin activity. A screening of available *in situ* data for genes expressed specifically at the MHB, revealed a gene encoding a calcium-binding protein, *calmodulin*

1a. We hypothesized that  $\text{Ca}^{2+}$  functions as a morphogenetic signal to mediate cell shape changes at the MHB to promote basal epithelial tissue folding because it is known to play a critical role in mediating phosphorylation of MRLC via myosin light chain kinase (MLCK) (Berridge et al., 2000; Somlyo and Somlyo, 2003; Vicente-Manzanares et al., 2009) and we know that NMII proteins are important for MHB cell length and cell width changes (Gutzman et al., 2015). Additionally, calcium signaling is critical for many other embryonic developmental processes such as gastrulation and neural tube closure (Slusarski and Pelegri, 2007; Webb and Miller, 2003).

During late MHB formation, MHBC cells basally constrict in the anterior-posterior direction (Figure 7C). Basal constriction was shown to be mediated by the basement membrane protein, laminin (Figure 7C) (Gutzman et al., 2008). Apical expansion is critical in late basal epithelial tissue folding and is mediated in part by midbrain and hindbrain ventricle inflation (Figure 7D). This was demonstrated in mutants of the  $\text{Na}^+/\text{K}^+$  ATPase encoding gene, *snakehead* (Gutzman et al., 2008). Because NMII and the basement membrane are found throughout the neural tube, but cell shaping for basal tissue folding of the MHB was region specific, a next logical step was to identify other potential upstream mediators of MHBC cell shaping.

From the screening of *in situ* data for genes expressed specifically at the MHB, the morphogen, *wnt5b*, was found (Gutzman et al., 2018). *Wnt5b*, from this study, is critical for the basal constriction of cells at the MHB (Gutzman et al., 2018). Focal adhesion kinase contributed to MHB tissue folding downstream and cooperatively of *Wnt5b* signaling (Gutzman et al., 2018). *Wnt5b* was discovered to be mediated through  $\text{GSK3}\beta$  (Gutzman et al., 2018). It is important to note it is not known what happens to



basal cell depth in the dorsal-ventral direction and whether the basal cell shape is isotropic or anisotropic for the tissue folding. Additionally, what happens apically to cell shape was not studied. Furthermore, it is not known if Wnt5b impacts MHBC cell shape by modulating the actin cytoskeleton, microtubule cytoskeleton, or is cytoskeleton-independent. We hypothesize that Wnt5b regulation of basal tissue folding is dependent on the cytoskeleton. One downstream effector of Wnt signaling, jun N-terminal Kinase (JNK) is known to regulate microtubule dynamics (Schambony and Wedlich, 2007; Yang, 2003). We hypothesize that Wnt5b signals to JNK to regulate microtubule dynamics during MHB morphogenesis.

Although we have previously characterized some of the cell shape changes that are critical for MHB basal epithelial tissue folding, we have not identified the following questions. What happens to cell shape on the apical and basal side? What are the potential upstream instructional cues of this process? How do these signaling cues mediate the cell shape changes? These questions will be the focus of this dissertation.

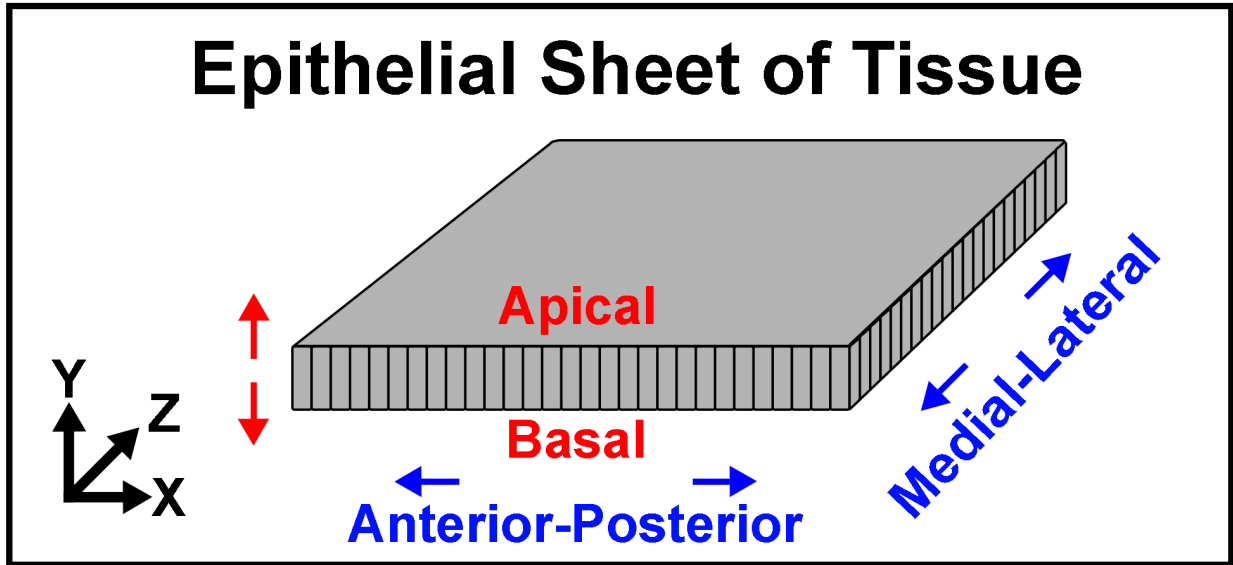


**Figure 1. Model of a single-cell layered epithelial tissue.** Illustration of a sheet of epithelial tissue. Y-axis indicates the apical-basal direction (red). X-axis indicates the anterior-posterior direction and the Z-axis indicates the medial-lateral direction (blue).

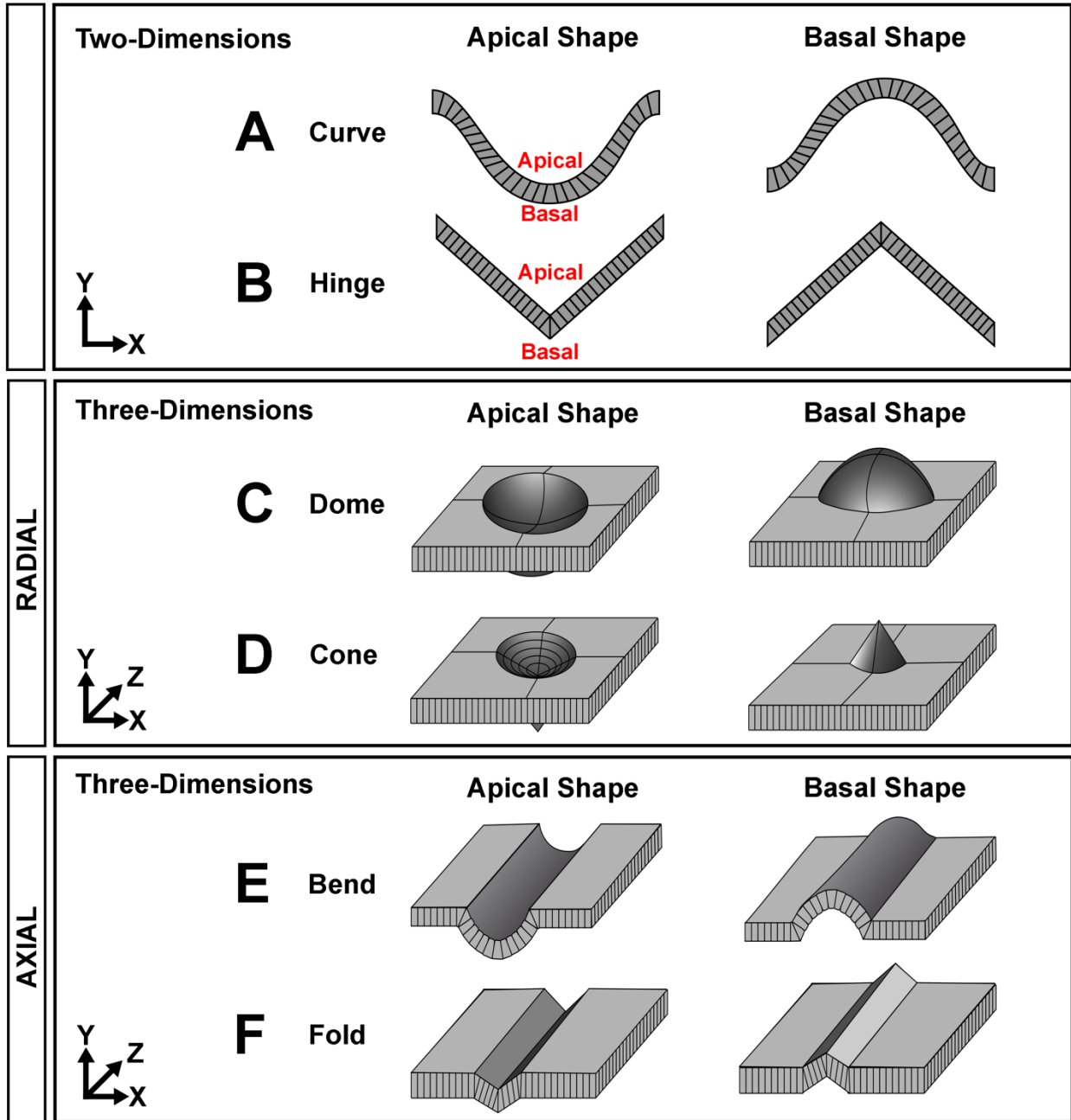


**Figure 2. Model of some possible epithelial tissue shapes.** (A-B) Illustration of tissue shapes from two-dimensions showing apical or basal tissue curve (A) or tissue hinge (B). (C-D) Illustration of radial tissue shapes from three-dimensions. (C) Apical or basal tissue domes can form from radial tissue curves. (D) Apical or basal tissue cones can form from radial tissue hinges. (E-F) Illustration of axial tissue shapes from three-

dimensions. (E) Apical or basal tissue bends can form from axial tissue curves. (F) Apical or basal tissue folds can form from radial tissue hinges.

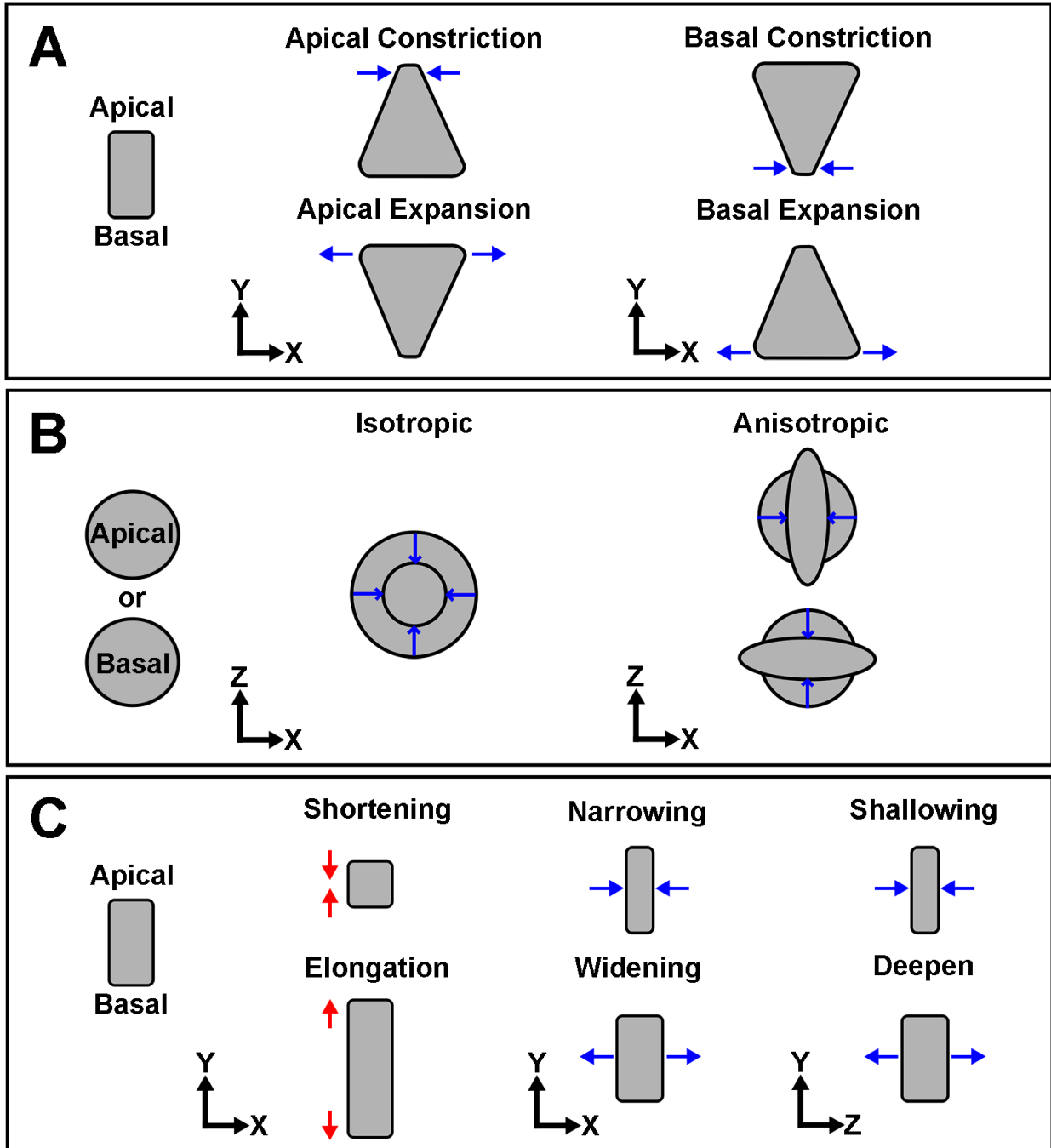


**Figure 3. Model of some possible epithelial cell shape changes.** (A) Cells can apically or basally constrict or expand. (B) Apically or basally, cells can change shape equally in all directions (isotropic) or in a specific direction (anisotropic). (C) Cells can elongate or shorten in the Y-axis. Cells can become wider or narrower in the X-axis or shallower or deeper along the Z-axis.

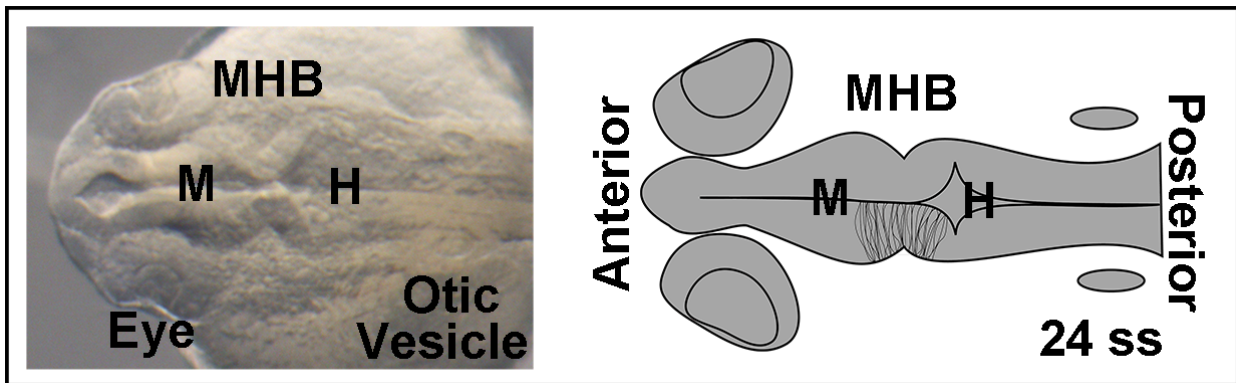


**Figure 4. Model of the zebrafish MHB.** Brightfield image (Left) and Illustration (Right) of dorsal view of zebrafish embryo at 24 somite stage (ss). Individual cells are illustrated at the midbrain-hindbrain boundary (MHB). M, midbrain; H, hindbrain.

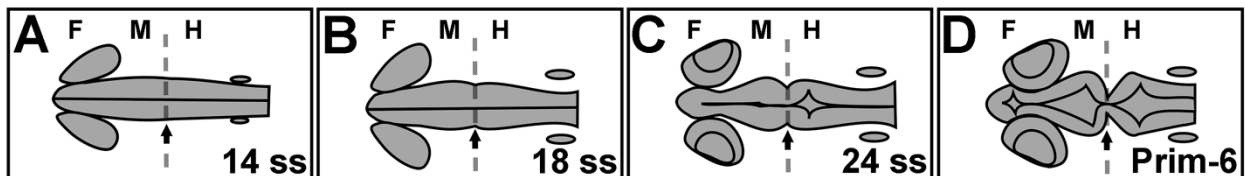


**Figure 5. Timeline of MHB formation in zebrafish.** (A-D) Illustrated dorsal view of zebrafish at indicated stages. Before MHB formation, the neural tube is straight, but patterned for the forebrain, F, midbrain, M, and hindbrain, H, at 14 ss (A). At the onset of MHB formation, 18 ss, the region between the midbrain and hindbrain begins to constrict (B). (C) By 24 ss, the hindbrain ventricle is inflating and a hinge point forms

between the midbrain and the hindbrain. (D) At Prim-6 stage, or about 24 hours post fertilization (hpf), the MHB forms a sharp fold. Dotted line indicates boundary between midbrain and hindbrain. Arrow indicates where MHB fold occurs.

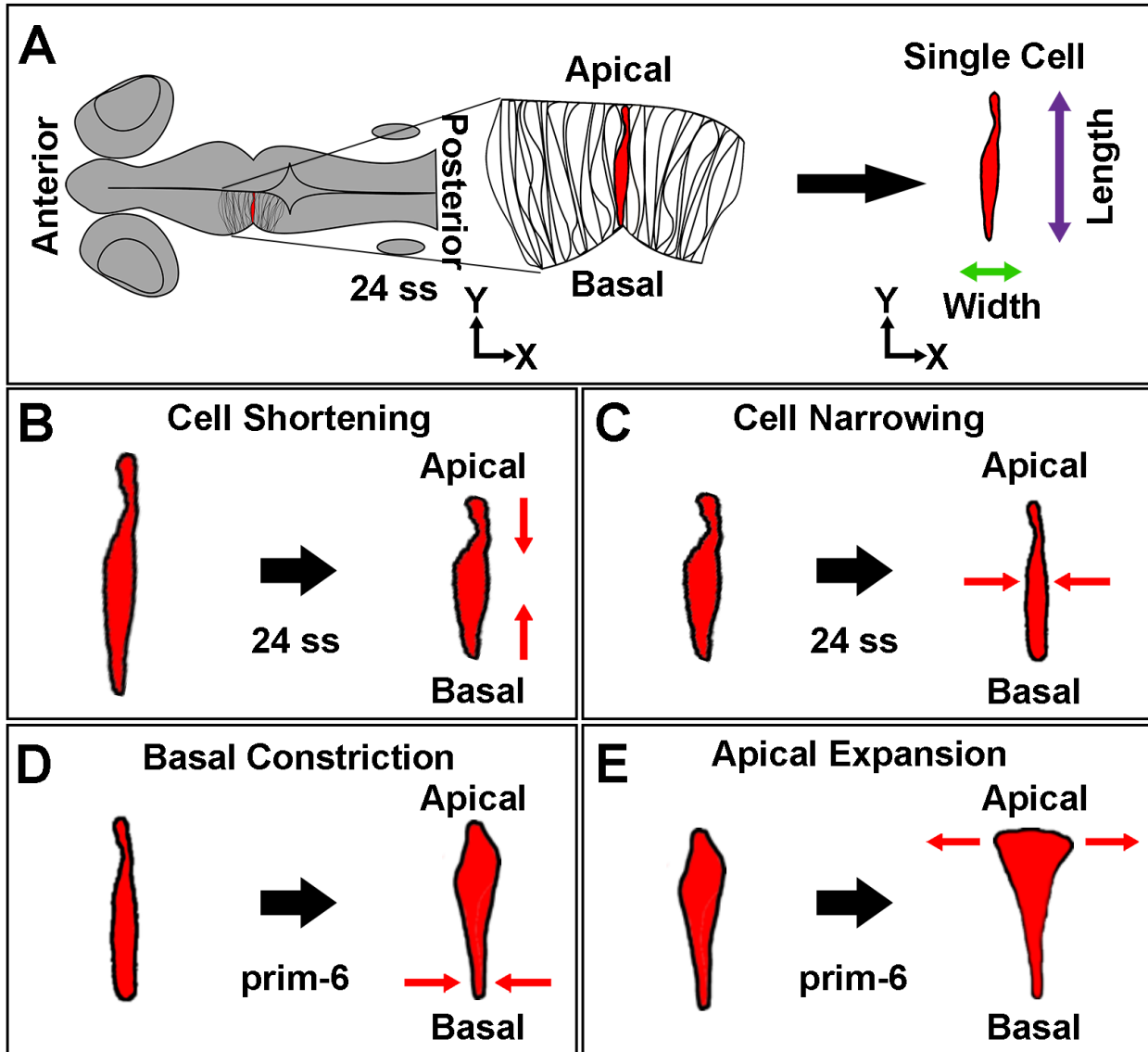


**Figure 6. Illustration of cell shape changes in the zebrafish MHB.** (A) Illustration of one side of the neuroepithelium at the MHB of a developing zebrafish embryo at 24 ss.

A single cell at the deepest hinge point of the MHB constriction (MHBC) is highlighted in red. To the right, cell length is characterized in the apical-basal direction (Y-axis) and cell width is in the anterior-posterior direction (X-axis). (B-E) Cell shape changes during MHB formation. At 24 ss, cells at the MHBC shorten (B) and cells throughout the MHB narrow (C). At prim-6 stage, cells at the MHBC constrict basally (D) and expand apically (E).

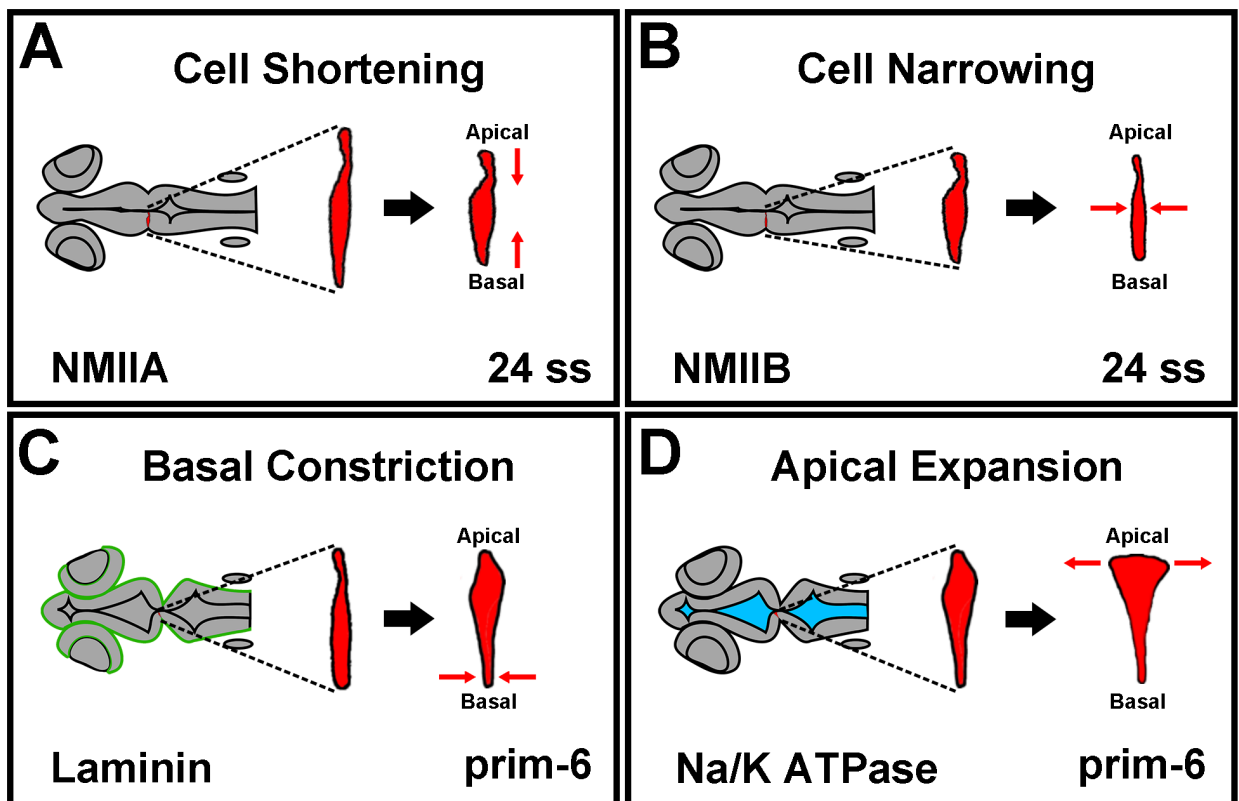


**Figure 7. Model of MHBC cell shape mediators required for basal epithelial tissue folding.** (A) Cell shortening occurs by 24 ss in the apical-basal direction and is mediated by the actin motor protein, non-muscle myosin IIA (NMIIA) isoform. (B) Cell narrowing occurs by 24 ss in the anterior-posterior direction and is mediated by the

actin motor protein, non-muscle myosin IIB (NMIIB) isoform. (C) Basal constriction occurs by prim-6 stage and is mediated by the basement membrane protein, laminin, illustrated in green. (D) Apical expansion occurs by prim-6 stage and is mediated by ventricle inflation, regulated through the Na/K ATPase.



## **1.7 Thesis statement**

How do epithelial tissues form basal tissue folds? This is the broader question that drives this dissertation work. Understanding the critical cellular and molecular mechanisms that produce a basal tissue fold will provide an updated model for the types of tissue shapes possible during development.

To understand basal epithelial tissue folding we looked in the early developing brain structure known as the neural tube. The neural tube generates a basal epithelial tissue fold to delineate formation of the midbrain from the hindbrain and is known as the midbrain-hindbrain boundary (MHB). We utilized the zebrafish MHB because it provides a rapid, transparent, and easily accessible model for characterizing basal epithelial tissue folding at single cell resolution.

We wanted to know what could be driving the cell shape changes critical for basal tissue folding of the MHB. We looked at what signaling components are specifically expressed at the MHB and that regulate morphogenesis during development. Using zebrafish gene expression data, we found *calmodulin 1a*, a gene encoding a calcium binding protein. Calcium is known to regulate morphogenesis. The screen further revealed *wnt5b*, a gene encoding an extracellular morphogen. We hypothesized that calcium and Wnt5b signaling are critical for mediating specific and different aspects of MHB cell shape during basal epithelial tissue folding. Using genetic and pharmacological manipulation of embryos, imaging, and various molecular analyses, we found that calcium signaling, through *calmodulin 1a*, is important for controlling cell length at the deepest hinge point of the tissue fold, known as the MHB

constriction (MHBC) during basal tissue folding. Furthermore, we found that calcium signaling shortens MHBC cells through MLCK and non-muscle myosin II.

We recently developed a three-dimensional morphometric technique for analyzing cell shapes within epithelial tissues. Using this technique, we have uncovered a novel role for a single morphogen, Wnt5b, in the regulation of apical and basal anisotropic cell shape. Moreover, we found that within the same epithelial cell context, Wnt5b specific regulation of basal anisotropic epithelial cell shape is differentially mediated by microtubules. This is in stark contrast to actomyosin contractility which is largely implicated in tissue morphogenesis, while microtubules within the context of tissue shaping has been poorly examined. Our current model suggests that Wnt5b mediates microtubules to regulate MHBC cell shape via jun N-terminal Kinase (JNK) signaling, a known downstream Wnt target and known microtubule regulator. Wnt5b- and JNK-mediated anisotropic basal cell shape is specifically important for basal tissue folding. Furthermore, the basal anisotropic cell shape is restricted to cells directly at the hinge point of the fold.

With our studies, we may continue to uncover the potential etiology of developmental structural birth defects. We can work towards a future that applies our findings to the development of *in vitro* tissue models for human diseases. Additionally, we can discover and test pharmacological treatments for diseases using these *in vitro* models or engineer complex tissues and organs for regenerative medicine.

## Chapter 2

### Calcium signals drive apical-basal cell length during basal epithelial tissue folding

This chapter is a modified version of a paper published in the Journal, Molecular Biology of the Cell (Sahu et al., 2017), and has incorporated online supplemental materials from the published work throughout the chapter.

#### **2.1 Abstract**

One of the first morphogenetic events in the vertebrate brain is the formation of the highly conserved midbrain-hindbrain boundary (MHB). Specific cell shape changes occur at the point of deepest constriction of the MHB, the midbrain-hindbrain boundary constriction (MHBC), and are critical for proper MHB formation. These cell shape changes are controlled by non-muscle myosin II (NMII) motor proteins which are tightly regulated via the phosphorylation of their associated myosin regulatory light chains (MRLC). However, the upstream signaling pathways that initiate the regulation of NMII to mediate cell shape changes during MHB morphogenesis are not known. We show that intracellular calcium signals are critical for the regulation of cell shortening during initial MHB formation. We demonstrate that the MHB region is poised to respond to calcium transients that occur in the MHB at the onset of MHB morphogenesis and that calcium mediates phosphorylation of MRLC specifically in MHB tissue. Our results indicate that *calmodulin 1a* (*calm1a*), expressed specifically in the MHB, and myosin light chain kinase (MLCK), together mediate MHBC cell length. Our data suggest that

modulation of NMII activity by calcium is critical for proper regulation of cell length to determine embryonic brain shape during development.

## **2.2 Introduction**

MHB basal tissue folding requires changes in apical-basal cell length and anterior-posterior cell width and these changes in cell shape are mediated differentially by NMIIA and NMIIB, respectively (Gutzman et al., 2015). It is known that NMII activity can be regulated by several different kinase cascades via phosphorylation of myosin regulatory light chain (MRLC). One molecular pathway that could potentially mediate MHB basal tissue folding is calcium ( $\text{Ca}^{2+}$ ) signaling. Calcium signaling is known to play a critical role in mediating phosphorylation of MRLC via myosin light chain kinase (MLCK) (Berridge et al., 2000; Somlyo and Somlyo, 2003; Vicente-Manzanares et al., 2009) and is critical for many embryonic developmental processes such as gastrulation and neural tube closure (Slusarski and Pelegri, 2007; Webb and Miller, 2003). However, the specific role for  $\text{Ca}^{2+}$  signaling in neuroepithelial tissue morphogenesis is unknown. Therefore, we hypothesized that  $\text{Ca}^{2+}$  functions as a morphogenetic signal to mediate cell shape changes at the MHB to promote basal tissue folding. We demonstrate that intracellular  $\text{Ca}^{2+}$  signals specifically determine apical-basal cell length at the MHBC and that  $\text{Ca}^{2+}$  regulation of this cell shape is dependent upon NMII activity. We further demonstrate that regulation of cell shape restricted to just the MHBC requires *calmodulin 1a* (*calm1a*) and MLCK. Our data show for the first time that modulation of NMII function by  $\text{Ca}^{2+}$  is critical for regulation of MHBC cell length to mediate the morphogenetic process of basal epithelial tissue folding.

## **2.3 Materials and methods**

### 2.3.1 Zebrafish husbandry and maintenance

Zebrafish husbandry, maintenance procedures, and staging were followed as per (Kimmel et al., 1995) and (Westerfield, 2007). Wild-type (AB and EK) zebrafish embryos were used for all experiments. Somites were counted to establish specific and consistent staging and to eliminate concerns regarding potential developmental delay for all experiments. This study was approved by the University of Wisconsin-Milwaukee Institutional Animal Care and Use Committee.

### 2.3.2 Live imaging of calcium transients and analysis

For imaging of  $\text{Ca}^{2+}$  transients, wild-type single-cell embryos were injected with 100 ng GCaMP6s-eGFP mRNA encoding the  $\text{Ca}^{2+}$  indicator, a gift from Dr. Philipp Keller and Yinan Wan from the HHMI Janelia Research Campus, and 100 ng memcherry mRNA. Live time-lapse imaging was conducted beginning at 18 ss, 20 ss, or 24 ss using a Nikon CS2 scanning confocal microscope. Time-lapse data sets were acquired as single slices or 5  $\mu\text{m}$  z-stacks and taken approximately 15–20  $\mu\text{m}$  into the neural tube tissue from the dorsal surface at a frame rate of 10-30 seconds per image. Overall capture time was between 10-120 minutes, with the average total time being 35 minutes per embryo.  $\text{Ca}^{2+}$  transients observed were quantified spatially within the MHB region (~10  $\mu\text{m}$  on either side of the MHBC, ~20  $\mu\text{m}$  total) and the Outside MHB region (~30  $\mu\text{m}$  on either side of the MHB region, ~60  $\mu\text{m}$  total). Therefore, the MHB region accounted for 25% of the total area analyzed, and the Outside MHB region accounted

for 75% of the total area analyzed. To determine  $\text{Ca}^{2+}$  transient frequency, the number of  $\text{Ca}^{2+}$  transients observed during each time-lapse experiment were normalized to number of transients per hour at an acquisition rate of 1 image per 10 seconds. Each region was normalized to represent an equal area of the neural tube tissue for comparison. To examine change in cell shape following  $\text{Ca}^{2+}$  transients, apical-basal length of single cells was measured using the memcherry cell outline images. Single cells were measured during the  $\text{Ca}^{2+}$  transient and the same cell was measured again immediately following the transient. Only cells in the MHB region demonstrated decreases in cell length following  $\text{Ca}^{2+}$  transients. To examine change in  $\text{Ca}^{2+}$  transients after pharmacological manipulation, embryos were injected with GCaMP6s-eGFP mRNA and imaged using live confocal microscopy at 18 ss before drug treatment and after the indicated drug treatments. All confocal images were analyzed using the Nikon Imaging Systems (NIS) Elements software.

### 2.3.3 Pharmacological manipulations

Wild-type embryos were injected at the one-cell stage with 200 ng/ $\mu\text{L}$  membrane GFP (memGFP) mRNA (CAAX-eGFP). At 18 ss, embryos were dechorionated and treated for 10 min with 100  $\mu\text{M}$  2-aminoethoxydiphenyl borate (2-APB, D9754-1G, Sigma), an inositol triphosphate receptor ( $\text{IP}_3\text{R}$ ) antagonist that blocks  $\text{Ca}^{2+}$  release from the endoplasmic reticulum, to decrease intracellular  $\text{Ca}^{2+}$  levels (Ashworth et al., 2007; Bootman et al., 2002). Or they were treated for 15 min with 2  $\mu\text{M}$  Thapsigargin (Thaps, T9033-1MG, Sigma) a sarcoplasmic and endoplasmic reticulum  $\text{Ca}^{2+}$  ATPase (SERCA) inhibitor that depletes  $\text{Ca}^{2+}$  stores, to increase intracellular  $\text{Ca}^{2+}$  levels (Kreiling et al.,

2008; Zhang et al., 2011). After the treatment times, embryos were washed and allowed to mature to 24 ss in 1% agarose-lined petri dishes at 28°C and imaged using live confocal microscopy. Dimethyl sulfoxide (DMSO) control treatments were conducted using the same volume percentage as other treatment groups in each experiment. For Thapsigargin/Blebbistatin combined drug treatment rescue experiments, wild-type embryos were injected at the one-cell stage with memGFP mRNA. At 18 ss, embryos were separated into two treatment groups: DMSO or 2  $\mu$ M Thaps. After treatment, embryos were washed and incubated at 28°C until 20-21 ss. At 20-21 ss, embryos from each treatment group were separated into two additional treatment groups: DMSO or 50  $\mu$ M Blebbistatin (Bleb, B0560-1MG, Sigma). Finally, each group was incubated at 28°C until 24 ss and imaged using live confocal microscopy.

#### 2.3.4 Live confocal imaging and cell shape analysis

All memGFP live confocal imaging was conducted as previously described (Graeden and Sive, 2009; Gutzman et al., 2015) using a Nikon CS2 scanning confocal microscope. Live confocal images presented in each figure are single slices taken from a z-series of images approximately 15–20  $\mu$ m into the tissue from the dorsal surface. All confocal images were processed using Nikon Imaging Systems (NIS) Elements software and Photoshop (Adobe). Cell shape analysis was performed as described in (Gutzman et al., 2015). Briefly, cell length was determined using the NIS-Elements software measurement tool by measuring a single cell spanning the neuroepithelium from apical to basal in the region described, either directly at the MHBC, or 40  $\mu$ m posterior to the MHBC (outside the MHBC) on the hindbrain side. The cell width

measurement was obtained from the NIS-Elements software as an average width of a cell as previously described (Gutzman et al., 2015). The angle measurement was determined by measuring the angle at the MHBC at 24 ss approximately 20  $\mu\text{m}$  into the neuroepithelial tissue from the dorsal surface.

### 2.3.5 Calmodulin 1a rescue construct

The zebrafish *calmodulin 1a* rescue construct was generated using the following primers each containing an EcoRI restriction site, based on the zebrafish Ensembl GRCz10 transcript sequence ENSDART00000034580. *calm1a* forward (5'–CCGGAATTCCGGAGTTGCACGGTGGAGCTTTA–3'); *calm1a* reverse (5'–CCGGAATTCCGGTTCTTTGGGAACAGGACCAC–3'). RT-PCR was conducted using 24 ss wild-type RNA. The 783 bp product was subcloned into pCS2+ and mRNA was *in vitro* transcribed using the SP6 mMessage mMachine Kit (AM1340, Ambion).

### 2.3.6 Antisense morpholino oligonucleotide and mRNA injections

All knockdown experiments were performed using splice site-blocking morpholino antisense oligonucleotides. Morpholino (MO) details are as follows: *mypt1* MO (5'-ATTTTTTGTGACTTACTCAGCGATG-3') (Gutzman et al., 2008; Gutzman et al., 2015) and *calmodulin 1a* ([ENSDART00000034580](#)) *calm1a* MO (5'-CCACAAACAGACTGCCTTACCTGCA-3'). Zebrafish *p53* MO (5'-GCGCCATTGCTTTTGCAAGAATTG-3') was used in conjunction with the *calm1a* MO at equal concentration. Standard Control MO (5'-CCTCTTACCTCAGTTACAATTTATA-



3'). All MOs are from Gene Tools, LLC. Morpholinos were injected into one-cell stage embryos either alone or in conjunction with memGFP mRNA as indicated. MO concentrations: 5 ng *mypt1* MO, 2 ng *calm1a* MO and 2 ng *p53* MO. Control MO concentration was equal to the highest concentration of any MO used in that experiment. For MLCK mRNA expression experiments, 50 ng MLCK mRNA (zfMLCK fused to Globin 3'UTR, kindly provided by Dr. Erez Raz, University of Munster, Munster, Germany) was injected with 200 ng/μL memGFP mRNA separately or combined with *calm1a* MO or Control MO. All mRNA was *in vitro* transcribed for injections using the mMessage mMachine Transcription Kit (AM1340, Ambion). Embryos were incubated at 28°C to 24 ss and imaged using live confocal microscopy. For *calm1a* MO rescue experiments 50 ng of memGFP mRNA was co-injected with 100 ng of *calm1a* mRNA or control mRNA (additional memGFP mRNA was used as control) and 2 ng of control MO + 2 ng *p53* MO or 2 ng *calm1a* MO + 2 ng *p53* MO.

### 2.3.7 In situ hybridization

*In situ* hybridization was conducted according to standard procedures. EST/cDNA Clone: *calm1a*, cb617, from ZFIN was used to produce the *calmodulin 1a in situ* probe. Brightfield imaging was conducted using an Olympus SZX12 stereomicroscope with an Olympus DP72 camera.

### 2.3.8 Analysis of apoptosis

Embryos were treated with DMSO, 100  $\mu$ M 2-APB for 10 min at 18 ss, or 2  $\mu$ M Thaps for 15 min at 18 ss. Embryos were incubated to 24 ss and fixed overnight with 4% paraformaldehyde (PFA) at 4°C. TUNEL assays were performed using a Millipore ApopTag Fluorescein *In Situ* Apoptosis Detection Kit (S7110) according to the provided protocol using fluorescent detection of apoptotic cells. Embryos were counterstained with propidium iodide (red) to label nuclei and imaged using a Nikon CS2 laser-scanning confocal microscope. Images were analyzed with NIS-Elements and Photoshop (Adobe) software.

### 2.3.9 Immunohistochemistry

Embryos were treated with DMSO, 2-APB or Thaps at 18 ss and fixed at 24 ss in 4% PFA at 4°C overnight. Staining was performed following the GeneTex Inc. recommended protocol. Briefly, embryos were dehydrated, kept at -20°C freezer overnight in 100% methanol, and rehydrated using a methanol/PBST series. Embryos were deyolked, equilibrated, blocked in 10% NGS/2% BSA/PBT, and incubated in *cdh2* primary antibody (GTX125885, GeneTex, Inc.) at 1:200 overnight at 4°C. Embryos were washed and incubated in secondary antibody (goat anti-rabbit Alexa Fluor 488, Life Technologies) diluted to 1:500 with 2% NGS/2% BSA/PBT for 3 hours at room temperature, then re-fixed with 4% PFA for 20 minutes, washed, and imaged using a Nikon CS2 laser-scanning confocal microscope. Images were analyzed with NIS-Elements and Photoshop (Adobe) software.

### 2.3.10 MHB microdissection

MHB tissue was dissected from 18-24 ss embryos using fine-tip forceps (Dumont No. 5). Dissections were performed in 1% agarose-lined petri dishes in E3 media. One dissection was made between the eyes and the MHB and a second dissection between the MHB and the otic vesicle to separate the MHB tissue from the remaining embryo tissue and yolk (See Figure 6). MHB tissue was collected in 1X lysis buffer containing 5 mM Tris, 400  $\mu$ M EDTA, 2% Glycerol, and 0.2% Triton X, with cOmplete Protease Inhibitor (#04693124001, Sigma-Aldrich) for Western blot analysis. 10  $\mu$ g of protein was analyzed by Western or RNA was isolated for RT-PCR.

### 2.3.11 Reverse transcription – PCR (RT-PCR)

To determine efficiency of MHB microdissection, total RNA was extracted from forebrain, MHB, and tail dissected-tissue of 24 ss WT embryos using Ambion Life Technologies TRIzol Reagent. cDNA was prepared using 100-200 ng RNA and SuperScript III reverse transcriptase (56575, Invitrogen). Manufacturer protocol was followed. PCR was performed for *six3b*, *engrailed 2b*, *starmaker*, and *Ef1 $\alpha$*  using the following primers: *six3b*: forward primer, 5' –GAAAAGGGAACTGGCACAAG -3', *six3b* reverse primer, 5'-GTTGAACACAAGCTGGCAAA-3'. *engrailed 2b*: forward primer, 5'-AAAGAGAGAACCGCTGTCCA-3', *engrailed 2b* reverse primer, 5'-GTTCTCGGACGCTTGTCTTC-3'. *starmaker*: forward primer, 5' –GCAATCACGCTGGAAAAGAT-3', *starmaker* reverse primer, 5'-CGAATCGTGGTCTTTGGATT-3'. *Ef1 $\alpha$* : forward primer, 5'-GATGCACCACGAGTCTCTGA-3', *Ef1 $\alpha$*  reverse primer, 5'-TGATGACCTGAGCGTTGAAG-3'. To confirm *calm1a* MO, total RNA was collected

using Ambion Life Technologies TRIzol Reagent at 24 ss, from whole embryos injected with either control MO or *calm1a* MO. cDNA was prepared as described above. The following primer pairs were used for RT-PCR reactions: *calm1a* forward (5'-AGTTGCACGGTGGAGCTTTA-3'), *calm1a* reverse (5'-CCCGTCCTTGTCAAACACTC-3'). *Ef1 $\alpha$*  was used as a control, primer sequences for *Ef1 $\alpha$*  above.

### 2.3.12 Western blot analysis with MHB specific tissue

Embryos were dechorionated and treated as described above with either DMSO or Thaps at 18 ss or embryos were injected with *calm1a* MO or control MO. MHB tissue was dissected from 18-24 ss for protein isolation and analysis (see Figure 6). Primary antibodies: pMLC2 (pMRLC) (#3671, Cell Signaling Technology) at 1:500 (Gutzman and Sive, 2010), anti-calmodulin (ab208911, Abcam) at 1:1000, and  $\alpha$ -tubulin (#T6199, Sigma Aldrich) at 1:1000. Secondary antibodies: anti-mouse HRP (Cell Signaling Technology, #7076S) and anti-rabbit HRP (#7074S, Cell Signaling Technology) at 1:2000. Blots were imaged on a UVP Biospectrum Imaging System.

### 2.3.13 Statistical analyses

Statistical analysis between two groups was carried out using the Mann-Whitney U-test, *P*-values denoting significance are reported within each figure legend. Statistical analysis for comparisons between more than two treatment groups was carried out by one-way ANOVA. For ANOVA *P*-values < 0.05, Tukey's Honest Significant Difference (HSD) post-hoc tests were performed to determine significance between control

treatment and experimental treatment groups. *P*-values for post-hoc comparisons are presented in each figure legend. All ANOVA and Tukey's HSD post-hoc analyses were carried out using R-3.1.2. At least three independent experiments were conducted for all data presented, *n* indicates total number of embryos analyzed, and numbers of single cells analyzed are indicated where necessary.

## **2.4 Results**

### **2.4.1 $Ca^{2+}$ mediates apical-basal cell length at the MHBC during basal tissue folding.**

In zebrafish,  $Ca^{2+}$  signals precede morphological patterning in the brain (Webb and Miller, 2007) and apical-basal cell thinning in the enveloping layer cells is dependent upon  $Ca^{2+}$  transients (Zhang et al., 2011).  $Ca^{2+}$  flashes have also been shown to drive apical constriction during neural tube closure (Christodoulou and Skourides, 2015). Therefore, we investigated intracellular  $Ca^{2+}$  flashes in the MHB during morphogenesis. We used 4D time-lapse imaging of GCaMP6s-eGFP mRNA injected embryos to determine if there were  $Ca^{2+}$  flashes in MHB cells at the time of initial MHB formation. We found single-cell  $Ca^{2+}$  transients to be enriched in the MHB region compared to surrounding regions at 18 ss, during the initiation of MHB morphogenesis (Figure 8 and Movie 1). We also found that apical-basal cell length decreased immediately following a  $Ca^{2+}$  transient specifically in the MHB region (Figure 9). Therefore, we hypothesized that  $Ca^{2+}$  signals may initiate MHB morphogenesis and that cells in this region are poised to respond to  $Ca^{2+}$  transients.

To further investigate the role of  $\text{Ca}^{2+}$  signals in regulating zebrafish MHB morphogenesis, we utilized pharmacological inhibitors to manipulate intracellular  $\text{Ca}^{2+}$  levels. 2-aminoethoxydiphenyl-borate (2-APB) was used to decrease intracellular  $\text{Ca}^{2+}$  levels (Ashworth et al., 2007; Bootman et al., 2002). Thapsigargin (Thaps) was used to increase intracellular  $\text{Ca}^{2+}$  levels (Kreiling et al., 2008; Zhang et al., 2011). Wild-type embryos were treated at 18 ss with DMSO, 2-APB, or Thaps. At 24 ss, after the initial morphogenetic events have occurred, cell shapes were analyzed (Figure 10, A-C'). We found that embryos with decreased intracellular  $\text{Ca}^{2+}$  (2-APB treated) had significantly longer cells at the MHBC while embryos with increased intracellular  $\text{Ca}^{2+}$  (Thaps treated) had significantly shorter cells at the MHBC (Figure 10D). However, cells 40  $\mu\text{m}$  posterior to the MHBC were not significantly different from controls after either treatment (Figure 10E), indicating a region-specific effect on cell shape with  $\text{Ca}^{2+}$  manipulation.

Efficacy of 2-APB and Thaps were determined using the genetically encoded calcium indicator GCaMP6s-eGFP (Figure 11, A-D). Embryos injected with GCaMP6s-eGFP mRNA demonstrated uniform expression throughout the brain, with low levels of background  $\text{Ca}^{2+}$  signal. Pharmacological manipulation of  $\text{Ca}^{2+}$  levels sometimes resulted in mosaic changes of the GCaMP6s-eGFP  $\text{Ca}^{2+}$  signal (Figure 11D), likely due to the dramatic changes in  $\text{Ca}^{2+}$  levels within the cells. Quantification of fluorescence intensity at the MHB before and after drug treatments revealed that 2-APB decreased intracellular  $\text{Ca}^{2+}$  levels by  $58\% \pm 7\%$  (mean  $\pm$  SEM,  $n=16$  embryos) and Thaps increased intracellular  $\text{Ca}^{2+}$  levels 5-fold  $\pm 1$  (mean  $\pm$  SEM,  $n=10$  embryos). Apoptosis and N-cadherin (cdh2) cell adhesion protein localization within the neuroepithelium, which are known to depend on intracellular  $\text{Ca}^{2+}$  homeostasis (Lagunowich et al., 1994;

Orrenius et al., 1992), were tested using immunohistochemistry, but were not affected by these treatments at the doses utilized (Figure 11, E-K).

Quantification of  $\text{Ca}^{2+}$  effects on tissue shape showed that the MHBC angle was abnormal, as expected with changes in MHBC cell length, while MHB cell width was only slightly affected with Thaps treatment (Figure 12). Together, these data demonstrate a novel role for  $\text{Ca}^{2+}$  signaling in regulating specifically apical-basal cell length at the deepest point of the hinge point during basal epithelial tissue folding of the MHB.

#### 2.4.2 Calcium signals to non-muscle myosin II to mediate cell shape at the MHB.

Based on our previous work demonstrating that NMII proteins are critical mediators of cell shape at the MHB (Gutzman et al., 2015) and the known role for  $\text{Ca}^{2+}$  in regulation of NMII activity (Somlyo and Somlyo, 2003), we hypothesized that  $\text{Ca}^{2+}$  may mediate its effects on MHB cell shape via downstream activation of NMII. In order to test this hypothesis we first determined whether or not increasing  $\text{Ca}^{2+}$  in the MHB would modulate phosphorylation of MRLC (pMRLC), an indicator of NMII activity (Vicente-Manzanares et al., 2009). We treated wild-type embryos with DMSO or Thaps and micro-dissected MHB tissue for Western analysis of pMRLC. MHB dissections were confirmed to be specific using RT-PCR with tissue specific markers (Figure 13). Western blot analysis of MHB protein showed that pMRLC levels increased approximately 2-fold following Thaps treatment (Figure 14, A-B), suggesting that increased intracellular  $\text{Ca}^{2+}$  leads to increased NMII activity. We were unable to detect a

change in pMRLC with 2-APB treatment. This is consistent with the observed difference in the magnitude of effects on  $Ca^{2+}$  between 2-APB and Thaps. Specifically, 2-APB decreases  $Ca^{2+}$  by half while Thaps increases  $Ca^{2+}$  by 5-fold (Figure 11, A-D).

Next, we tested our hypothesis that  $Ca^{2+}$  mediates cell shape via NMII protein function using two complimentary rescue experiments that coupled modulation of intracellular  $Ca^{2+}$  levels with manipulation of NMII function. 2-APB or Thaps treatments were used to manipulate  $Ca^{2+}$  levels as described in Figure 10. NMII activity was manipulated using the pharmacological reagent Blebbistatin (Bleb) or with *mypt1* gene knockdown to inhibit or activate NMII respectively. Bleb is a well-established myosin II inhibitor (Kovacs et al., 2004) and *mypt1* encodes for the regulatory subunit of myosin phosphatase and is required to inactivate pMRLC. Therefore, *mypt1* knockdown leads to an increase in pMRLC resulting in NMII over-activation (Gutzman and Sive, 2010; Ito et al., 2004).

In our first rescue experiments we increased  $Ca^{2+}$  levels and rescued the cell length phenotype with inhibition of NMII. We hypothesized that we could rescue Thaps-induced short cells by inhibiting NMII with Bleb (Figure 14C). As predicted, we found that Thaps decreased cell length and Bleb increased cell length at the MHBC, and treatment of embryos with Thaps followed by Bleb rescued the abnormal cell length phenotypes specifically at the MHBC (Figure 14, D-I). These data suggest that the  $Ca^{2+}$  signal affects cell length via modulation of NMII function. Quantification of tissue shape showed that the MHBC angle was abnormal as expected with changes in MHBC cell length, but was also partially rescued with Thaps and Bleb treatment together. Bleb had a slight effect on MHB cell width which is expected since Bleb inhibits both NMIIA and



NMIIB and we know that NMIIB is essential in mediating cell width (Figure 15 and (Gutzman et al., 2015)). Cell length outside of the MHBC was not significantly different from controls for any treatment (Figure 14I), suggesting that MHBC cells are poised to respond to slight changes in intracellular  $\text{Ca}^{2+}$  levels.

In a complementary set of experiments, we over-activated NMII and rescued the cell length phenotype by decreasing  $\text{Ca}^{2+}$  levels. We hypothesized that decreasing  $\text{Ca}^{2+}$  with 2-APB would specifically rescue short cells induced by NMII over-activation (Figure 16A). *mypt1* morphants demonstrated cells that were both shorter and wider than controls, as we have previously reported (Figure 16B and (Gutzman et al., 2015; Gutzman and Sive, 2010)). As predicted, cell length in *mypt1* morphants treated with 2-APB was rescued compared to *mypt1* morphant controls (Figure 16, B-D). No other significant differences were observed (Figure 16E and Figure 17). We did not observe a rescue of the MHB tissue angle in these experiments, which is expected since we know cell width also contributes to normal MHB tissue angle (Figure 17). Taken together, these data shows *in vivo* that MHBC cell length is regulated by  $\text{Ca}^{2+}$  and NMII activity.

#### 2.4.3 Calmodulin and MLCK regulate MHBC cell shape during basal tissue folding

Since  $\text{Ca}^{2+}$  is a ubiquitous molecule and additional manipulations of  $\text{Ca}^{2+}$  levels are not region-specific, the question remains as to how  $\text{Ca}^{2+}$  transients might lead to modulation of cell shape specifically at the MHBC.  $\text{Ca}^{2+}$  interacts with calcium-binding proteins to initiate downstream signaling cascades (Berridge et al., 2000). Therefore, one possible mechanism for a region-specific  $\text{Ca}^{2+}$  response to transient activity would

be through tissue specific expression of a calcium-binding protein required to mediate cell shape changes. We hypothesized that the calcium-binding partner, Calmodulin, a highly conserved multifunctional  $\text{Ca}^{2+}$  sensor and signal transducer (Crivici and Ikura, 1995; Tidow and Nissen, 2013), may play a role in allowing MHBC cells to respond specifically to  $\text{Ca}^{2+}$ .

Mammalian vertebrates express three *calmodulin* genes, while zebrafish have 6 *calmodulin* genes due to genome duplication, that all encode for the same Calmodulin protein (Friedberg and Taliaferro, 2005). In zebrafish, *calmodulin 3b* is ubiquitously expressed in the brain during development, while other *calmodulin* genes have region specific expression (Thisse et al., 2004; Thisse, 2001) and the protein exhibits cell-type specific subcellular localization (Barreda and Avila, 2011; Caceres et al., 1983). Of particular interest is *calmodulin 1a* (*calm1a*) which was shown to have potential MHB specific expression during development (Thisse, 2001). Differential expression patterns of *calmodulin* has been observed in the eye and nervous system in other vertebrates (Friedberg and Rhoads, 2001; Kobayashi et al., 2015; Thut et al., 2001); however, comparative expression patterns during neural tube formation and brain morphogenesis at the time points examined here have not been reported. We used *in situ* hybridization to confirm the MHB localized expression of *calm1a* during brain morphogenesis. We found that *calm1a* is expressed specifically at the MHB before and during the initiation of MHB morphogenesis, with other specific expression detectable in the trigeminal ganglia and otic vesicles (Figure 18). Therefore, we hypothesized that the spatial localization of *calm1a* expression may provide an MHBC region-specific response to the  $\text{Ca}^{2+}$  transients. In order to test this we knocked down *calm1a* using morpholino

antisense oligonucleotides. We chose a knockdown method rather than a mutant approach because we hypothesize that the multiple *calmodulin* genes, all encoding the same protein, would lead to gene compensation masking any specific role for *calm1a* in MHB tissue (Rossi et al., 2015). The *calm1a* MO effectiveness and specificity was confirmed using RT-PCR, MHB tissue specific Western analysis, and *calm1a* mRNA rescue (Figure 19). The morpholino resulted in a deletion of exon 2 and an early stop codon as well as an approximate 50% reduction in Calmodulin protein within the MHB region (Figure 19, A-C). We found that *calm1a* knockdown resulted in longer MHBC cells but had no effect on cell length outside of the MHBC (Figure 20). The MHBC cell length defect was rescued by *calm1a* mRNA expression (Figure 19, D-H). The *calm1a* knockdown also had a dramatic effect on MHBC angle as expected with the cell length phenotype but had no effect on MHB cell width (Figure 21). These results indicate a requirement for *calm1a* in mediating cell length at the MHBC.

One known downstream target of Calmodulin is activation of MLCK (Holzapfel et al., 1983) and activated MLCK is known to phosphorylate MRLC (Somlyo and Somlyo, 2003). Therefore, we investigated the role for MLCK in regulation of cell shape at the MHBC. We overexpressed MLCK and found that cells at the MHBC, and outside the MHBC were slightly shorter than control cells, indicating overexpression of MLCK increased cell shortening throughout the region (Figure 20, C-D' and E-F). MLCK expression had no effect on overall MHB angle because all cells had a cell length defect (Figure 21). From these results we hypothesized that *calm1a* and MLCK may function in the same pathway to mediate MHBC cell length. In order to test this, we co-injected embryos with *calm1a* MO and MLCK mRNA, which rescued the MHBC cell length

phenotype (Figure 20, C-F), further suggesting that Calmodulin works in conjunction with MLCK to regulate cell shape specifically at the MHBC. In addition, we hypothesized that *calm1a* knockdown would influence activation of NMII. Therefore, we analyzed phosphorylated MRLC levels in MHB tissue micro-dissected from control and *calm1a* MO injected embryos by Western blot analysis, as in Figure 10. Western blot analysis of MHB protein demonstrated that pMRLC levels decreased approximately 50% with *calm1a* knockdown (Figure 22A-B), further indicating a requirement for *calm1a* at the MHB for NMII activity. Together our results suggest a model where specific expression of Calmodulin at the MHB poises the cells within this region to respond to the  $\text{Ca}^{2+}$  signal (Figure 22C). This in turn would lead to the specific activation of MLCK at the MHBC and mediate apical-basal cell shortening via regulating NMII function (Figure 22C).

**MOVIE 1. Calcium transients at the MHB.** A representative wild-type embryo injected with 100 ng/ $\mu$ l pCS2+GCaMP6s-eGFP mRNA encoding the  $Ca^{2+}$  indicator. This construct was kindly provided by Dr. Philipp Keller and Yinan Wan from the HHMI Janelia Research Campus. Live imaging demonstrates  $Ca^{2+}$  transients during early MHB formation from 18-20 ss, ~1 h. 4D data was collected using a Nikon CS2 laser-scanning confocal microscope. Each frame represents a 5 micron z-stack, images were collected approximately 20 microns into the neural tube from the dorsal surface. One z-stack of images was taken every 10 seconds.  $Ca^{2+}$  transients are found in neuroepithelial cells that span the neural tube in the MHB region (cells numbered 1-6) and specifically in cells at the MHBC (cells 2,3,5). Cells are numbered based on the order in which transients appear in the movie. Some cells flash more than once during this time interval and cell 6 is only partially visible on the basal side due to the size of the z-stack used for 4D data collection. Transients are also visible in post-mitotic cells at the midline (example indicated with an asterisk \*). Arrowhead indicates MHBC. Representative embryo shown. Total number of embryos imaged using 4D imaging at 18 ss (n=11). Movie Link (Sahu et al., 2017):

[https://www.molbiolcell.org/doi/video\\_original/10.1091/mbc.e16-08-0561/mc-e16-08-0561-s02.mov](https://www.molbiolcell.org/doi/video_original/10.1091/mbc.e16-08-0561/mc-e16-08-0561-s02.mov)

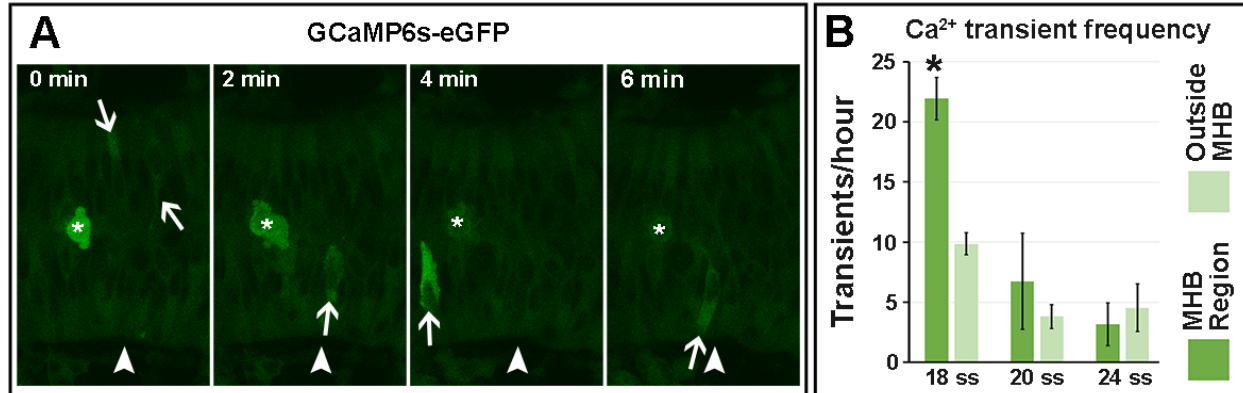


**Figure 8. Calcium transients are enriched in the MHB at 18 ss.** (A) Representative wild-type 18 ss time-lapse images of intracellular Ca<sup>2+</sup> transients (panels from Movie 1). Asterisks indicate mitotic cells and arrows indicate examples of Ca<sup>2+</sup> transients analyzed (B) Quantification of Ca<sup>2+</sup> transients at 18, 20, and 24 ss. Statistical analysis: one-way ANOVA with Tukey's HSD post-hoc test was conducted for Ca<sup>2+</sup> transient frequency. \*P<0.05, mean ± SEM. Embryos analyzed: 18 ss (n=11), 20 ss (n=10), 24 ss (n=8). Arrowheads indicate the MHBC.

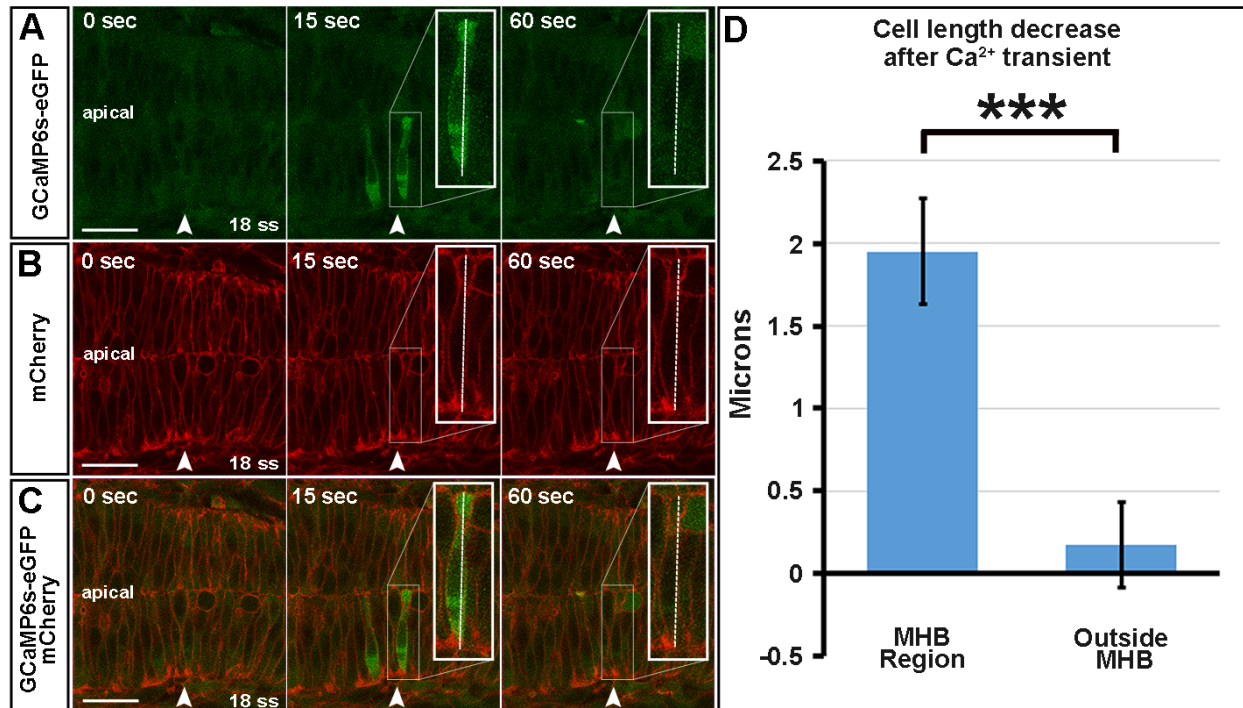


**Figure 9. Calcium transients promote decreases in cell length at the MHBC.** (A-C) Representative wild-type images at 18 ss analyzed for cell length changes following Ca<sup>2+</sup> transients. (A) Representative GCaMP6s-eGFP image at 0, 15, and 60 seconds. (B) Representative memcherry image at 0, 15, and 60 seconds. (C) Representative overlay of A and B. (D) Quantification indicating the amount of decrease in cell length immediately following Ca<sup>2+</sup> transients. Mann-Whitney U Test was performed for analysis of cell length decrease after Ca<sup>2+</sup> transients. \*\*\*P<0.001, mean ± SEM. Embryos analyzed (n=10), (MHB region cells=17), (Outside MHB cells=6). Arrowheads indicate the MHBC. Scale bars: 25 μm.

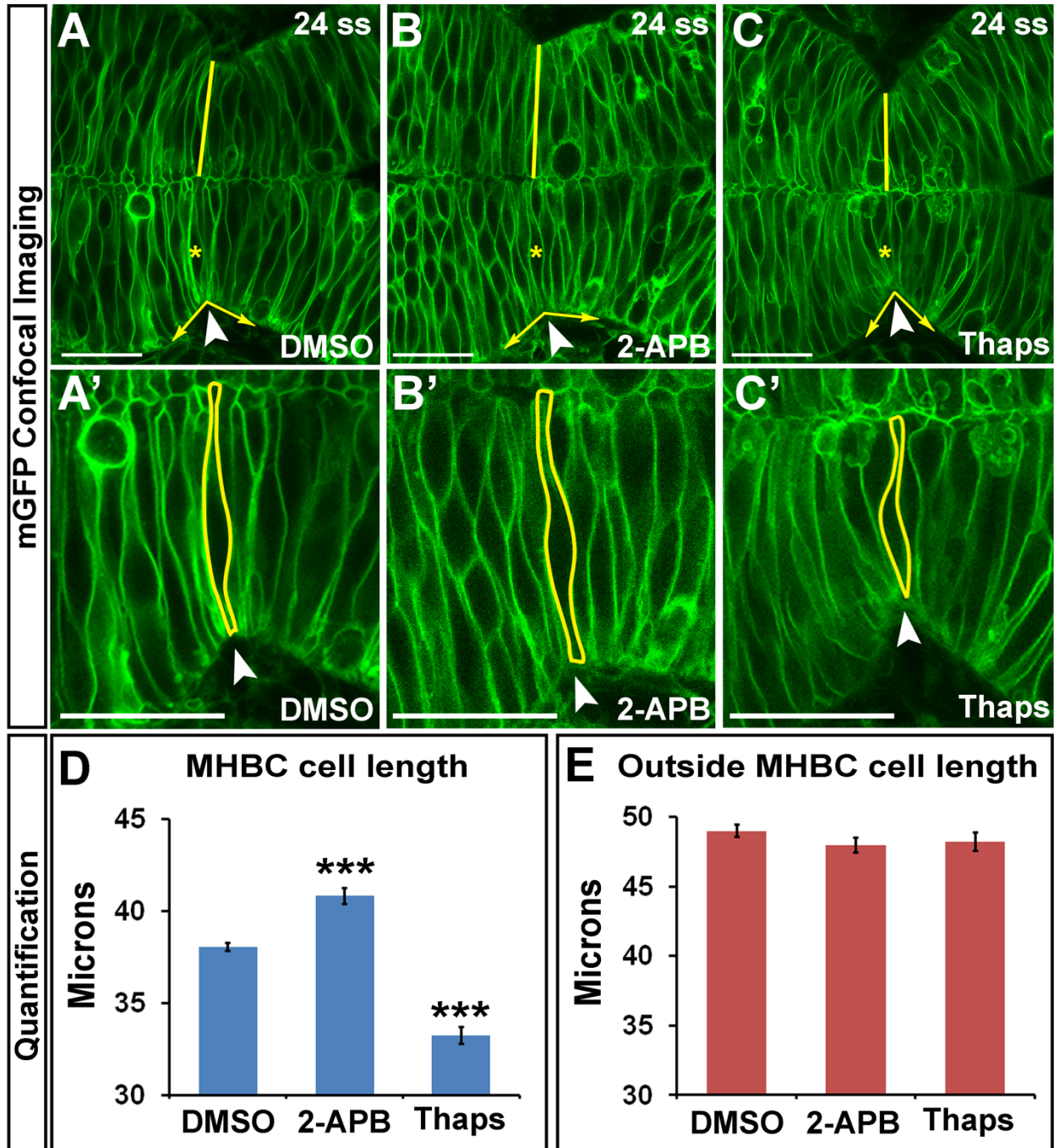


**Figure 10. Calcium regulates cell length at the MHBC.** (A-C') Confocal images of 24 ss embryos injected with memGFP mRNA and treated at 18 ss with (A,A') DMSO, (B,B') 100  $\mu$ M 2-APB, or (C,C') 2  $\mu$ M Thaps. (A'-C') Magnification of A-C. Arrowheads indicate the MHBC. Asterisks in A-C indicate cell outlined in A'-C'. (D-E) Cell length



quantification: at the MHBC (D) and 40  $\mu\text{m}$  outside the MHBC (E). Statistical analysis: one-way ANOVA with Tukey's HSD post-hoc test. \*\*\* $P < 0.001$  compared to DMSO, mean  $\pm$  SEM. For each measurement: DMSO (n=29, cells=58), 2-APB (n=16, cells=32), Thaps (n=14, cells=28). Scale bars: 25  $\mu\text{m}$ .

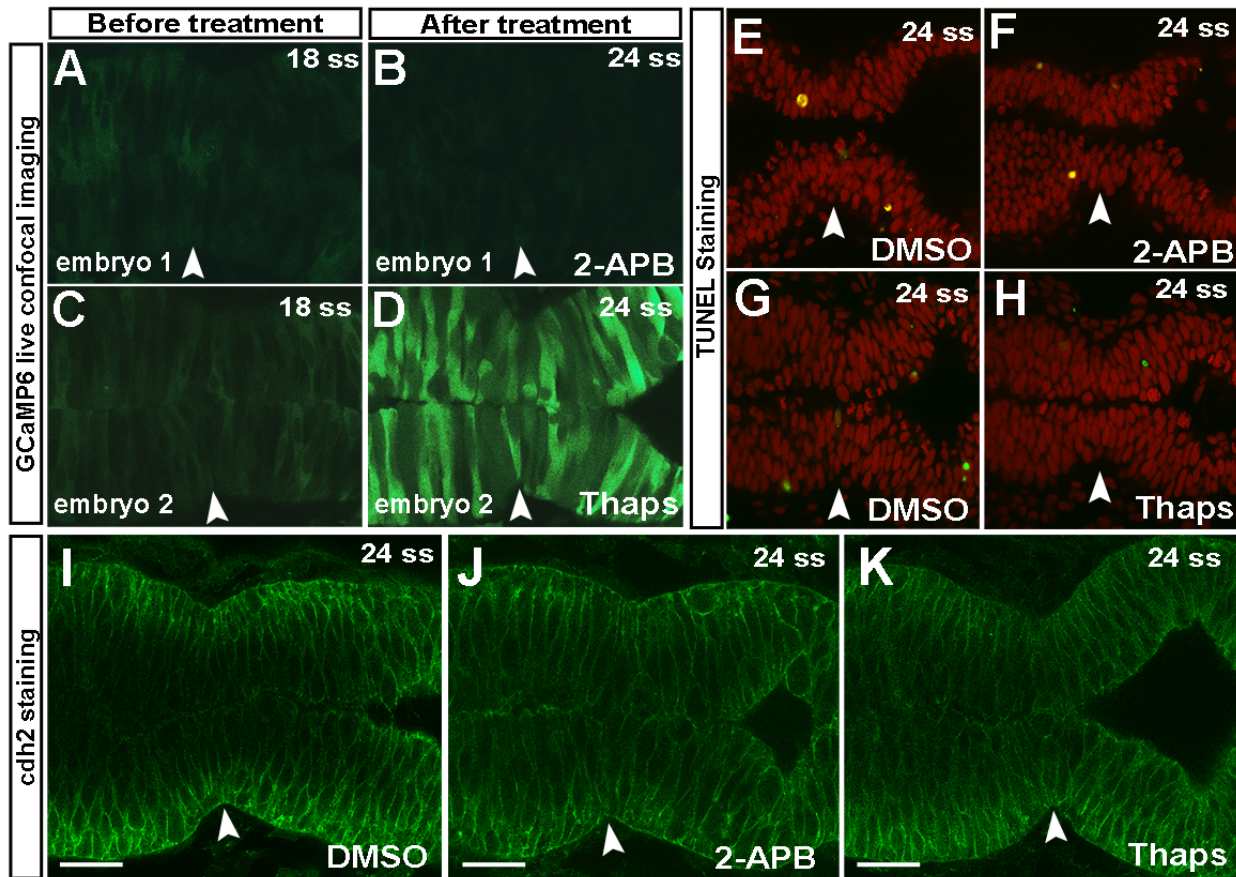


**Figure 11. Pharmacological manipulations change intracellular  $\text{Ca}^{2+}$  levels and do not increase apoptosis or affect N-cadherin localization in the MHB.** (A-D) Live confocal imaging of intracellular  $\text{Ca}^{2+}$  levels following drug treatments using the  $\text{Ca}^{2+}$  indicator GCaMP6s-GFP at 18 ss before drug treatment (A, C) and after the indicated drug treatments (B,D). Pharmacological manipulation of  $\text{Ca}^{2+}$  levels sometimes resulted in mosaic changes of the GCaMP6s-eGFP  $\text{Ca}^{2+}$  signal as seen in panel D, likely due to

the dramatic changes in  $\text{Ca}^{2+}$  levels within the cells. Quantification of fluorescence intensity at the MHB before and after drug treatments revealed that 2-APB decreased intracellular  $\text{Ca}^{2+}$  levels by  $58\% \pm 7\%$  (mean  $\pm$  SEM,  $n=16$  embryos) and Thaps increased intracellular  $\text{Ca}^{2+}$  levels 5-fold  $\pm 1$  (mean  $\pm$  SEM,  $n=10$  embryos). (E-H) Representative confocal images of DMSO controls (E,G), 2-APB treated (F), and Thaps treated (H) embryos TUNEL labeled (green) to indicate apoptotic cells. (E-F) DMSO ( $n=8$ ), 2-APB ( $n=12$ ); (G-H) DMSO ( $n=15$ ), Thaps ( $n=20$ ). (I-K) Analysis of cell adhesion using N-cadherin (*cdh2*) immunostaining at 18 ss of embryos treated with either DMSO (I), 2-APB (J) or Thaps (K). DMSO ( $n=7$ ), 2-APB ( $n=11$ ), Thaps ( $n=8$ ). Scale bars: 25  $\mu\text{m}$ .

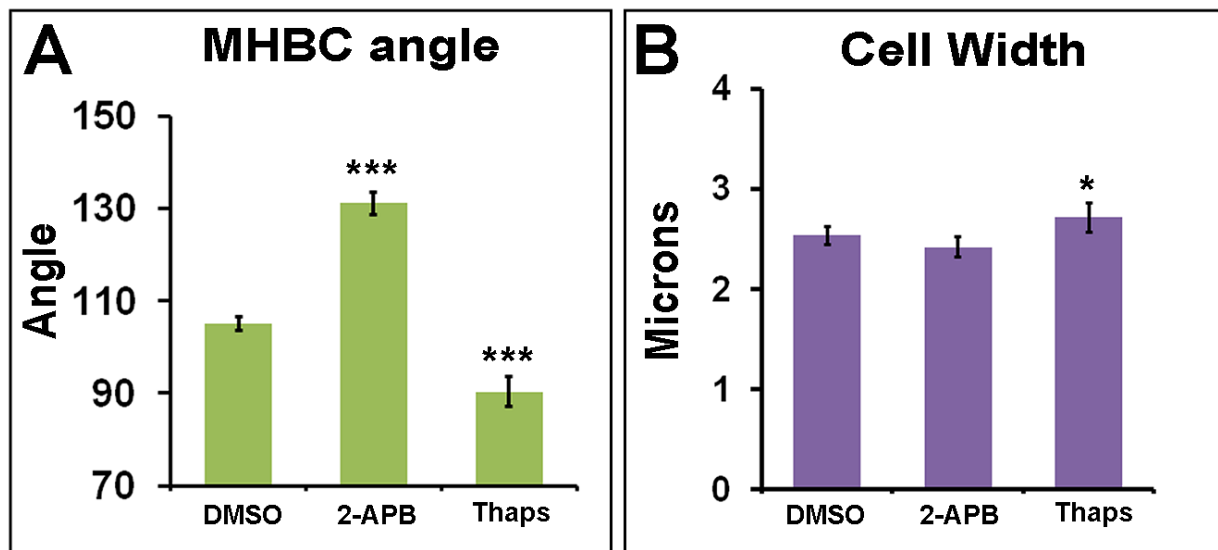


**Figure 12. Calcium regulates MHB basal tissue folding.** (A-B) Quantification of MHB angle and cell width at the MHB for DMSO, 2-APB and Thaps treated embryos (See Figure 4). MHB angle measurements: DMSO ( $n=29$ ), 2-APB ( $n=16$ ), Thaps ( $n=14$ ). Cell width measurements: DMSO ( $n=28$ , cells=92), 2-APB ( $n=14$ , cells=77), Thaps ( $n=15$ ,

cells=86). One-way ANOVA followed by Tukey's HSD was performed to determine significance. Comparisons shown as significant are compared to DMSO treatments.

\*\*\*P<0.001, \*\*P<0.01, \*P≤0.05, (mean ± SEM).

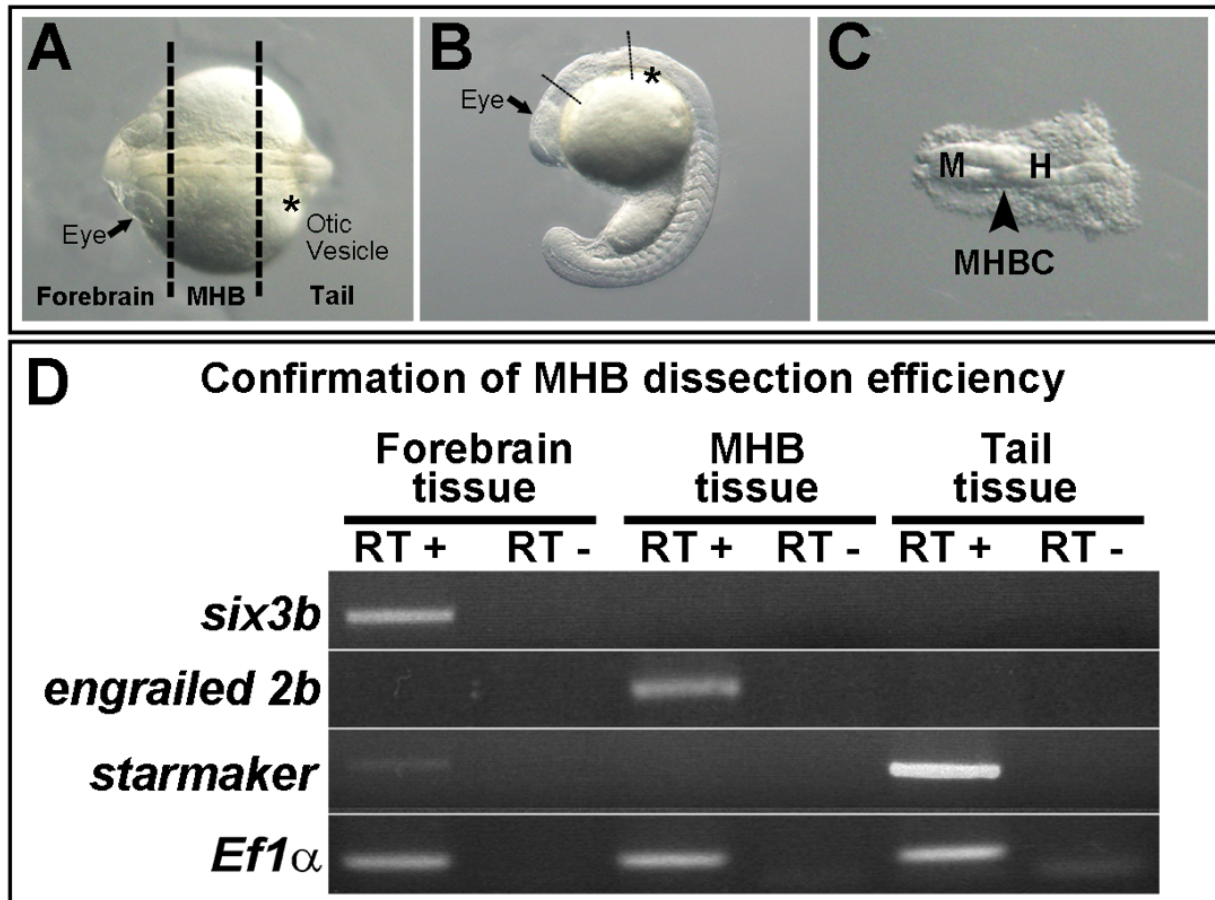


**Figure 13. Confirmation of MHB tissue dissection.** (A-B) Representative brightfield images of a 21 ss embryo, dorsal (A), lateral (B), indicating dissection points for extracting MHB tissue using fine-tip forceps (Dumont No. 5). One dissection was made between the eyes and the MHB and a second dissection between the MHB and the otic vesicle to separate the MHB tissue from the remaining embryo tissue and yolk, shown with dotted lines (A-B). Brightfield image of isolated MHB tissue (C). (D) Reverse Transcriptase - PCR showing forebrain marker: *six3b*, MHB marker: *engrailed 2b*, and

otic vesicle marker: starmaker, and loading control Ef1 $\alpha$  in Forebrain, MHB, and tail tissue, confirming specificity of tissue micro-dissection. M, midbrain, H, hindbrain.

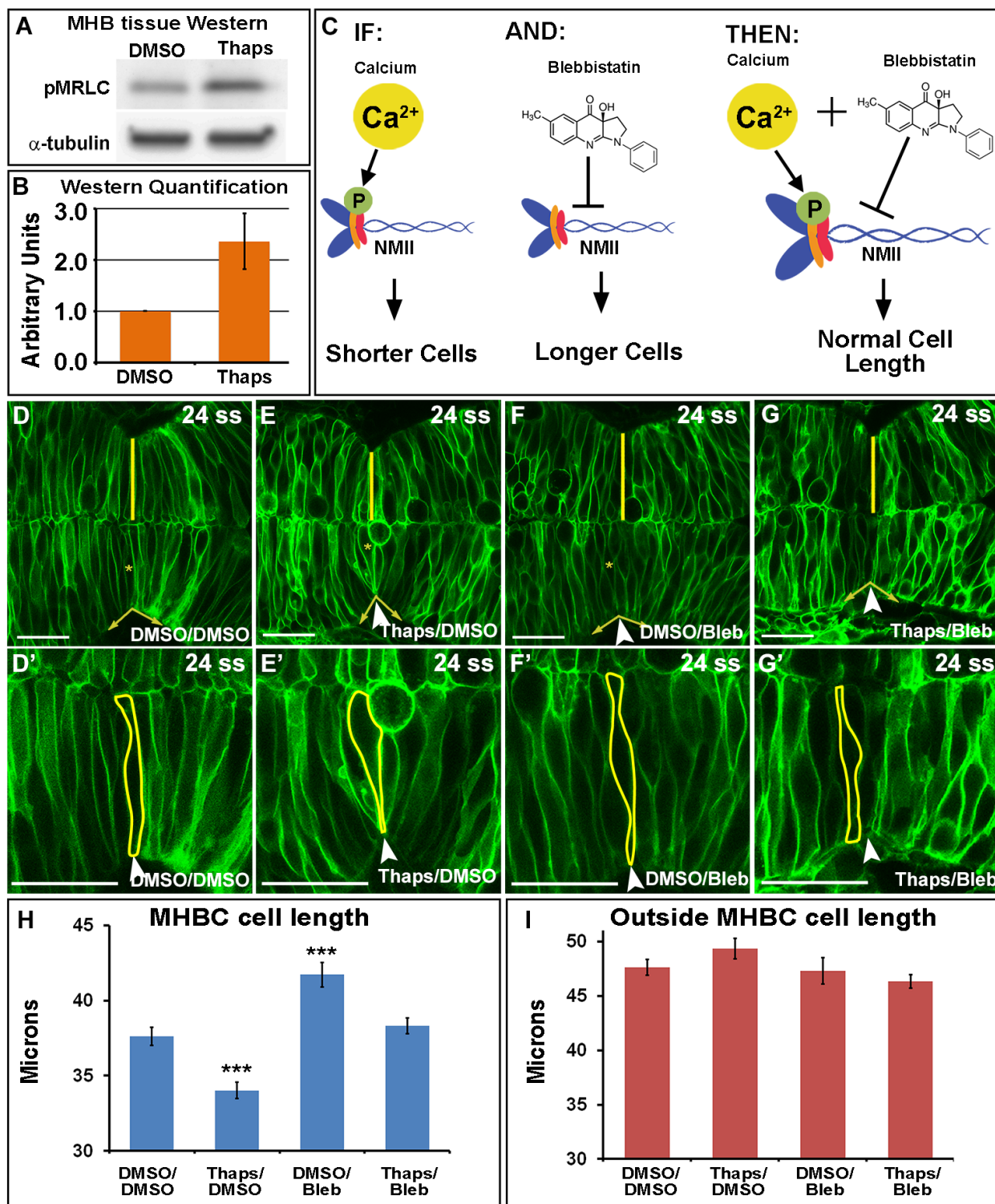


**Figure 14. Calcium signals to NMII at the MHB to modulate MHBC cell length. (A)**

Representative Western blot for pMRLC in MHB specific tissue dissected after DMSO

or 2  $\mu\text{M}$  Thaps treatment. (B) pMRLC Western quantification using  $\alpha$ -tubulin as a control (n=4). (C) Hypothesized role of  $\text{Ca}^{2+}$  and NMII interactions. IF: Increase in  $\text{Ca}^{2+}$  leads to increased pMRLC to activate NMII and causes shorter cells at the MHBC, AND: Blebbistatin inhibits NMII function, THEN: Thaps treatment to increase  $\text{Ca}^{2+}$  leading to shorter cells can be rescued with NMII inhibition by Bleb. (D-G') Confocal images of memGFP injected embryos treated with (D,D') DMSO/DMSO, (E,E') Thaps/DMSO, (F,F') DMSO/Bleb, (G,G') Thaps/Bleb. (D'-G') Magnification of D-G. Arrowheads indicate the MHBC. Asterisks in D-G indicate cell outlined in D'-G'. (H-I) Cell length quantification: at the MHBC (H) and 40  $\mu\text{m}$  outside the MHBC (I). Statistical analysis: one-way ANOVA with Tukey's HSD post-hoc test. \*\*\*P<0.001 compared to DMSO/DMSO, mean  $\pm$  SEM. For each measurement: DMSO/DMSO (n=9, cells=18), Thaps/DMSO (n=9, cells=18), DMSO/Bleb (n=7, cells=14), Thaps/Bleb (n=8, cells=16). Scale bars: 25  $\mu\text{m}$ .

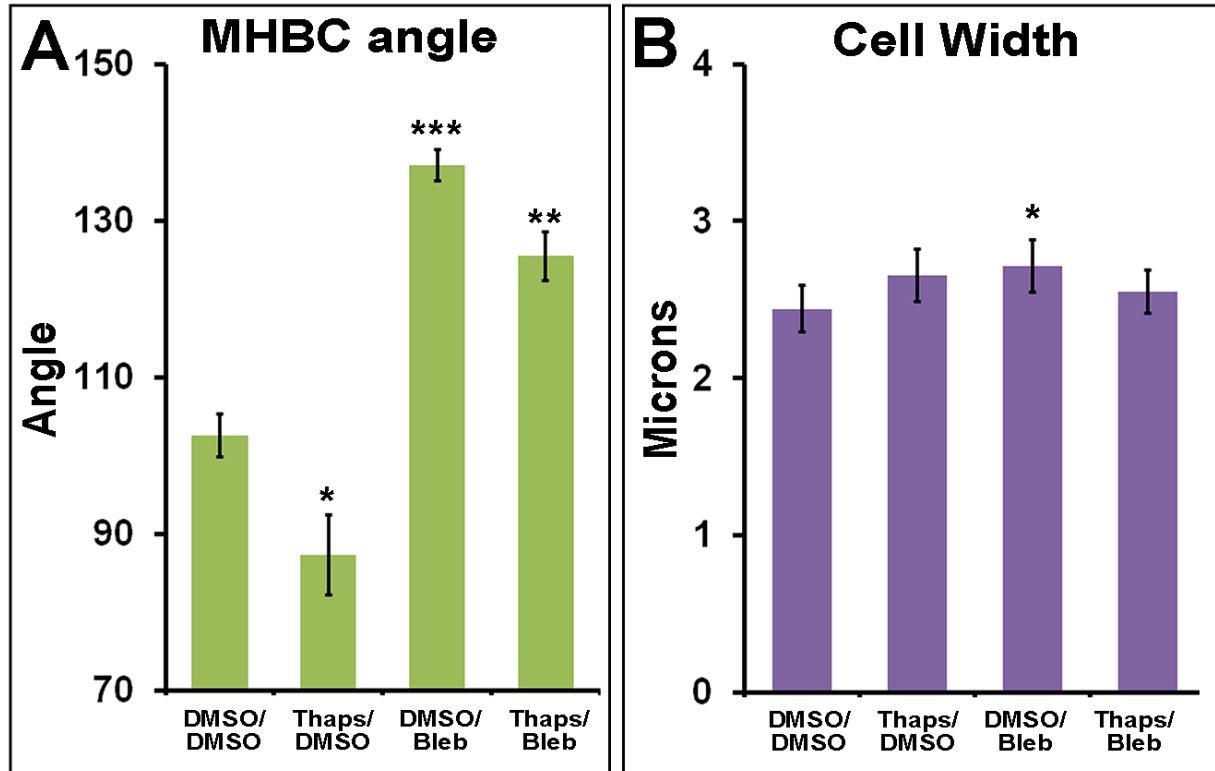


**Figure 15. Calcium regulates MHB basal tissue folding, but not cell width, through NMII.** (A-B) Quantification of MHB angle and cell width at the MHB for DMSO/DMSO, Thaps/DMSO, DMSO/Bleb, and Thaps/Bleb treated embryos. MHB angle measurements: DMSO/DMSO (n=9), Thaps/DMSO (n=9), DMSO/Bleb (n=7), Thaps/Bleb (n=8). Cell width measurements: DMSO/DMSO (n=7, cells=42), Thaps/DMSO (n=11, cells=55), DMSO/Bleb (n=6, cells=31), Thaps/Bleb (n=7, cells=41). One-way ANOVA followed by Tukey's HSD was performed to determine significance. Comparisons shown as significant are compared to DMSO treatments or control treatments. \*\*\*P<0.001, \*\*P<0.01, \*P<0.05, (mean ± SEM).



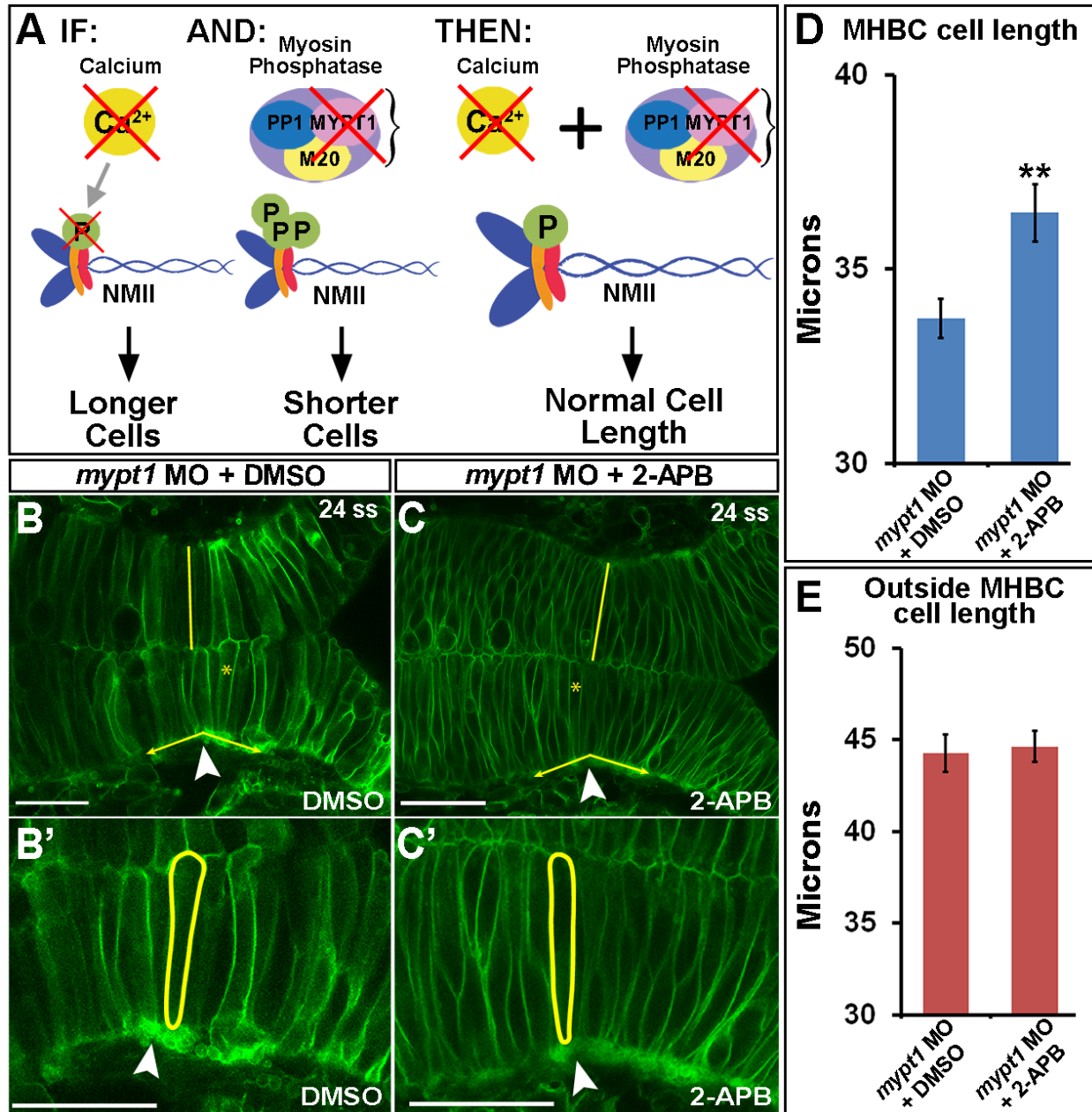


**Figure 16. Calcium inhibition rescues NMI over-activation at the MHBC. (A)**

Hypothesized role of  $Ca^{2+}$  and NMI interactions. IF: inhibition of  $Ca^{2+}$  by 2-APB results in longer MHBC cells, AND: *mypt1* knockdown results in overactivation of MRLC causing shorter and wider MHB cells, THEN: inhibition of  $Ca^{2+}$  in *mypt1* knockdown embryos would rescue MHBC cell length. (B-C) Confocal images of 24 ss embryos co-injected with memGFP and *mypt1* MO and treated with (B) DMSO or (C) 2-APB. (B'-C')



Magnified images from B-C. Arrowheads indicate MHBC. (D-E) Cell length quantification: at the MHBC (D) and 40  $\mu\text{m}$  outside the MHBC (E). Statistical analysis: Mann-Whitney U-test.  $**P < 0.01$ , mean  $\pm$  SEM. For each measurement: *mypt1* MO+DMSO (n=11, cells=22), *mypt1* MO+2-APB (n=13, cells=26). Scale bars: 25  $\mu\text{m}$ .

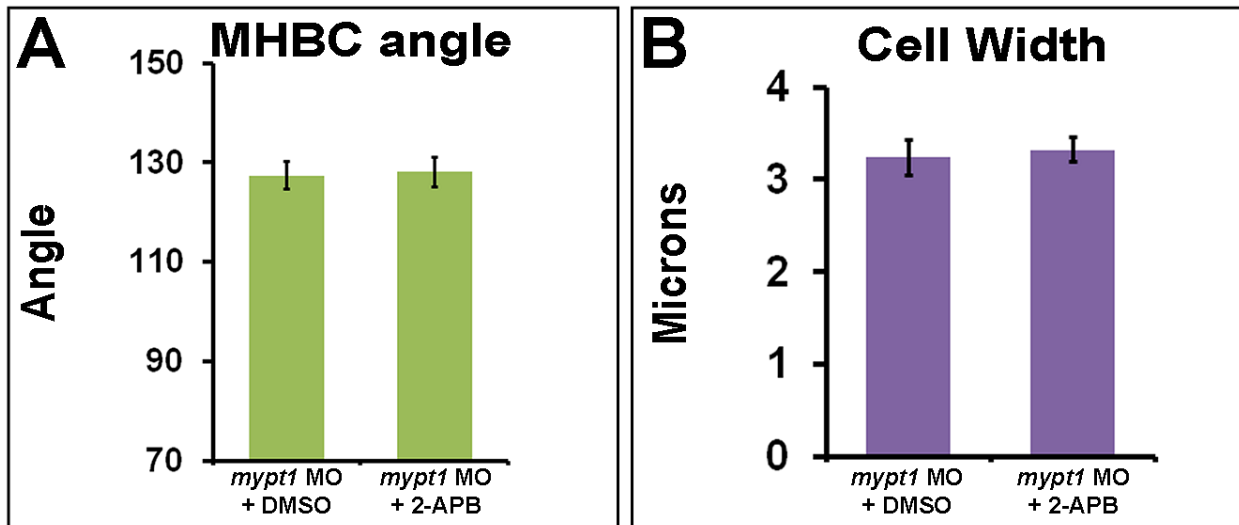


**Figure 17. Calcium does not affect NMII-mediated cell width during MHB basal tissue folding.** (A-B) Quantification of MHB angle and cell width at the MHB for *mypt1* MO + DMSO and *mypt1* MO + 2-APB treated embryos (See Figure 9). MHB angle measurements: *mypt1* MO + DMSO (n=11), *mypt1* MO + 2-APB (n=13). Cell width measurements: *mypt1* MO + DMSO (n=9, cells=42), *mypt1* MO + 2-APB (n=10, cells=29). Mann-Whitney U-test was performed to determine significance between two groups, DMSO and 2-APB treatment groups.  $***P < 0.001$ ,  $**P < 0.01$ ,  $*P \leq 0.05$ , (mean  $\pm$  SEM).

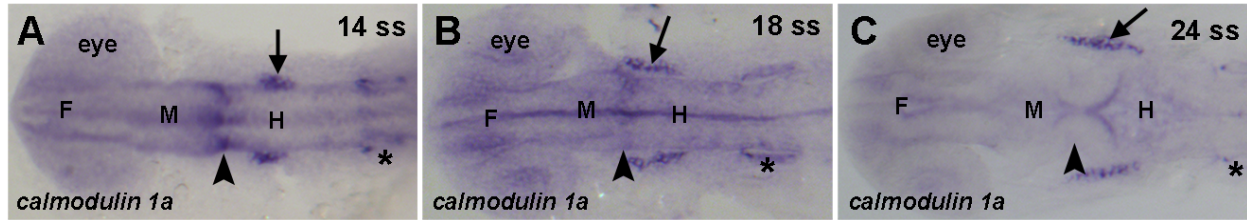


**Figure 18. Calmodulin 1a is expressed at the MHBC before and at the onset of MHB morphogenesis.** (A-C) *calm1a* gene expression by in situ hybridization at 14 ss (A), 18 ss (B), and 24 ss (C). Arrowheads indicate MHBC, arrows indicate trigeminal ganglia, asterisks indicate otic vesicle. F, forebrain; M, midbrain; H, hindbrain.

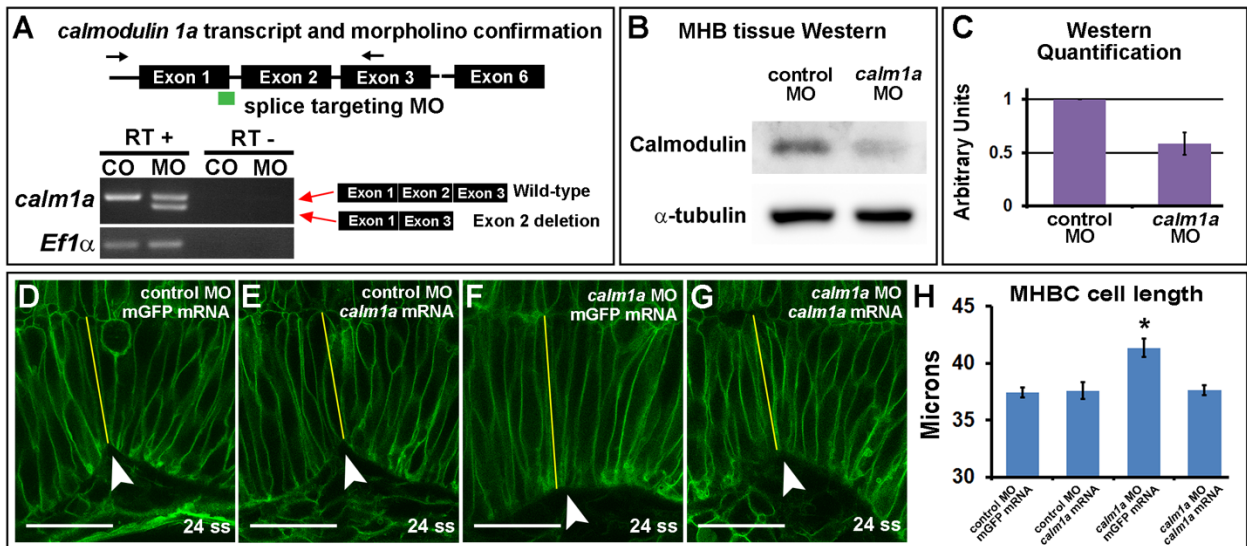


**Figure 19. Confirmation of calmodulin1a morpholino-mediated knockdown.** (A) Diagram depicts location of primers, morpholino target, and abnormal splicing product with MO injection on *calm1a* RNA transcript. Representative reverse transcriptase – PCR showing truncated *calmodulin1a* RNA transcript and *Ef1α* as a control with morpholino-mediated *calm1a* knockdown. (B-C) Representative Western blot (B) and quantification (C) for Calmodulin in MHB specific tissue. (D-G) Representative live confocal images in control MO (D,E) or *calm1a* MO (F,G) injected embryos co-injected

with either memGFP mRNA alone (D,F) or with *calm1a* mRNA (E,G). (H) Quantification of MHBC cell length. Statistical analysis: one-way ANOVA with Tukey's HSD post-hoc test. \* $P < 0.001$  compared to all experimental groups, mean  $\pm$  SEM. Control MO + control mRNA (n=14, cells=28), control MO+*calm1a* mRNA (n=11, cells=22), *calm1a* MO + control mRNA (n=17, cells=32), *calm1a* MO + *calm1a* mRNA (n=17, cells=34). Scale bars: 25  $\mu$ m.

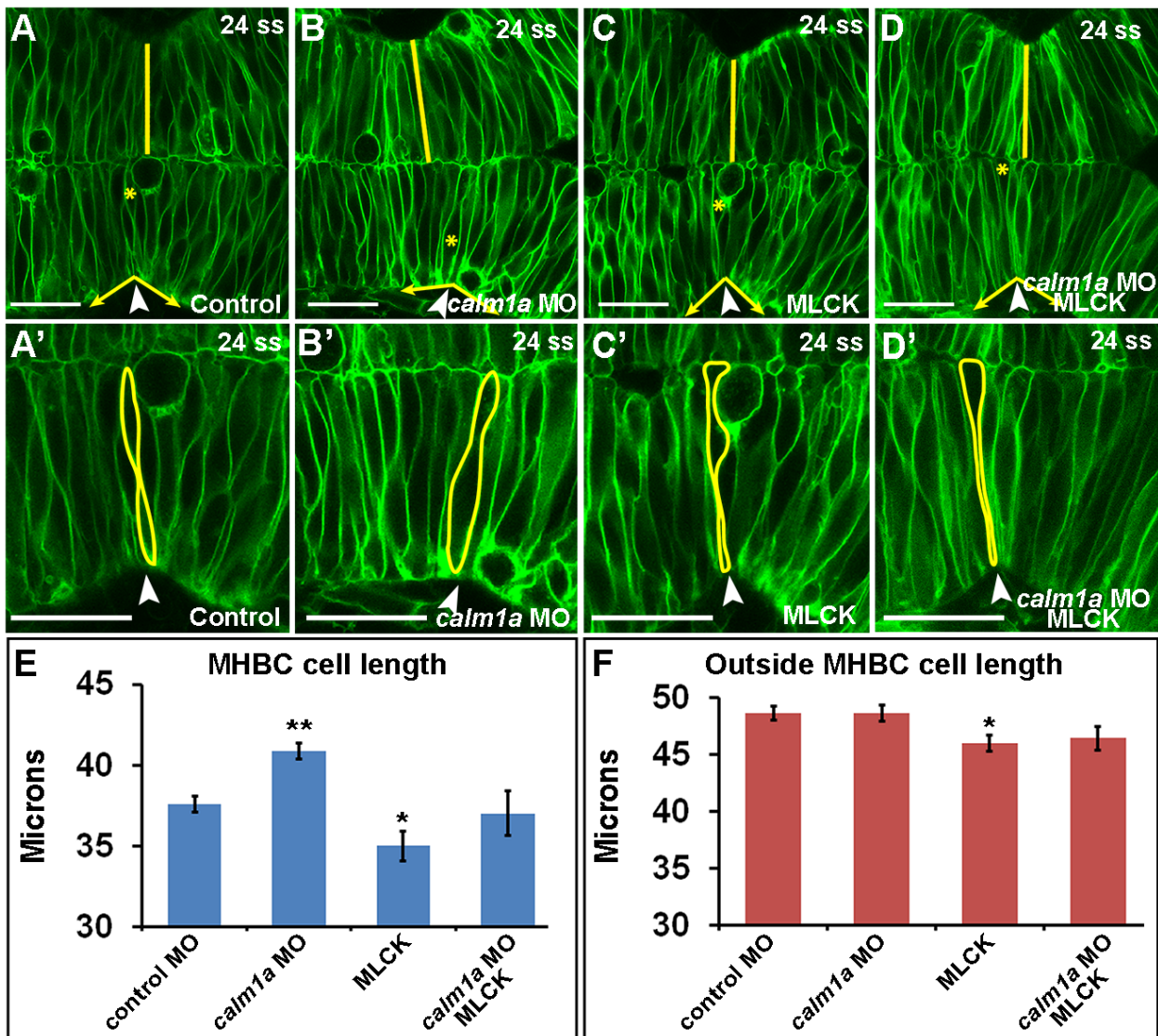


**Figure 20. Calmodulin 1a and MLCK mediate cell length at the MHBC. (A-D')**

Confocal images of embryos injected with memGFP mRNA and (A,A') Control MO, (B,B') *calm1a* MO, (C,C') MLCK mRNA, or (D,D') *calm1a* MO and MLCK mRNA. (A'-D') Magnification of A-D. Arrowheads indicate the MHBC. Asterisks in A-D indicate cell outlined in A'-D'. (E-F) Cell length quantification: at the MHBC and 40  $\mu\text{m}$  outside the MHBC. Statistical analysis: one-way ANOVA with Tukey's HSD post-hoc test. \*\* $P < 0.01$ , \* $P < 0.05$  compared to Control, mean  $\pm$  SEM. Control MO (n=17, cells=34), *calm1a* MO (n=19, cells=38), MLCK mRNA (n=13, cells=26), *calm1a* MO+MLCK (n=9, cells=18). Scale bars: 25  $\mu\text{m}$ .

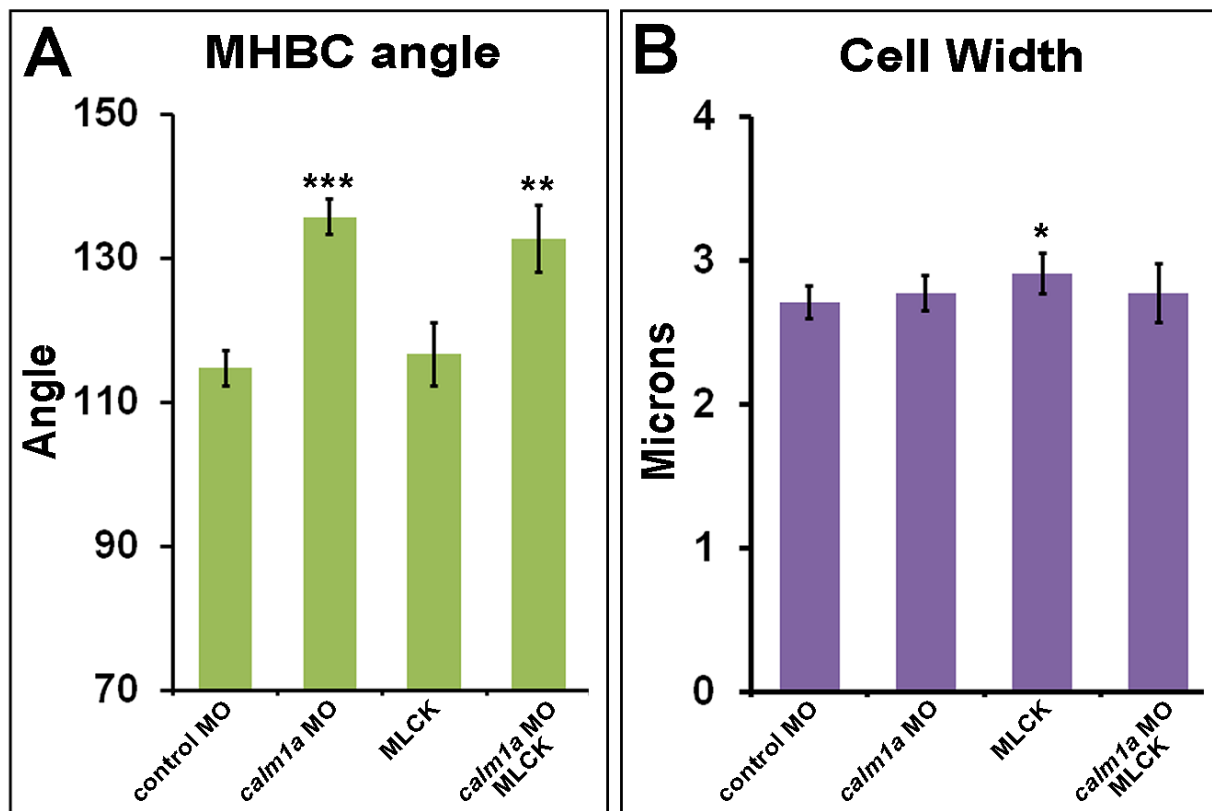


**Figure 21. Quantification of MHBC angle and MHB cell width. (A-B)** Quantification of MHB angle and cell width at the MHB for experimental data presented in Figure 13.

MHB angle measurements: Control MO (n=17), *calm1a* MO (n=19), MLCK mRNA (n=13), *calm1a* MO+MLCK mRNA (n=9). Cell width measurements: Control MO (n=18, cells=108), *calm1a* MO (n=14, cells=82), MLCK mRNA (n=12, cells=72), *calm1a* MO+MLCK mRNA (n=8, cells=48). One-way ANOVA followed by Tukey's HSD was performed to determine significance. Comparisons shown as significant are compared to DMSO treatments or control treatments.

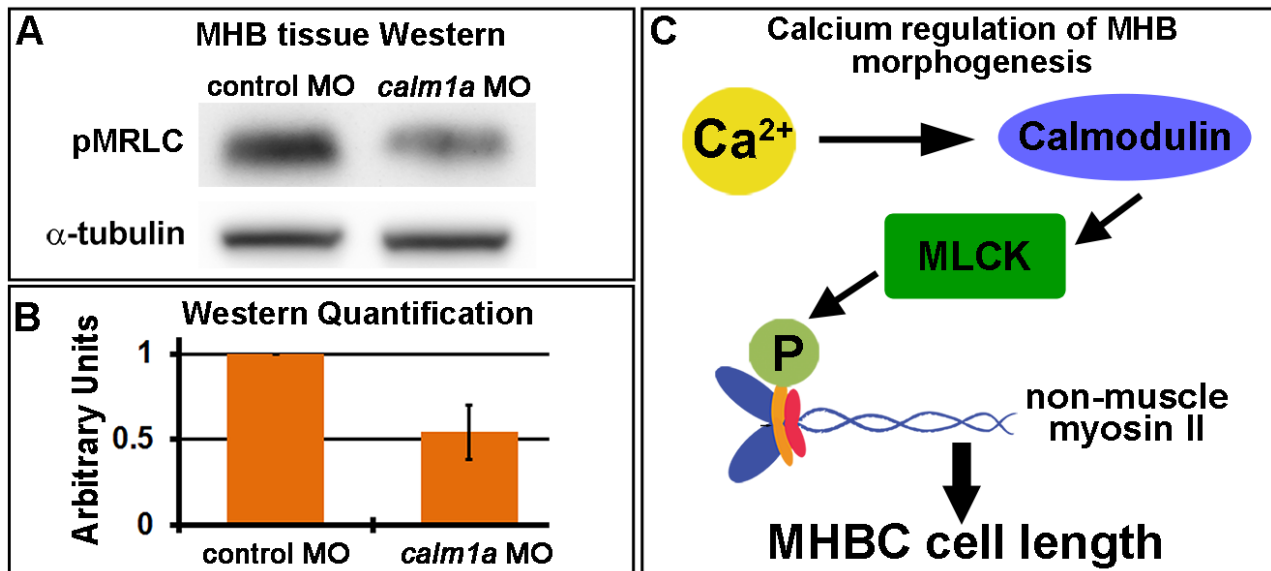


**Figure 22. *Calmodulin 1a* mediates pMRLC levels at the MHB during basal tissue folding.** (A) Representative Western blot for pMRLC in MHB specific tissue dissected after control MO or *calm1a* MO injection. (B) pMRLC Western quantification using  $\alpha$ -tubulin as a control (n=5). (C) Proposed signaling pathway for  $Ca^{2+}$  regulation of cell length at the MHBC.

## 2.5 Discussion

$\text{Ca}^{2+}$  has been previously reported to regulate cell shape in different tissue contexts. Our study shows for the first time, *in vivo*, that intracellular  $\text{Ca}^{2+}$  is an upstream regulator of cell shape during basal epithelial tissue folding. During MHB morphogenesis,  $\text{Ca}^{2+}$  signaling specifically regulates apical-basal cell length at the fold hinge point. Consistent with our previous work showing the role of NMII in MHBC cell shape (Gutzman et al., 2015), we have demonstrated that calcium mediates cell length but not cell width via NMII activation. We determined that NMII activation is carried out by regulation of MLCK via Calmodulin (Figure 20). NMII overactivation using *mypt1* knockdown results in both longer and wider MHBC cells (Gutzman et al., 2015). Reducing intracellular  $\text{Ca}^{2+}$  rescued the MHBC cell length, but not cell width, phenotype in *mypt1* morphants (Figure 16). Interestingly, we know that of the two NMII isoforms responsible for mediating MHBC cell shape, NMIIA differentially regulates apical-basal cell length but not anterior-posterior cell width (Gutzman et al., 2015), consistent with the observed role for  $\text{Ca}^{2+}$ . These results lead us to speculate that  $\text{Ca}^{2+}$  may signal through intermediate molecules, including MLCK, specifically to NMIIA to differentially mediate cell length at the MHBC. However, additional experiments are needed to test and confirm this hypothesis.

We observed that  $\text{Ca}^{2+}$  transients are not restricted to the cells at the MHBC, but are found to occur throughout the neuroepithelium. Similarly, during neural tube closure in *Xenopus*, the spatial occurrence of cell-autonomous and asynchronous calcium transients was unrestricted (Christodoulou and Skourides, 2015). Tracking of cell shape after  $\text{Ca}^{2+}$  transients revealed contraction of the cell membrane and increases in apical

actin accumulation in neuroepithelial cells (Christodoulou and Skourides, 2015). However, tracking apical-basal cell length before and after a  $\text{Ca}^{2+}$  transient event at the MHBC versus outside of the MHBC in our model revealed that only cells at the MHBC decreased in cell length after the  $\text{Ca}^{2+}$  transient. We saw that cell shape changes occur at the hinge point of the fold, but not outside of that region; therefore, we asked the question of how do we get this spatially restricted cell shape change? We did observe an enrichment of calcium transient events at the MHBC, suggesting that perhaps there may be threshold of transient frequency to affect cell shape. We additionally hypothesized that the specific expression of *calm1a* in this region is what allows the MHBC neuroepithelial cells to respond to the  $\text{Ca}^{2+}$  transients at the MHBC. Although the  $\text{Ca}^{2+}$  signal may be more ubiquitous, the cellular context within that restricted region is poised to respond with morphological changes.

During a  $\text{Ca}^{2+}$  transient event, the intracellular  $\text{Ca}^{2+}$  level is high throughout the cell cytoplasm. However, the cell shape change that depends on calcium is only observed in one dimension, apical-basal cell length. In the context of MHB basal tissue folding,  $\text{Ca}^{2+}$  may be providing an activation cue for NMII activity but may not directly relay information on the subcellular localization of the shape changes. We show that MLCK overexpression decreases apical-basal cell length and increases anterior-posterior cell width (Figure 21). With over expression of MLCK, we hypothesized increased phosphorylation of MRLC and increased cell contractility. Increased contractility was observed in the cell length direction with MLCK overexpression, but we see a potential loss of contractility when observing cell width (Figure 21). One potential hypothesis for loss of cell width contractility is that cell volume remains unchanged in

these cells, and cell length when decreased significantly results in increase of a different cell dimension to accommodate the same cytoplasmic volume. If this is true, these data would further support a hypothesis in which MLCK differentially regulates NMIIA activity. One other possibility is that cell adhesion may be perturbed, as we know MLCK function is critical for tight junctions and adherens junctions in gut epithelia (Du et al., 2016). However, when we investigated localization of N-cadherin (*cdh2*) using immunohistochemistry, there was no difference at the MHBC when calcium levels were manipulated (Figure 11).

During MHB morphogenesis, MLCK may differentially localize to the cell cortices to mediate cell contractility. As an example, apical constriction during neural tube formation in chick is mediated at the cell cortices by recruitment and alignment of actin and myosin regulating proteins, RhoGEF and ROCK (Nishimura et al., 2012). MHBC cells contract in the apical-basal direction; therefore, we hypothesize that active MLCK localizes along the lateral edges of the cell from apical to basal.

This work reveals a novel, but singular aspect of the multifaceted epithelial cell shape responsible for basal epithelial tissue folding, which we term as apical-basal cell length. However, we are left to question what other mediators are responsible for controlling the epithelial cell shapes required to promote MHB tissue folding including width and depth. This will be discussed in the next chapter.

## **2.6 Contributions**

This chapter includes and expands upon the earlier work performed and partially published in the Master's thesis of Srishti U. Sahu (Sahu, 2015). Figures 17 and 18 from



Sahu, 2015 Master's thesis demonstrate how reduction in intracellular  $\text{Ca}^{2+}$  by means of 2-APB drug treatment perturbs specifically MHBC cell length and MHB tissue angle. These data have also been incorporated into this dissertation as new figures (Figures 10 and 12). Figures 20 and 21 from Sahu, 2015 Master's thesis demonstrate that NMII mediated MHBC cell length is calcium-dependent. This was done by rescuing the MHBC cell length defect of *mypt1* morpholino knockdown with 2-APB drug treatment. These data have also been included in this dissertation as new figures (Figures 16 and 17). The contributions for this overall work are provided as follows: Srishti U. Sahu performed experiments and assisted in conceptualizing ideas. Mike R. Visetsouk performed experiments, conceptualized ideas, and completed all statistical analysis. Ryan J. Garde, Leah Hennes, and Constance Kwas performed experiments. Jennifer H. Gutzman conceptualized ideas, performed experiments, and drafted the manuscript. All contributed to drafting and revision of the manuscript. This work was funded in part by the UWM Research Growth Initiative.

## Chapter 3

### **Differential regulation of microtubules drive basal anisotropic cell shape during basal epithelial tissue folding**

This chapter is a modified version of a paper published in the Journal, Development (Visetsouk et al., 2018), and has incorporated online supplemental materials from the published manuscript throughout the chapter.

#### **3.1 Abstract**

The folding of epithelial tissues is critical for development of three-dimensional structure and function. Understanding this process can assist in determining etiology of developmental disease and engineering of tissues for the future of regenerative medicine. Folding of epithelial tissues towards the apical surface has long been studied, while the molecular mechanisms that mediate epithelial folding towards the basal surface are just emerging. Here we utilize the zebrafish neuroepithelium to identify mechanisms that mediate basal tissue folding to form the highly conserved embryonic midbrain-hindbrain boundary. Live imaging revealed *Wnt5b* as a mediator of anisotropic epithelial cell shape, both apically and basally. In addition, we uncovered a *Wnt5b* mediated mechanism for specific regulation of basal anisotropic cell shape that is microtubule-dependent and likely to involve JNK signaling. We propose a model by which a single morphogen can differentially regulate apical versus basal cell shape during tissue morphogenesis.

### **3.2 Introduction**

Basal epithelial tissue folding is important for the development of structures like the midbrain and the hindbrain. Using the zebrafish midbrain-hindbrain boundary (MHB) as a model, we have begun to elucidate the cell shapes and molecular mechanisms that are critical for generating the MHB basal fold. Our work has identified several cell shape changes at the MHB hinge point that mediate the tissue fold. Cells specifically at the MHBC were found to contract in the apical-basal direction (Gutzman et al., 2015). MHBC cells contract in the anterior-posterior direction, throughout the MHB region (Gutzman et al., 2015). Later, cells are found to constrict basally and expand apically (Gutzman et al., 2008). However, cell shape in the third dimension along the dorsal-ventral direction has not been previously characterized.

We have recently demonstrated that calcium signaling modulates apical-basal cell length of MHBC cells during basal epithelial tissue folding (Sahu et al., 2017). Next, we asked what other potential upstream signaling cues are required to regulate other cell shape changes during MHB basal tissue folding? We hypothesized that signals of interest would be specifically expressed in the region where cell shape changes occur. Screening of the ZFIN gene expression database revealed *wnt5b* to be specifically enriched at the MHB, and was later confirmed by *in situ* hybridization to turn on at the onset of morphogenesis and persist throughout MHB development (Gutzman et al., 2018). *Wnt5b* is a secreted signaling molecule with known roles throughout development as a morphogen and was found to be important for basal constriction in the anterior-posterior direction during late MHB development (Gutzman et al., 2018). Wnt signaling during the gastrulation event of convergent extension mediate actomyosin

activity via downstream signaling factors, RhoGEF and ROCK, as well as localization of planar cell polarity factors such as vangl2 via microtubules (Lin et al., 2010; Lopez-Escobar et al., 2018; Nishimura et al., 2012; Ossipova et al., 2015b; Sepich et al., 2011).

Here, we demonstrate that Wnt5b also plays an earlier role in the regulation of cell shape at the MHBC, prior to the prim-6 stage. Specifically, we identified that cells at the MHBC have apical and basal anisotropic cell shape, while basally during MHB development anisotropic cell shape is enhanced. We determined that Wnt5b is important for this anisotropic cell shape. We discovered that Wnt5b differentially and specifically mediates basal anisotropic cell shape through the regulation of microtubules. Our data further suggests that Wnt5b regulation of basal anisotropic cell shape is potentially mediated through JNK. These findings provide a new model of three dimensional cell shaping required for basal epithelial tissue folding, in which anisotropic cell shape is enhanced basally over time. This anisotropic cell shape enhancement is Wnt5b, JNK, and microtubule-dependent.

### **3.3 Materials and methods**

#### **3.3.1 Zebrafish husbandry, maintenance, and strains**

Zebrafish (*Danio rerio*) embryos were used for these studies and include Wild-type (AB) and *wnt5b* mutants, *pipetail*<sup>(ti265)</sup> (Hammerschmidt et al., 1996). Zebrafish husbandry, maintenance, and embryo care were performed according to (Westerfield, 2007). For all experiments, embryo stage was determined according to somite number

following standard guidelines (Kimmel et al., 1995). Somite number was utilized to account for any possible developmental delays. This study was conducted under the approval and supervision of the University of Wisconsin-Milwaukee Institutional Animal Care and Use Committee.

### 3.3.2 Antisense morpholino oligonucleotide and mRNA injections

Microinjections were performed at the one-cell stage using the following reagents and concentrations. For mRNA injections: CAAX-eGFP (memGFP), 150 pg/embryo; membrane Cherry (memCherry), 50 pg/embryo; EMTB-GFP, 100 pg/embryo; EB3-GFP, 100 pg/embryo; MRLC-GFP, 150 pg/embryo. All mRNA was synthesized using SP6 mMessage mMachine Transcription Kit (AM1340, Ambion). EMTB-GFP, EB3-GFP, and MRLC-GFP constructs were kindly provided by Dr. Caren Norden, Max Planck Institute of Molecular Cell Biology and Genetics, Dresden, Germany (Norden et al., 2009). For anti-sense morpholino (MO)-mediated knockdown experiments: Standard Control MO (5'-CCTCTTACCTCAGTTACAATTTATA-3'), 3 ng/embryo. Zebrafish *p53* MO (5'-GCGCCATTGCTTTTGCAAGAATTG-3'), 3 ng/embryo (Robu et al., 2007). Splice site-blocking *wnt5b* MO (5'-TGTTTATTTCTCACCATTCTCCG-3') 3 ng/embryo (De Rienzo et al., 2012; Gutzman et al., 2018; Robu et al., 2007; Young et al., 2014). For all MO experiments, *p53* MO was co-injected. All morpholino (MO) oligonucleotides were obtained from (Gene Tools, LLC). MO injected embryos are referred to as morphants.

### 3.3.3 Live confocal imaging and cell shape analysis

Live confocal imaging was carried out as previously described using a Nikon C2 laser scanning confocal and a 40X water-immersion objective lens (NA 1.15) at room temperature (Gutzman et al., 2015; Sahu et al., 2017). Embryos were oriented on a microscope slide in 1% agarose wells with the anterior region of the embryo facing the left and posterior region facing the right. The dorsal side of the embryo, at the MHB, is positioned closest to the cover slip such that the midline of the embryo is parallel to the X-axis and the MHBC is centered. This was done to ensure consistency in tissue and cellular orientation when imaged and quantified for each embryo. Images were acquired in a Z-series spanning 15-25  $\mu\text{m}$  in depth for each embryo. Stacks were collected starting 15 microns below the dorsal surface at the MHB. Each figure contains representative images of a single slice from a Z-series (X-Y plane) or a view of the projected X-Z plane utilizing Nikon Imaging System (NIS) Elements Software to acquire a digital orthogonal cross-section of the Z-series (Digital slice) (See Appendix A). All confocal images were processed and analyzed using NIS Elements, Fiji (ImageJ), or Photoshop (Adobe). Cell length (Y-axis) measurements and MHB angle analyses were performed as previously described (Gutzman et al., 2015; Sahu et al., 2017).

To ensure that cells within the image are consistently aligned for proper quantification of anterior-posterior (X-axis) cell width and dorsal-ventral (Z-axis) cell depth, the following cell alignment protocol was followed (See Appendix A). First, Z-stacks of data were rotated in the X-Y plane to orient the apical-basal length of MHBC cells parallel to the Y-axis. Next, X-Z digital sections were taken from the newly oriented Z-stack both apically and basally perpendicular to the length of the cell (Y-axis). This allowed for generation of X-Z plane digital sections that aligned the same MHBC cells in

both the apical and basal X-Z images. In order to measure cell length, we identify one MHBC cell at the deepest point of constriction within the confocal Z-series dataset that clearly spans the entire distance from the apical surface of the tissue at the midline to the basal surface of the tissue and take a Y-axis measurement (Gutzman et al., 2015). MHBC cell length was then divided into 6 equal sections along the apical-basal cell axis. Using these sections as guides, two digital slices in the X-Z plane were generated from the NIS Elements Software Slices View Module. On each side of the neural tube, one slice was generated at the section point immediately below the apical cell surface and one slice was generated immediately above the basal surface. On average, these digital slices were about 5-7 microns into the cell from the apical or basal cell surface (see Fig. 23D-L; Appendix A). Apical and basal digital slices were then used for the quantification of apical and basal X:Z cell shape. The dotted yellow line shown in each figure indicates apical and basal section positions, where digital slices were generated.

Three measurements were acquired for cell shape analysis from each digital slice: Cell area, Z-dimension (depth), and X-dimension (width). Cell area was quantified using the free-hand selection tool in Fiji to outline individual cells in the X-Z plane. Each cell outline was then defined as a region of interest (ROI). In the ROI manager, cell area was calculated from the ROIs in micron units. The Z-dimension of the MHBC cells was measured using the line and measure tool along the deepest point of the cell, within 45° of the Z-axis. The X-dimension was measured at the widest point of the cell, perpendicular to the Z-dimension measurement (see Fig. 23C; Appendix A). To quantify anisotropic cell shape, the X-dimension measurement was divided by the Z-dimension measurement resulting in an X:Z ratio. Data are presented as X:Z ratios. Ratios with

values that are greater than one, or less than one, indicate anisotropic, or polarized, cell shape. To quantify cell shape posterior of the MHBC, cells 40 microns posterior of the MHBC at the midline chosen and the same procedure was followed for acquiring digital slices (See Appendix B).

#### 3.3.4 Western blot and two-dimension SDS PAGE analysis

For Western blot analysis, 22-24 ss embryos were dechorionated in embryo media and head tissue was dissected using fine-tip forceps. Tissue was collected in 1.5 mL Eppendorf tubes on ice containing buffer comprising 25mM Tris (pH 8.0), 2mM EDTA (pH 8.0), 10% glycerol, 1% Triton-X-100, phosphatase inhibitor (#88667, Pierce) and protease inhibitor (#04693124001, Roche). Total protein was isolated, and concentration measured by Bradford assay. 25 µg of protein were separated on 4-20% gradient SDS-PAGE and subsequent Western blot analysis was conducted with the following conditions. Blots were blocked for 2 hours at room temperature in 5% milk in 1X TBST, then washed 3X30 min in 1X TBST and incubated overnight at 4 degrees in primary antibody. pJNK and β-tubulin primary antibodies made in 5% milk in 1X TBST, all other primary antibodies were made in 0.25% gelatin in 1X TBST. The next day, blots were washed 3X30 min in 1X TBST and incubated for 1 hour in secondary antibody in 5% milk in 1X TBST. Following secondary antibodies, blots were washed and imaged using ECL Western blotting substrate (#1705060, Bio-rad). Primary antibodies: 1:2000 α-tubulin (#T6199, Sigma Aldrich), 1:2000 β-tubulin (E7-5, Developmental Studies Hybridoma Bank) 1:1000 phosphorylated-JNK (pJNK) (#4668, Cell Signaling Technology), 1:2000 β-actin (#A5441, Sigma-Aldrich). Secondary



antibodies: 1:2000 anti-mouse HRP (#7076, Cell Signaling Technology) and anti-rabbit HRP (#7074, Cell Signaling Technology). Blots were imaged on a Syngene G:BOX Chemi XRQ imaging system.

For two-dimension SDS PAGE analysis (See Appendix C), 22-24 ss embryos were dechorionated in embryo media and MHB tissue was dissected using fine-tip forceps as previously described [Sahu Ref]. Tissue was collected in 1.5 mL Eppendorf tubes on ice containing embryo media buffer containing protease inhibitor (#04693124001, Roche). Total protein was isolated using Bio Rad ReadyPrep™ Sequential Extraction kit (#1632100, Bio Rad) as per manufacturer protocol, and concentration was measured by Bradford assay. 30 µg of protein were separated on pH 3-10 IPG strip (#1632014, Bio Rad) using a PROTEAN IEF system. Separation by size was carried out on 4%-20% Criterion™ TGX Precast gels (#5671091, Bio Rad) and subsequently stained for total protein using SYPRO Ruby protein gel stain (S12000, Invitrogen). Gels were then imaged and compared to determine differences in protein spot. Differential spots of interest were then excised from the gel and identified by mass spectrometry.

### 3.3.5 Microtubule imaging and analysis

We examined microtubule filaments with live confocal imaging of EMTB-GFP, and plus-end microtubule dynamics with live confocal imaging of EB3-GFP. We quantified filament intensity, comet number, comet size, and comet speed. Analyses were conducted on wild-type embryos that had been co-injected with memCherry

mRNA, EB3-GFP, or EMTB-GFP mRNA either alone, or combined with Control MO or *wnt5b* MO.

To quantify microtubule filaments, EMTB-GFP injected embryos were live imaged at 24 ss. We used a Nikon CS2 laser scanning confocal microscope and collected a 15-25  $\mu\text{m}$  Z-series of images. The stack was cropped to 10  $\mu\text{m}$  and was analyzed using the average intensity projection of a Z-series in Fiji. To quantify MHBC-specific EMTB-GFP intensity, 40  $\mu\text{m}$  X 50  $\mu\text{m}$  ROIs were drawn using the rectangle selection tool and analyzed using the measure tool. ROIs were drawn at the MHBC, immediately adjacent to the MHBC in the midbrain region, and immediately adjacent to the MHBC in the hindbrain region (see Appendix D). An intensity measurement of each region was obtained using Fiji. Each side of the neuroepithelium was analyzed for each embryo. To compare MHBC average intensity across embryos and experiments, we divided the MHBC average intensity by the average of the intensity at the midbrain and hindbrain within each individual embryo, then we compared multiple embryos under different conditions (with or without *wnt5b* knockdown). We term this ratio as the normalized MHBC EMTB-GFP intensity (see Appendix D).

To quantify the plus-ends of microtubules, EB3-GFP injected embryos were imaged at 21-24 ss. We used a Nikon CS2 laser scanning confocal microscope and imaged in a single plane, 15-20  $\mu\text{m}$  into the tissue from the dorsal side of the embryo. Time-lapse data were collected for 10 minutes at a scanning speed of 1 frame per 4 seconds. Data were then cropped to 200 seconds and analyzed for EB3-GFP comet speed, comet number, and comet size using Fiji software. In Fiji, each image series was cropped to equal size (50  $\mu\text{m}$  X 40  $\mu\text{m}$ ) in the region at the MHBC on one side of the

neural tube at a time. The ROI used for EB3-GFP analysis does not include the apical region of the cells to avoid quantification of microtubules within dividing cells and to avoid the mitotic organizing center population of microtubules at the apical midline. Next, each image series was converted into 8-bit gray scale. The cropped data were segmented for EB3-GFP comets using the Threshold plugin and Otsu method, followed by the Analyze Particle plugin. EB3-GFP comets were then analyzed using the Fiji TrackMate plugin (Szikora et al., 2017). Particle detection was performed using the Laplacian of Gaussian detector method with an estimated blob diameter of 1  $\mu\text{m}$  and a threshold of 0.5  $\mu\text{m}$  with sub-pixel localization. Auto initial thresholding of spot quality was used to filter spots. Tracks were detected using the Linear motion LAP Tracker. (See Movies 2-9).

### 3.3.6 MRLC-GFP imaging and analysis

To quantify MRLC-GFP localization, average intensity projections of a 10  $\mu\text{m}$  Z-series of 24 ss embryos injected with MRLC-GFP mRNA were acquired. Average intensity was quantified for apical, middle, and basal regions of the MHBC (See Appendix E). Apical or basal MHBC average intensity was divided by the average intensity of the middle MHBC region within the same embryo. Control and *wnt5b* MO injected embryos were compared for each normalized intensity.

### 3.3.7 Immunohistochemistry

For  $\beta$ -tubulin immunostaining, embryos were fixed at 24 ss in 4% paraformaldehyde with 80mM KPIPES, 5mM EGTA, 1mM  $\text{MgCl}_2$ , and 0.2% Triton X, pH

6.4 for 5 minutes at 28 degrees C, followed by three hours at room temperature and washed with Tris buffered saline and 0.1% NP-40 (TBS-NP40) (155mM NaCl, 10mM tris HCl, and 0.1% NP-40, pH 7.6), three times for 10 minutes each at room temperature. Embryos were then deyolked and blocked (5% normal goat serum, 2% BSA, 1% Triton-X in TBS-NP40) for one hour at room temperature. After blocking, embryos were incubated in  $\beta$ -tubulin antibody (1:200, E7-5, Developmental Studies Hybridoma Bank) in block for 72 hours at 4 degrees C and then washed three times for ten minutes each at room temperature. After the embryos were washed, they were incubated in Alexa-Fluor 555 secondary antibody (1:500, A21422, Invitrogen) in block overnight at 4 degrees C. After three washes in PBT for ten minutes each, embryos were flat-mounted in glycerol and imaged using a Nikon C2 confocal with a 60X oil immersion objective lens. Quantification was carried out as follows:  $\beta$ -tubulin average intensity was quantified in a 10  $\mu\text{m}^2$  box for middle and basal regions of the MHBC within each embryo (See Appendix F). The average intensity at the basal and apical MHBC region was divided by the average intensity at the middle MHBC region in the same embryo. This normalization was used for comparison of basal and apical MHBC intensity across embryos and for comparisons between Control MO and *wnt5b* MO injected embryos.

To examine cell proliferation, embryos were fixed at 24 ss in 4% paraformaldehyde in phospho-buffered saline with 0.1% Tween-20 (PBT) for 2 hours and immunostained for phospho-histone 3 (1:800, Millipore, #06-570) and counter-stained with propidium iodide, and flat mounted for imaging on a confocal microscope.

In order to examine  $\beta$ -catenin localization at the MHBC, the following procedure was followed. Embryos were fixed in Dents (80% Methanol, 20% DMSO) for 1 hour at room temperature and washed in PBT three times for 30 minutes each. Embryos were deyolked, washed three times for 10 minutes in PBT, and incubated in block solution (1% Boehringer Mannheim Blocking Reagent, 10% lamb serum, 80% Maleic Acid Buffer) overnight at 4 degrees C, followed by incubation with 2.5  $\mu$ g/ml  $\beta$ -catenin primary antibody (ab6301, Abcam) in PBT overnight at 4 degrees C. The next day, embryos were washed four times for 1.5 hrs each in PBT and incubated in secondary antibody overnight at 4 degrees C, 1:2500 goat anti-mouse AlexaFluor-555 (A21422, Invitrogen) in PBT. Next, embryos were washed in PBT three times for 30 minutes each, flat mounted in glycerol, and imaged using confocal microscopy.

In order to analyze actin localization with *wnt5b* KD, phalloidin staining was conducted as follows: embryos were fixed at 24 ss in 4% paraformaldehyde in phosphate buffered saline with 0.1% Tween (PBT) for two hours, washed with PBT three times for 10 minutes each, deyolked, and incubated in phalloidin (1:40, A12379, Invitrogen) in PBT overnight at 4 degrees C. Next, embryos were washed three times for ten minutes each in PBT, flat-mounted in glycerol, and imaged using confocal microscopy. To quantify actin, average intensity projections of a 10  $\mu$ m Z-series of 24 ss embryos injected with MRLC-GFP mRNA were acquired. Average intensity was quantified for apical, middle, and basal regions of the MHBC (See Appendix E). Apical or basal MHBC average intensity was divided by the average intensity of the middle MHBC region within the same embryo. Control and *wnt5b* MO injected embryos were compared for each normalized intensity.

### 3.3.8 Pharmacological manipulations

For all pharmacological manipulations, embryos were dechorionated at 15 ss-17 ss and placed in 1% agarose coated petri-dishes containing embryo media. Normal media was then replaced with embryo media containing pharmacological reagents and embryos were bathed in the treatment from either 16-24 ss or 18-24 ss, as indicated per experiment, then live imaged at 24 ss. Concentrations of reagents are as follows: JNK inhibitor SP600125 (#420119, Calbiochem) was solubilized in DMSO and used at a final concentration of 5  $\mu$ M. Colchicine (#C9754, Sigma-Aldrich) was solubilized in water and used at a final concentration of 100  $\mu$ M. Paclitaxel (#T7191, Sigma-Aldrich) was solubilized in DMSO and used at a final concentration of 100  $\mu$ M. All DMSO control treatments utilized the same volume percentage of DMSO as the compared pharmacological reagent treatment group.

### 3.3.9 Statistical analyses

R-3.4.2 was used for all statistical analyses. Statistical comparisons between two groups were conducted using the Welch's T-Test. For analyses of experiments with more than 2 treatment groups, one-way ANOVA was performed with experimental batch effect factored in. ANOVA analyses that yielded a  $p$ -value less than 0.05 were subjected to Tukey's Honest Significant Difference (HSD) post hoc tests to determine significant differences between each of the treatment groups. For each figure, \* indicates  $p < 0.05$ , \*\* indicates  $p < 0.01$ , \*\*\* indicates  $p < 0.005$ . In each figure legend,  $n$  represents the number of embryos and the number of independent experiments conducted is

presented. All box and whisker plots and scatter plot overlays were generated using the ggplot2 package in R. All other bar graphs were generated using Excel (Microsoft).

### **3.4 Results**

#### **3.4.1 Three-dimensional neuroepithelial cell shape analysis reveals anisotropic cell shape.**

To begin to identify cellular and molecular mechanisms that mediate basal tissue folding, we used the developing zebrafish MHB as a model. We examined the deepest point of the MHB fold, termed as the midbrain-hindbrain boundary constriction (MHBC) (Figure 23A) (Gutzman et al., 2008). The cells at the MHBC are part of a single layer of pseudostratified neuroepithelium with apical-basal polarity (Figure 23B). The brain ventricles develop along the apical cell surface and the basement membrane lines the basal cell surface. We have characterized the cell shape changes that form the MHB by measuring cell length (apical-basal, Y-axis) and cell width (anterior-posterior, X-axis) (Figure 23B) (Gutzman et al., 2015). In order to fold the neuroepithelium, we found that cells at the deepest point of the constriction decrease in length relative to cells outside of the MHBC and cells decrease in width in this region (Gutzman et al., 2015). These cell shape changes are critical to the formation of the basal tissue fold, as failure of either one of these cell shape changes results in an overall tissue shape defect. The defect is the formation of an obtuse MHB tissue angle, which looks grossly similar even though the specific cell shape abnormalities can be different (Gutzman et al., 2015). Here, we developed a method to analyze and quantify cell shape in the third dimension,

cell depth (dorsal-ventral, Z-axis) and investigate its role in regulating basal tissue folding (Figure 23C).

Cells were visualized by injecting one-cell stage embryos with membrane Cherry (memCherry) or membrane GFP (memGFP) mRNA followed by live confocal microscopy of the MHB neuroepithelium during the early stages of MHB formation, between 18 and 24 somite stage (ss) (Figure 19D-L). Using Z-series data, digital orthogonal slices were generated from the apical and basal sides of the MHBC cells (Figure 23G-L; See Appendix A). From these images, we observed that wild-type MHBC cells had different properties in different dimensions. MHBC cells appeared to have greater depth in the Z-dimension and less width in the X-dimension, revealing that these cells exhibit anisotropic cell shape in the X-Z plane.

#### 3.4.2 Basal anisotropic cell shape is significantly enhanced between 18 ss and 24 ss.

In order to quantify these morphological differences in the X-Z plane, we took three different measurements of the MHBC cells (Figure 23C; See Appendix A). First, we measured cell area in the X-Z plane by manually outlining cells at the MHBC from both apical and basal digital slices (yellow outlines in Figure 23G-L). Second, we measured the maximal depth of cells in the Z-dimension, within 45° of the Z-axis (demonstrated by red lines in Figure 19C; See Appendix A). Finally, we measured the maximal width of the cells in the X-dimension, perpendicular to the Z measurement (demonstrated by blue lines in Figure 23C; See Appendix A). Then, we quantified the anisotropic shape of the cells in the X-Z plane using an X:Z ratio, dividing the width (X-



dimension) by the depth (Z-dimension). Anisotropic cell shape is defined as an X:Z ratio greater than or less than one.

Using this quantification method we examined apical and basal cell area and X:Z ratios of MHBC cells at 18 ss, 22 ss, and 24 ss (Figure 23G-L). MHBC cells had a significantly greater area on the apical side compared to the basal side at each time point examined (Figure 23M). However, when we compared apical cell area over time or basal cell area over time, no significant differences were detected. X:Z ratio measurements were  $< 1$ , both apically and basally, which confirmed that the MHBC cells are anisotropic (Figure 23N). This is consistent with MHBC cells being described as “wedge-shaped”(Gutzman et al., 2018). When we compared only apical X:Z ratios, no significant differences were found (Figure 23G-I,N), suggesting that the apical anisotropic cell shape is not changing during this developmental window. Interestingly, comparison of X:Z ratios among basal digital slices revealed significant changes between 18 and 22 ss, and those changes were further enhanced by 24 ss (Figure 23J-L,N). Together, these data demonstrate that during the early stages of MHB morphogenesis, MHBC cells have apical and basal polarized cell shape and anisotropic cell shape in the X-Z plane. In general, cells are narrower along the X-axis and deeper along the Z-axis. Since cell area in the X-Z plane did not change at these time points, our data suggest that the enhancement of basal anisotropic cell shape contributes to early MHB formation. These cell shape quantification methods, and wild-type characterization, provide a platform for elucidating the molecular mechanisms that mediate basal tissue folding.

### 3.4.3 *Wnt5b* is required for anisotropic cell shape both apically and basally at the MHBC.

To test for upstream mediators of MHBC cell shape, we have hypothesized that signaling molecules would be specifically expressed in the MHB region during morphogenesis (Gutzman et al., 2018; Sahu et al., 2017). *wnt5b*, a known morphogen, is expressed at the MHB at the onset of tissue folding (18 ss) (Duncan et al., 2015; Gutzman et al., 2018; Thisse, 2005) and has been demonstrated to have a role in basal constriction of MHBC cells late in MHB morphogenesis, at prim-6 (Gutzman et al., 2018). Given the anisotropic cell shape changes we identified between 18 to 24 ss, we further hypothesized that *Wnt5b* could play an earlier role in MHB formation. In order to test this hypothesis, we utilized live cell imaging of *wnt5b* anti-sense oligonucleotide morpholino (MO) knockdown embryos (morphants) (Figure 24) (De Rienzo et al., 2012; Freisinger et al., 2010; Gutzman et al., 2018; Lin et al., 2010; Young et al., 2014) and *wnt5b pipetail*<sup>(*ti265*)</sup> mutants (Figure 25) (Hammerschmidt et al., 1996). Multiple publications confirm the ability of *wnt5b* MOs to clearly phenocopy *pipetail* mutants (Cirone et al., 2008; Lele et al., 2001; Robu et al., 2007), this is also validated here (Figure 25).

Wild-type embryos were co-injected with memGFP mRNA and either Control MO or *wnt5b* MO and imaged at 24 ss. We found that by 24 ss *wnt5b* knockdown perturbed the MHB tissue fold, represented by the MHB angle measurements, but did not affect MHBC cell length (Figure 24A-C), suggesting that *Wnt5b* mediates cell shape in a dimension other than the Y-axis to affect overall tissue shape. From examination of digital slices in the X-Z plane, we found that *wnt5b* knockdown did not affect apical or

basal cell area (Figure 26A). However, quantification of X:Z ratios revealed that knockdown of *wnt5b* perturbed cell depth in the Z-dimension and cell width in the X-dimension, demonstrating that Wnt5b was required to regulate anisotropic cell shape, both apically and basally (Figure 24D-H). Similar anisotropic cell shape defects were demonstrated using *pipetail*<sup>(*ti265*)</sup> mutants (Figure 25E-K); therefore, subsequent experiments were performed using the *wnt5b* MO. We also found no change in the percentage of PH3 positive cells with *wnt5b* knockdown (Figure 26B-D) suggesting that cell proliferation does not play a role in Wnt5b mediation of MHB morphogenesis. In order to confirm that the abnormal tissue shape observed in *wnt5b* morphants was due to cell shape defects specifically at the MHBC, we measured X:Z ratios in cells 40 microns outside and posterior to the MHBC (Figure 26E-I, See Appendix B). Differences in either apical or basal anisotropic cell shape were not observed between Controls and *wnt5b* morphants, demonstrating that *wnt5b*-dependent cell shape changes are region specific (Figure 26E-I). Together, these data indicate that Wnt5b is required in the early stages of MHB morphogenesis to promote proper MHB tissue folding via regulation of apical and basal anisotropic MHBC cell shape in the X-Z plane.

#### 3.4.4 Wnt5b regulates tubulin during MHB morphogenesis.

Next, we aimed to identify downstream targets of Wnt5b that mediate MHBC anisotropic cell shape. We hypothesized that potential targets would be regulated at the protein level due to the short time-span between the onset of *wnt5b* expression and MHB morphogenesis. Taking a global approach, we micro-dissected MHB specific tissue from Control and *wnt5b* knockdown embryos at 22-24 ss using our established

method (Figure 13) (Sahu et al., 2017), and compared protein populations with 2-dimensional SDS-PAGE (Figure 27; See Appendix C). Using mass spectrometry, we identified  $\alpha$ -tubulin and  $\beta$ -tubulin as proteins that were reduced in abundance upon knockdown of *wnt5b* (Figure 27D). We confirmed our 2D gel analysis by Western blot and demonstrated that both  $\alpha$ -tubulin and  $\beta$ -tubulin were reduced by approximately 50% in *wnt5b* morphants compared to Controls (Figure 28A-B).

$\alpha$ -tubulin and  $\beta$ -tubulin are the monomeric building blocks for the microtubule cytoskeleton and both are required for microtubule filament assembly (Etienne-Manneville, 2010). Therefore, we hypothesized that *wnt5b* knockdown, and the observed decrease of  $\alpha$ -tubulin and  $\beta$ -tubulin at the MHB, would affect the microtubules within the MHBC cells. We investigated the microtubule filament population *in vivo* with a widely used marker, EMTB-GFP, a chimeric GFP-tagged protein containing the N-terminal microtubule binding domain of ensconsin, a known microtubule-associated protein (MAP) (Bulinski et al., 1999; Norden et al., 2009). Wild-type embryos were co-injected with memCherry and EMTB-GFP mRNA and either Control MO or *wnt5b* MO and live imaged at 24 ss. To compare EMTB levels in cells at the MHBC between Control and *wnt5b* morphants, MHBC specific EMTB-GFP intensity was normalized within each embryo by dividing the average EMTB intensity of the MHBC region by the average EMTB intensity of the adjacent midbrain and hindbrain regions (Figure 28C-E; See Appendix D). We found that the normalized MHBC EMTB-GFP intensity was significantly decreased in *wnt5b* morphants when compared to Controls (Figure 28E), suggesting that *wnt5b* knockdown leads to decreased microtubule filaments within the MHBC. Next, we used  $\beta$ -tubulin immunohistochemistry to examine and quantify the

basal specific population of microtubules within the MHBC cells. We compared basal and apical  $\beta$ -tubulin levels in Controls and *wnt5b* morphants within each embryo by dividing  $\beta$ -tubulin intensity in the basal or apical MHBC region by the  $\beta$ -tubulin intensity in the middle MHBC region (Figure 28F-I; See Appendix D). We found a significant decrease in  $\beta$ -tubulin levels in the basal domain of MHBC cells in *wnt5b* morphants when compared to Controls (Figure 28F-H), demonstrating that Wnt5b is critical for the basal microtubule population at the MHBC. There were no differences in apical  $\beta$ -tubulin intensity (Figure 28I).

From these data, we uncovered an important role for Wnt5b in mediating the microtubule cytoskeleton during MHB basal tissue folding. However, it is known that Wnt signals mediate actomyosin dynamics in other morphogenetic contexts such as gastrulation, heart tube remodeling, and lung epithelial morphogenesis (Fumoto et al., 2017; Kim and Davidson, 2011; Lee et al., 2006; Merks et al., 2018). In addition, our previous work revealed a critical role for non-muscle myosins in mediating the cell shape changes required for MHB basal tissue folding (Gutzman et al., 2015). Therefore, we investigated a potential role for *wnt5b* in mediating actomyosin at the MHBC by examining *in vivo* localization of myosin using GFP-tagged myosin regulatory light chain (MRLC-GFP) (Norden et al., 2009) and actin using phalloidin staining. Following quantification, no differences were detected in apical or basal MRLC-GFP and actin localization at the MHBC when comparing Controls to *wnt5b* knockdowns (Figure 29), suggesting that Wnt5b does not act directly through the actomyosin network to mediate MHB basal tissue folding.

Together, these data demonstrate a role for *wnt5b* in the regulation of tubulin levels and suggest that Wnt5b is important for regulating the microtubule cytoskeleton within the MHBC during early MHB morphogenesis.

#### 3.4.5 Wnt5b regulates microtubule dynamics during early MHB morphogenesis.

Since we determined that *wnt5b* mediates  $\alpha$ -tubulin,  $\beta$ -tubulin and microtubule filament levels in the MHBC region and basally at the MHBC, we hypothesized that Wnt5b would also be required to regulate microtubule dynamics during early MHB morphogenesis. In order to test this hypothesis, we analyzed microtubule plus-end dynamics *in vivo* by following the fast-growing plus-end microtubule binding protein, EB3, tagged with GFP (Norden et al., 2009). We co-injected memCherry and EB3-GFP mRNA with Control MO or *wnt5b* MO and performed time-lapse imaging of the MHB region for 10 minutes at 24 ss (Movies 2-5). We quantified EB3-GFP microtubule comet speed, comet number, and comet size using Fiji (Figure 30). The EB3-GFP dynamic microtubule quantification was focused below the apical mitotic organizing center, in the more basal domain. We found that EB3-GFP comets moved significantly faster in *wnt5b* morphants compared to controls, at an average of 5  $\mu\text{m}$  per minute compared to 4.5  $\mu\text{m}$  per minute, respectively (Figure 30A). The number of EB3-GFP comets was also significantly higher in *wnt5b* morphants relative to Control morphants (Figure 30B); however, there was no difference in comet size (Figure 30C). These data revealed that *wnt5b* is required for regulation of microtubule dynamics within the MHBC.

3.4.6 Microtubule polymerization is required for basal, but not apical, anisotropic cell shape in MHBC cells at 24 ss.

Microtubules are well-established as important mediators of cell shape during neural tube formation (Burnside, 1971; Cearns et al., 2016; Jayachandran et al., 2016). As a next logical step in understanding the role of microtubules as a target for Wnt5b, we tested the hypothesis that disruption of microtubule polymerization would affect early MHB morphogenesis. We employed the widely used microtubule-destabilizing reagent, Colchicine (Dostal and Libusova, 2014; Ravelli et al., 2004), combined with live confocal imaging of memGFP injected embryos. As predicted, Colchicine treatment administered at 18 ss disrupted microtubule dynamics (Figure 31) and resulted in abnormal MHB tissue folding, but did not affect MHBC apical-basal cell length (Figure 32A-C). Quantification of anisotropic cell shape revealed that preventing microtubule polymerization significantly increased the basal X:Z ratio at the MHBC, with values closer to one (Figure 32D-H). Apical anisotropic cell shape remained unchanged (Figure 32D-H); however, we observed an increase in apical cell area (Figure 33) possibly due to an effect of Colchicine on cell cycle progression and cell proliferation (Brues and Cohen, 1936; Ghawanmeh et al., 2018). In addition, Colchicine did not affect cell shapes outside of the MHBC (Figure 34). Together, these data indicate that microtubule polymerization plays a region-specific role in the basal domain of MHBC cells to regulate anisotropic cell shape during early MHB tissue folding, which is independent from regulation of apical anisotropic cell shape.

#### 3.4.7 Microtubule filament stability is required for Wnt5b-mediated basal anisotropic cell shape.

We established that Wnt5b has a role in mediating apical and basal anisotropic cell shape,  $\alpha$ -tubulin and  $\beta$ -tubulin levels, and microtubule dynamics within the MHB. We also demonstrated that microtubule polymerization is required specifically for basal anisotropic cell shape. These data led us to hypothesize that Wnt5b mediates MHBC anisotropic cell shape by regulating microtubule stability. To test this hypothesis, we performed a rescue experiment using Paclitaxel, a microtubule-stabilizing reagent (Dostal and Libusova, 2014; Elie-Caille et al., 2007; Jayachandran et al., 2016), in combination with *wnt5b* knockdown. We predicted that stabilization of microtubules would rescue the *wnt5b* knockdown induced defects in anisotropic cell shape. Embryos were co-injected with memGFP and either Control or *wnt5b* MO, then treated at 18 ss with DMSO or Paclitaxel and imaged at 24 ss. Apical and basal digital slices were analyzed for anisotropic cell shape (Figure 35). Control and *wnt5b* morphants treated with DMSO demonstrated apical and basal anisotropic cell shapes that were similar to those observed in Figure 24 (Figure 35A-B,E-F). However, when quantified, apical anisotropic cell shape of Control morphants compared to *wnt5b* morphants was not significantly different (Figure 35A,E,I). This may be due to the microtubule polymerizing effect of DMSO treatment (Katsuda et al., 1987; Robinson and Engelborghs, 1982). Paclitaxel did not have a significant effect on Control morphant anisotropic cell shape apically or basally (Figure 35A-D,I). However, when we treated *wnt5b* morphants with Paclitaxel, we found that basal anisotropic cell shape was rescued (Figure 35F,H-I), and there was no effect on apical anisotropic cell shape (Figure 35E,G,I). Together, these



data indicate that basal anisotropic cell shape is specifically dependent on *wnt5b*-mediated microtubule stability.

#### 3.4.8 JNK is regulated by Wnt5b and mediates microtubule dynamics at the MHBC.

To examine what could mediate Wnt5b regulation of anisotropic MHBC cell shape, we investigated a known downstream effector of Wnt signaling that is also known to regulate microtubule dynamics, jun N-terminal Kinase (JNK) (Schambony and Wedlich, 2007; Yang, 2003). JNK plays an important role in the brain during neurite growth and regeneration, notably through the phosphorylation of downstream microtubule-associated proteins (MAPs) (Feltrin et al., 2012). This known role for JNK, and our finding that Wnt5b regulates microtubules to mediate basal anisotropic cell shape, led us to hypothesize that JNK is regulated by Wnt5b during early MHB morphogenesis. We investigated the effect of *wnt5b* knockdown on JNK activation by examining levels of JNK phosphorylation (pJNK) (Figure 36). *wnt5b* knockdown decreased pJNK levels by approximately 40% (Figure 36B), suggesting JNK is a potential mediator of the Wnt5b signal.

Since we found that Wnt5b-mediated anisotropic cell shape is specific to the MHBC, we hypothesized that downstream effectors the Wnt5b signal would also have subcellular specificity to elicit mechanistic differences in cell shape basally versus apically. It was previously demonstrated that inhibition of GSK3 $\beta$ , which normally targets  $\beta$ -catenin for degradation in the absence of Wnt signals, is sufficient to rescue the basal tissue folding defect observed in *wnt5b* morphants (Gutzman et al., 2018). In addition,

JNK cooperates with GSK3 $\beta$  to mediate microtubule stability (Ciani and Salinas, 2007) and studies have demonstrated a link between JNK and  $\beta$ -catenin localization (Lee et al., 2009; Liao et al., 2006). Therefore, we hypothesized that *wnt5b* could mediate the subcellular localization of  $\beta$ -catenin in MHBC cells. Immunohistochemistry revealed that *wnt5b* regulates basal, but not apical accumulation of  $\beta$ -catenin and this basal accumulation of  $\beta$ -catenin is specific to the MHBC region (Figure 37). These data suggest potential subcellular variations in Wnt5b signaling to mediate basal cell shape.

Next, we asked whether or not JNK modulates microtubules at the MHBC by tracking EB3-GFP in either DMSO control or JNK inhibitor, SP600125 (He et al., 2016) treated embryos (Figure 38 and Movies 6-9). Quantification of EB3-GFP comet speed, comet number, and comet size were compared between treatments (Figure 38). We observed that SP600125 JNK inhibitor treatment resulted in a significant increase in EB3-GFP comet speed and comet number (Figure 38A-B). However, we did not detect a significant difference in EB3-GFP comet size (Figure 38C). These data are consistent with the microtubule effects observed following *wnt5b* knockdown (see Figure 30) and indicate that JNK regulates microtubule dynamics in the MHBC at 24 ss during basal tissue folding.

#### 3.4.9 JNK is required for basal anisotropic MHBC cell shape

We demonstrated that Wnt5b regulates microtubules to establish basal anisotropic cell shape. We have also shown that Wnt5b regulates JNK, and that JNK modulates microtubule dynamics at the MHBC. Therefore, we hypothesized that JNK would also be required for MHB tissue and cell shape. We treated memGFP injected

embryos with DMSO control or the JNK inhibitor SP600125 at 18 ss and analyzed MHB tissue and cell shape at 24 ss (Figure 39). SP600125 treatment perturbed the MHB angle, indicating that JNK has a role in MHB basal tissue folding (Figure 39A-C), but not via mediation of apical-basal cell length (Figure 39C). Next, we characterized anisotropic cell shape using the X:Z ratio from apical slices and did not detect a significant difference with JNK inhibition (Figure 39D,F,H). However, when we quantified anisotropic cell shape in basal slices, JNK inhibition resulted in a significant increase in the X:Z ratio (Figure 39E,G-H). Differences in anisotropic cell shape were not observed in cells outside the MHBC with JNK inhibition (Figure 40). Together, these results indicate that JNK is required for MHB basal tissue folding through specific modulation of MHBC basal anisotropic cell shape.

#### 3.4.10 Microtubule filament stability is required for JNK-mediated basal anisotropic cell shape.

We have shown that JNK is required for mediating microtubule dynamics and basal anisotropic cell shape at the MHBC to control MHB basal tissue folding. These data led us to hypothesize that JNK mediates basal MHBC anisotropic cell shape by regulating microtubule stability as we have shown with Wnt5b. To test this hypothesis, we performed a rescue experiment using Paclitaxel in combination with the JNK inhibitor, SP600125. Wild-type embryos were injected with memGFP, treated at 16 ss with either DMSO or SP600125, and then treated at 18 ss with DMSO or Paclitaxel. At 24 ss embryos were imaged and basal anisotropic cell shape was analyzed (Figure 41). Control and SP600125-treated embryos, that were additionally treated with DMSO at 18

ss, demonstrated basal anisotropic cell shapes similar to the treatment with JNK inhibitor presented in Figure 39 (Figures 39E,G and 41A,C). However, when we treated SP600125-treated embryos with Paclitaxel, we found that basal anisotropic cell shape was rescued (Figure 41C,D,E). Together, these data indicate that basal MHBC anisotropic cell shape is dependent on JNK-mediated microtubule stability.

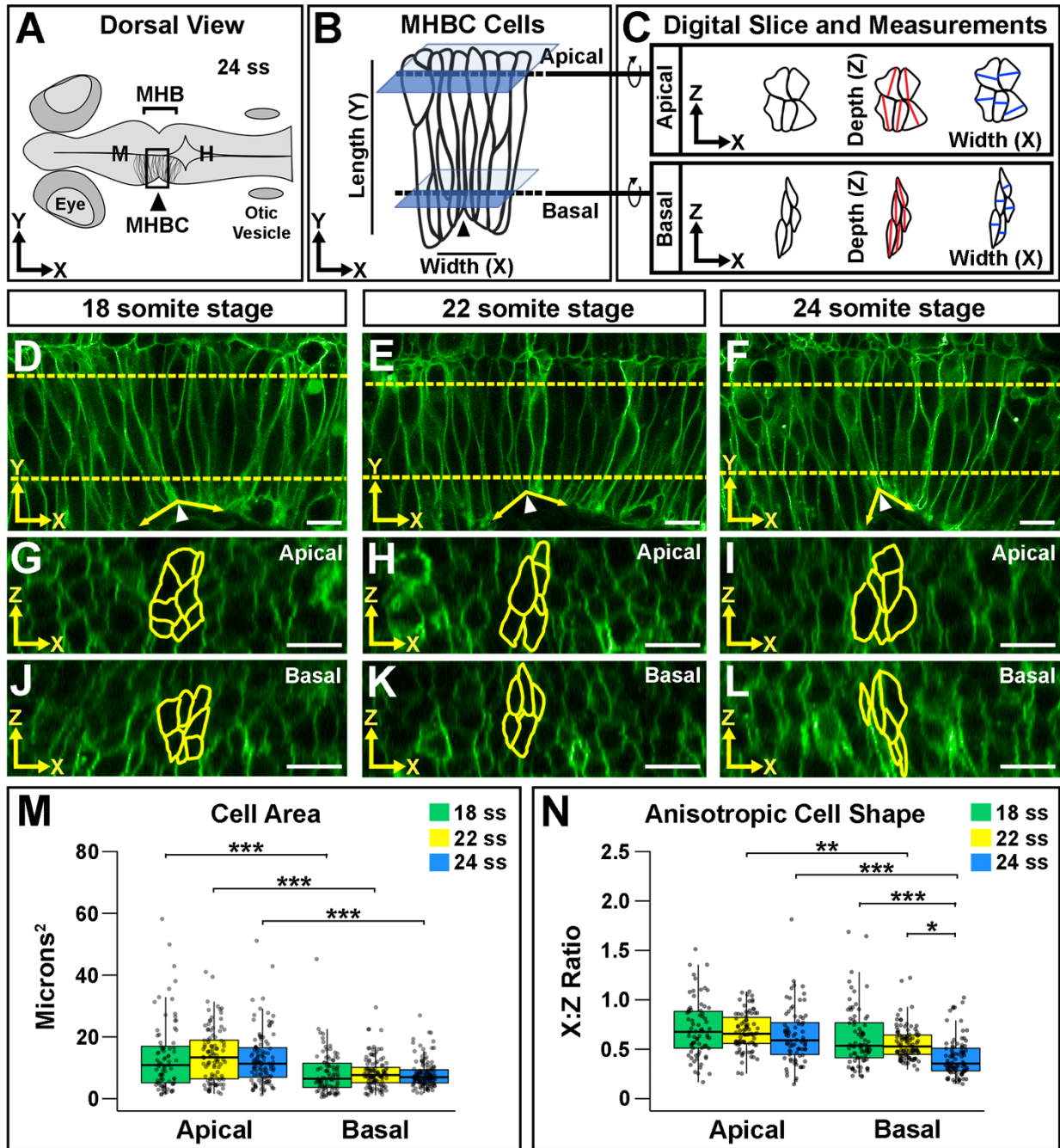


**Figure 23. Neuroepithelial cell shape analysis reveals anisotropic shape that is enhanced basally during morphogenesis.** (A) Diagram of a 24 somite stage (ss) zebrafish embryo. M, midbrain. H, hindbrain. (B) Zoom of boxed MHBC region in A. Cell orientation is demonstrated. Length (apical-basal, Y-axis), width (anterior-posterior, X-

axis). Dotted lines indicate where apical and basal digital orthogonal slices are generated for analyses. (C) Digital slices are rotated 90° to the right to reveal apical and basal cell shape in the X-Z plane. Cell area is measured by outlining cells. Cell depth is measured at the deepest point of the cell within 45° of the Z-axis (red lines). Cell width is measured at the widest point of the cell along the X-axis, perpendicular to the depth measurement (blue lines). See also Appendix I. (D-L) Live confocal images of wild-type embryos injected with memcherry mRNA at 18 ss (D,G,J), 22 ss (E,H,K), and 24 ss (F,I,L). Apical digital slices (G-I), basal digital slices (J-L), at indicated time points. MHBC cells are outlined in yellow. (M) Quantification of apical and basal cell area. (N) Quantification of anisotropic cell shape using the width (X) to depth (Z) ratio (X:Z ratio). Box plots indicate the 25th and 75th percentiles and the median. Three independent experiments are represented. 18 ss, n=6; 22 ss, n=6; 24 ss, n=6. \* indicates  $p < 0.05$ , \*\* indicates  $p < 0.01$ , \*\*\* indicates  $p < 0.005$ . Arrowhead indicates MHBC. Anterior is to the left in all images. Scale bars: 10  $\mu\text{m}$ .

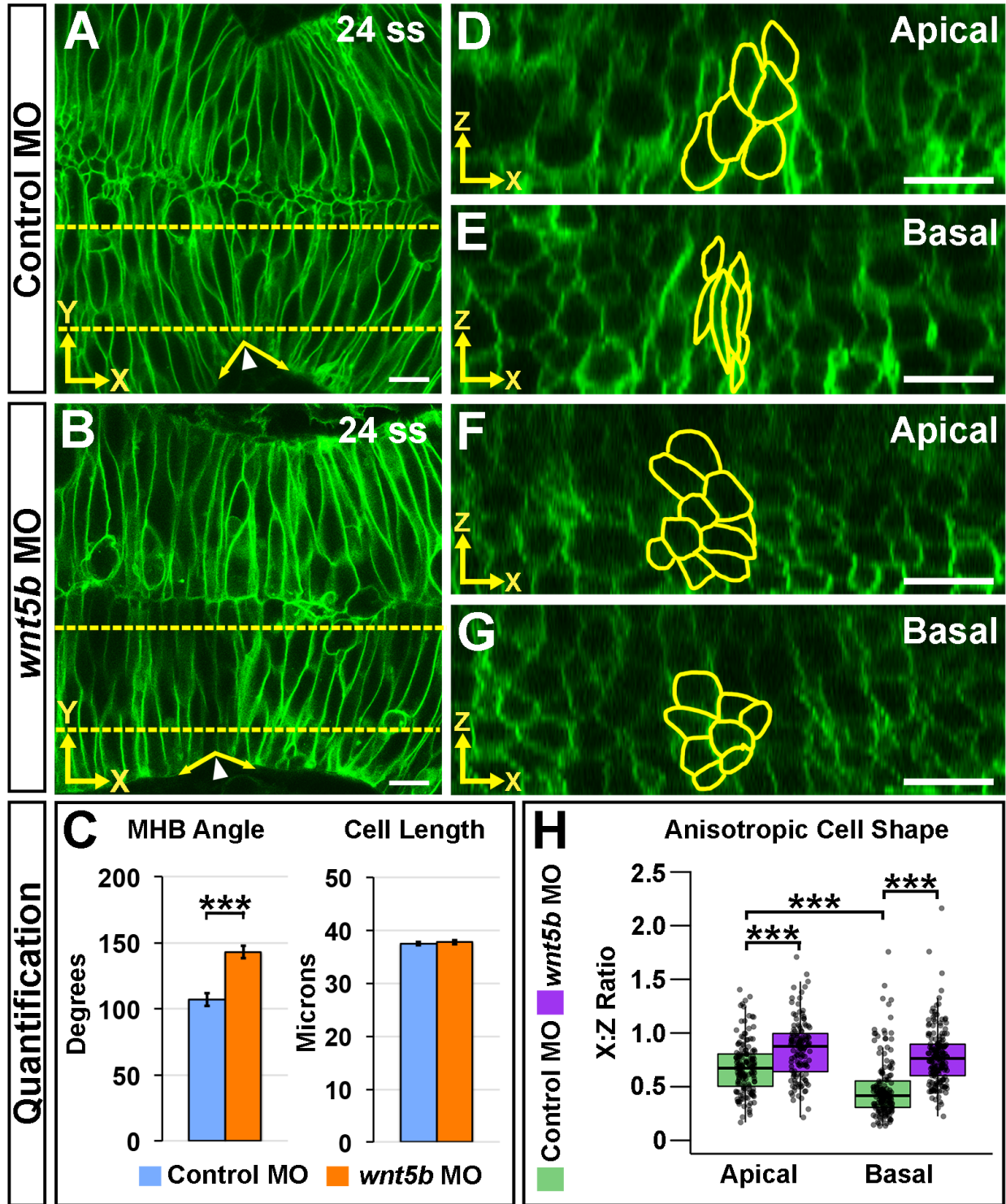
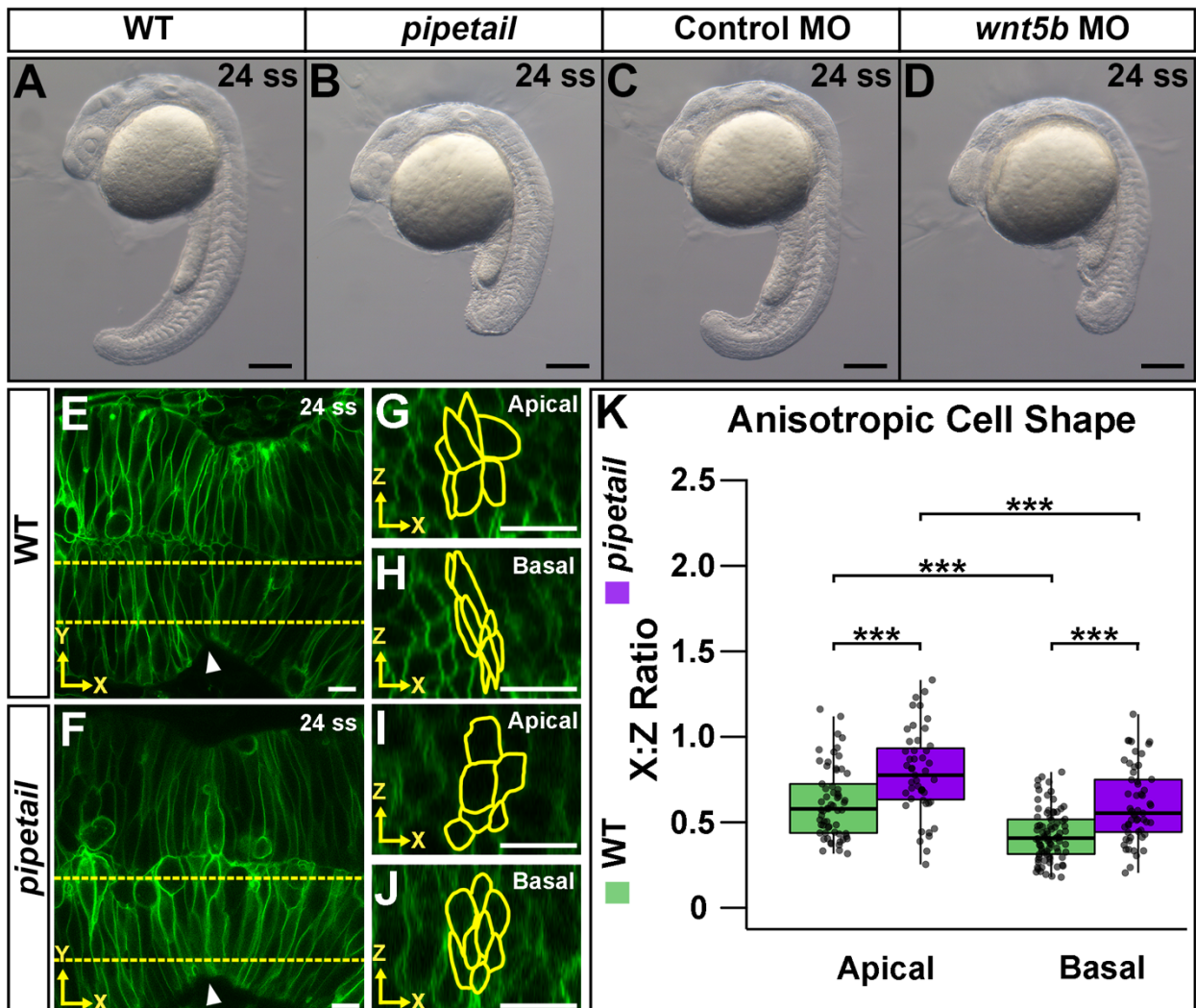


Figure 24. Wnt5b is required for anisotropic cell shape both apically and basally at the MHBC. (A-B) Live confocal images of 24 ss wild-type embryos co-injected with memGFP and Control MO (A) or *wnt5b* MO (B). (C) Quantification of MHB angle and



MHBC cell length (Y-axis). Data are represented as mean  $\pm$  SEM from eight independent experiments. (D-E) Representative apical (D) and basal (E) digital slices of Control morphants. MHBC cells are outlined in yellow. (F-G) Representative apical (F) and basal (G) digital slices of *wnt5b* morphants. MHBC cells are outlined in yellow. (H) Quantification of anisotropic cell shape using X:Z ratio. Boxplots indicate the 25th and 75th percentiles and the median. Eight independent experiments are represented. Control MO, n=10; *wnt5b* MO, n=10. \*\*\* indicates  $p < 0.005$ . Arrowhead indicates MHBC. Scale bars: 10  $\mu\text{m}$ .





**Figure 25. *wnt5b* morpholino knockdown phenocopies *wnt5b pipetail*<sup>(*ti265*)</sup>**

**mutants, including defects in anisotropic cell shape at the MHBC. (A-D)** Lateral brightfield images of 24 ss Wild-Type (WT) (A), *pipetail* (B), Control morphant (C), or *wnt5b* morphant (D) embryos. Scale bars: 200  $\mu$ m. (E-F) Live confocal imaging of 24 ss WT (E) or *pipetail* (F) embryos injected with memGFP. (G-H) Apical (G) and basal (H) digital slices of WT embryos at 24 ss. (I,J) Apical (I) and basal (J) digital slices of *pipetail* mutant embryos at 24 ss. (K) Quantification of X:Z ratio. Box plots indicate the 25th and 75th percentiles and the median. Three independent experiments are represented. WT, n=6; *pipetail*, n=4. \*\*\* indicates P<0.005. Arrowhead indicates MHBC. Scale bars: 10  $\mu$ m.

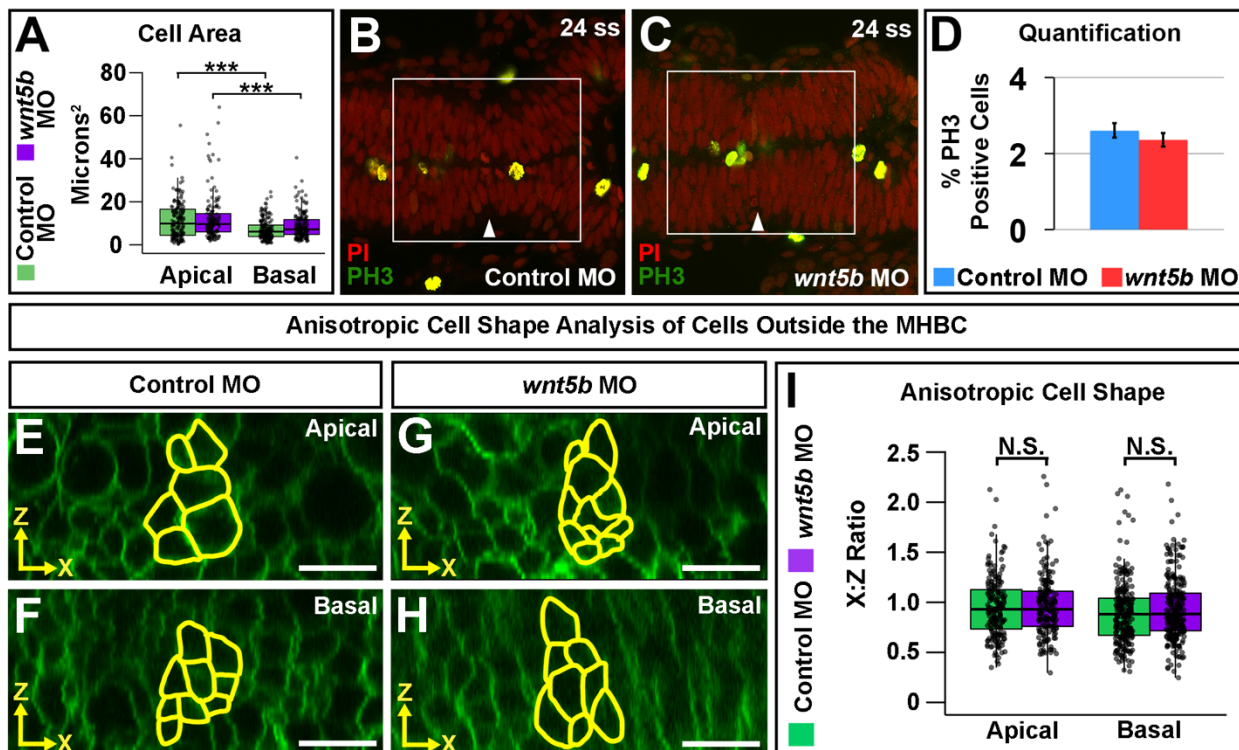


**Figure 26. *wnt5b* knockdown does not affect apical or basal MHBC cell area, MHB cell proliferation, or anisotropic cell shape outside of the MHBC during early**

**morphogenesis.** (A) Quantification of apical and basal cell area of 24 ss wild-type embryos co-injected with memGFP mRNA and Control or *wnt5b* MO. Boxplots indicate the 25th and 75th percentiles and the median. Eight independent experiments are represented. \*\*\* indicates  $P < 0.005$ . Control MO,  $n=10$ ; *wnt5b* MO,  $n=10$ . (B-D) Confocal images were acquired of Control MO (B) and *wnt5b* MO (C) injected embryos. (D) Quantification of PH3 positive cells as a percentage of total cells in the region indicated by the white box. Data represented as mean  $\pm$  SEM from three independent experiments. Control MO,  $n=3$ ; *wnt5b* MO,  $n=3$ . (E-H) Representative digital slices of cell shape outside of the MHBC in Control (E,F) and *wnt5b* (G,H) morphants. Apical (E,G) and basal (F,H) digital slices of WT 24 ss embryos co-injected with memGFP and either Control MO (G,H) or *wnt5b* MO (I,J). Cells that are 40 microns posterior to the MHBC are outlined in yellow. (K) Quantification of X:Z ratio. Box plots indicate the 25th and 75th percentiles and the median. Eight independent experiments are represented. Control MO,  $n=10$ ; *wnt5b* MO,  $n=10$ . N.S. (not significant) indicates  $P > 0.05$ . Scale bars: 10  $\mu\text{m}$ .

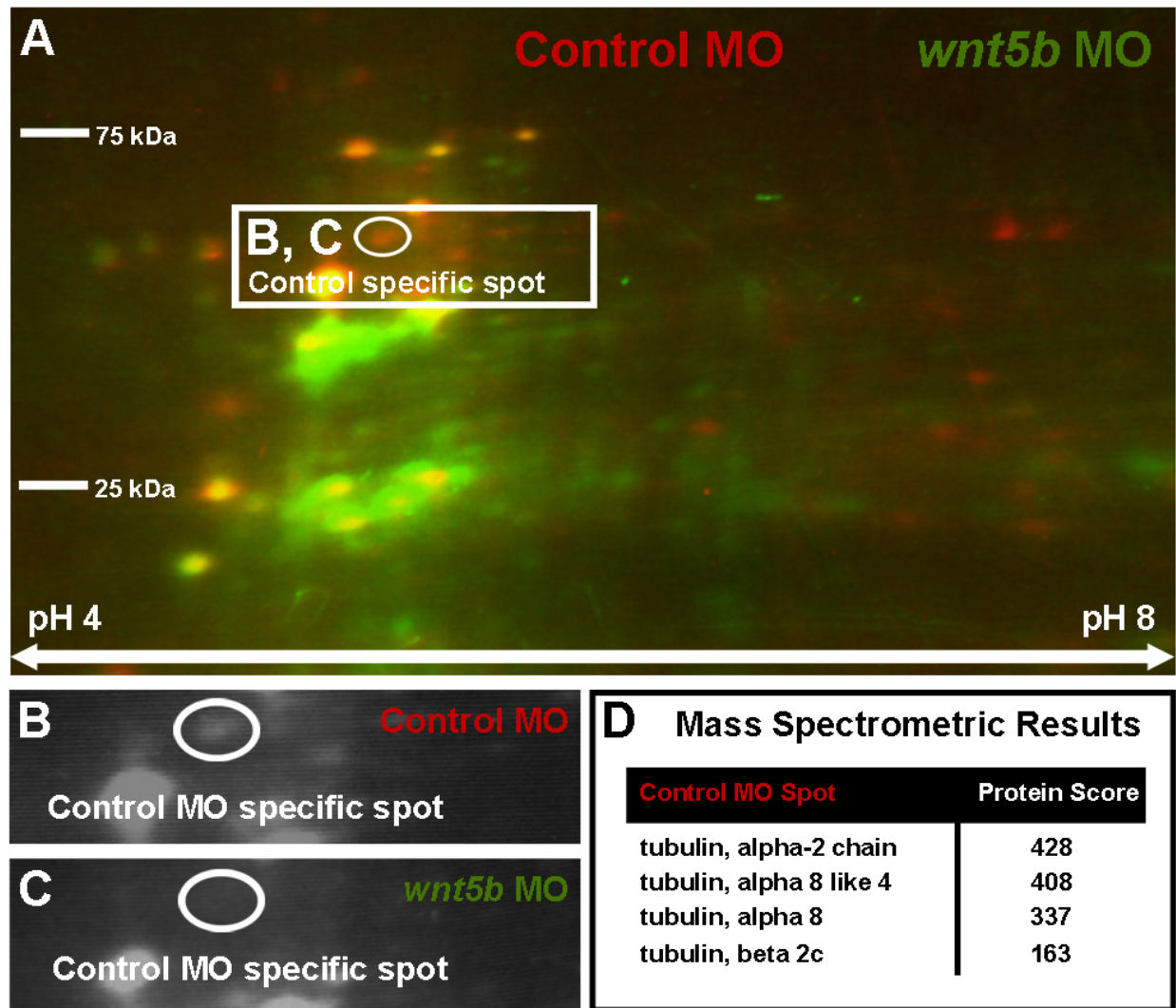


**Figure 27. Differential two-dimensional SDS-PAGE and mass spectrometry reveal Wnt5b may be important for tubulin protein levels at the MHB.** (A) 2D Gel overlay of Control MO MHB protein (Red) compared to *wnt5b* MO MHB protein (Green). Yellow spots indicate proteins of relatively the same abundance between conditions. Spots that are either red or green indicate proteins with differential abundance. Circle indicates spot present in the Control MO protein gel but absent in the *wnt5b* MO protein gel. (B,C) Boxed region of panel A is enlarged in panel (B) depicting the Control MO protein gel and panel (C) depicting the *wnt5b* MO protein gel. (D) Mass spectrometric analysis

results for the control specific protein spot. Protein score indicates the sum of the ion scores for the peptide.

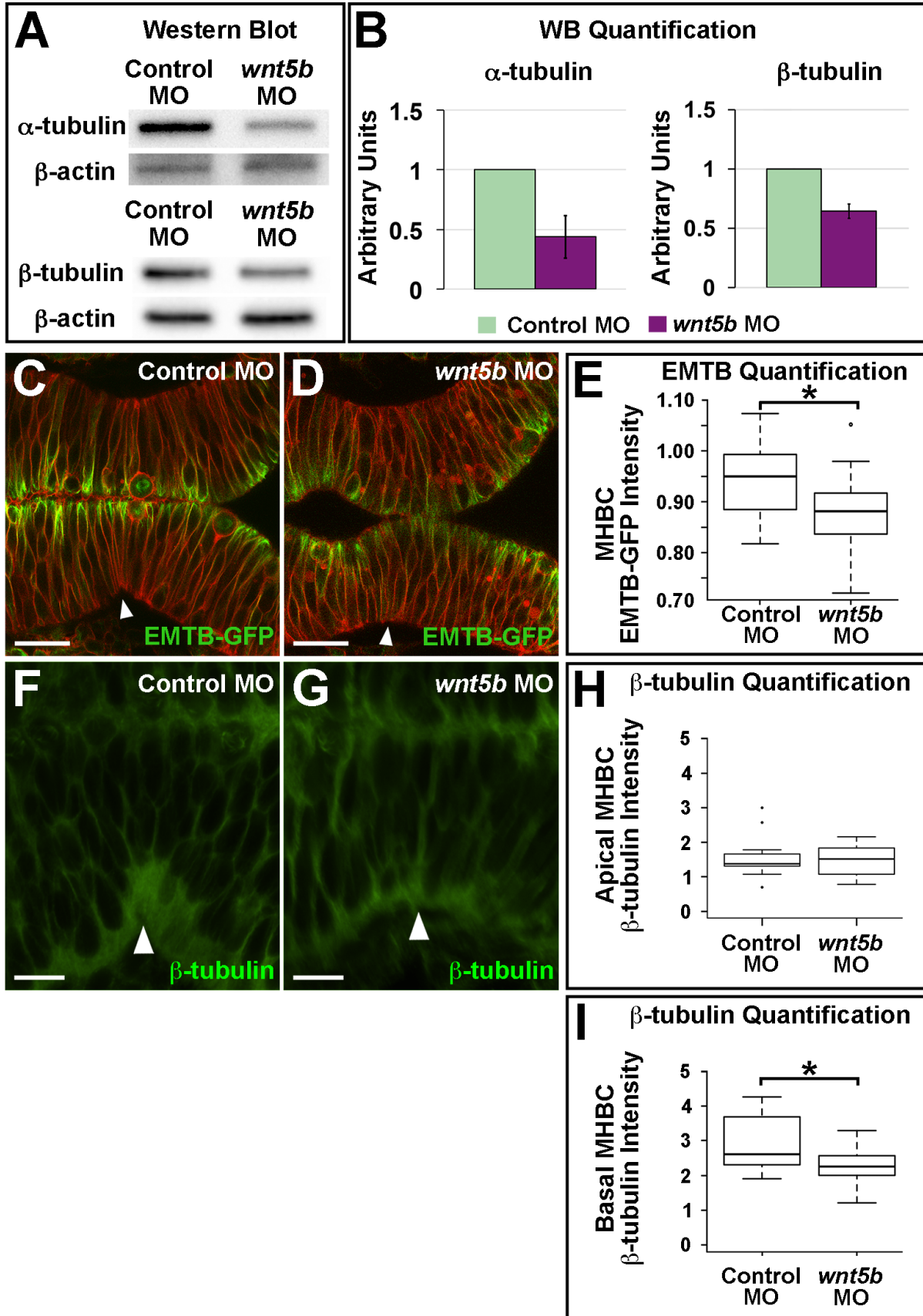


**Figure 28. Wnt5b regulates tubulin protein levels at the MHB.** (A) Representative Western blot for  $\alpha$ -tubulin and  $\beta$ -tubulin, with  $\beta$ -actin as the control, comparing Control MO and *wnt5b* MO injected embryos. Head tissue protein was analyzed. (B) Quantification of at least three independent Western blot (WB) experiments,  $\alpha$ -tubulin and  $\beta$ -tubulin levels were normalized to  $\beta$ -actin. Data are represented as mean  $\pm$  SD. (C,D) Representative live confocal images showing 10  $\mu$ m average intensity projections at 22-24 ss of wild-type embryos co-injected with EMTB-GFP, memCherry, and Control MO (C) or *wnt5b* MO (D). (E) Quantification of the normalized MHBC EMTB-GFP intensity in Control versus *wnt5b* morphants (Fig. S4). Box plots indicate the 25th and 75th percentiles and the median. Three independent experiments are represented. Control MO, n=10; *wnt5b* MO, n=7. Scale bars: 20  $\mu$ m. (F,G) Representative confocal images of  $\beta$ -tubulin immunostaining showing 10  $\mu$ m average intensity projections at 24 ss of wild-type embryos injected with either Control MO (F) or *wnt5b* MO (G). (H) Quantification of the normalized apical MHBC intensity in Control versus *wnt5b* morphants. Apical MHBC intensity was divided by the intensity in the middle of the cell (See Appendix B). (I) Quantification of the normalized basal  $\beta$ -tubulin intensity at the MHBC in Control versus *wnt5b* morphants. basal MHBC intensity was divided by the intensity in the middle of the cell. Box plots indicate the 25th and 75th percentiles and the median. Three independent experiments are represented. Control MO, n=7; *wnt5b* MO, n=6. Scale bars: 10  $\mu$ m. Arrowhead indicates MHBC.



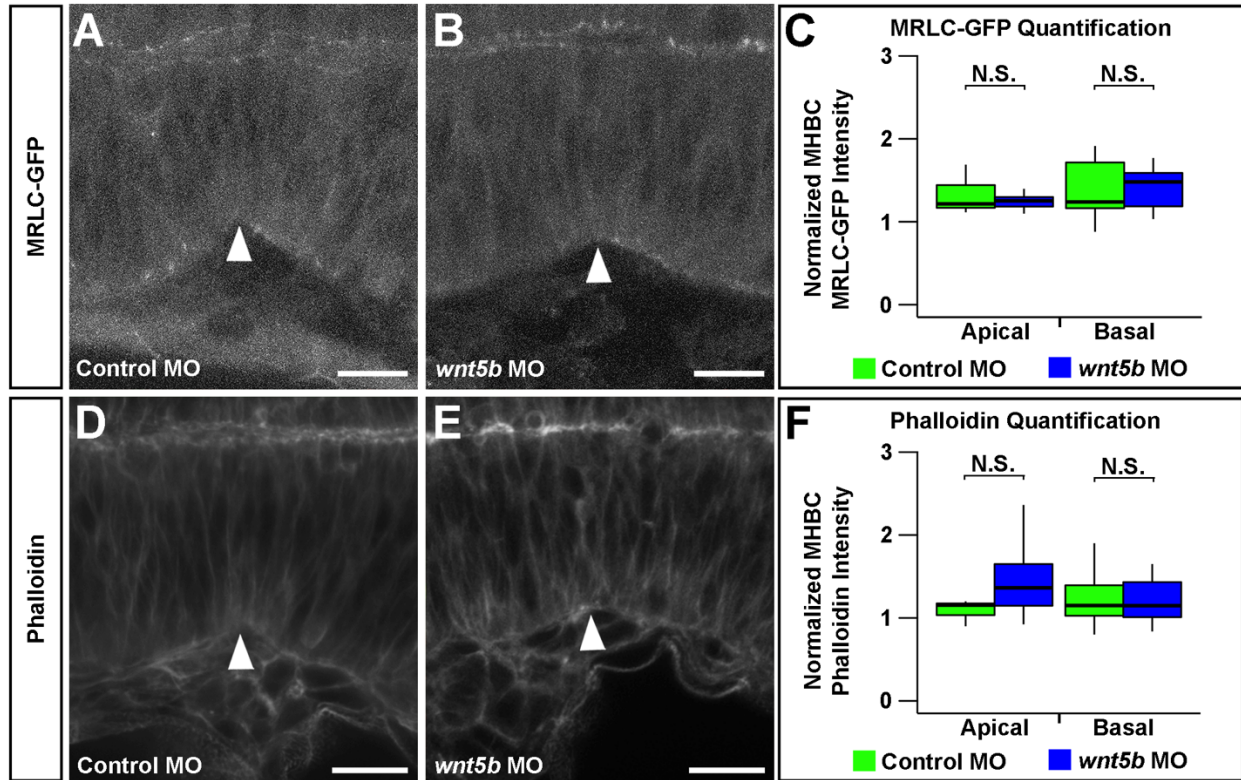


**Figure 29. *wnt5b* knockdown does not affect apical or basal localization of myosin regulatory light chain (MRLC) or actin at the MHBC.** (A,B) Representative confocal images of 10 μm average intensity projections at 24 ss of wild-type embryos co-injected with 150 pg/embryo MRLC-GFP, 50 pg/embryo memCherry, 3 pg/embryo *p53* MO and either 3 pg/embryo Control MO (A) or 3 pg/embryo *wnt5b* MO (B). (C) Quantification of the normalized apical and basal MHBC MRLC-GFP intensity in Control versus *wnt5b* morphants demonstrate no significant difference apically or basally. Box plots indicate the 25th and 75th percentiles and the median. Three independent experiments are represented. Control MO, n=9; *wnt5b* MO, n=8. Scale bars: 10 μm. (D,E) Representative confocal images of 10 μm average intensity projections at 24 ss of phalloidin stained wild-type embryos that were co-injected with 3 pg/embryo *p53* MO and either 3 pg/embryo of Control MO (D) or 3 pg/embryo *wnt5b* MO (E). (F)

Quantification of the normalized apical and basal MHBC intensity in Control versus *wnt5b* morphants demonstrated no significant differences. Box plots indicate the 25th and 75th percentiles and the median. Three independent experiments are represented. Control MO, n=6; *wnt5b* MO, n=7. N.S. (not significant) indicates  $P > 0.05$ . Scale bars: 10  $\mu\text{m}$ . Arrowhead indicates MHBC.

**Movie 2. Control MO EB3-GFP Raw Data Timelapse.** Representative live confocal timelapse at the MHB of an embryo co-injected with memCherry, EB3-GFP mRNA, and Control MO. Timelapse data were acquired at 21-24 ss for 10 minutes at 1 frame per 4 seconds and cropped to 100 seconds. Video plays at 5 frames per second for 5 seconds and shows raw EB3-GFP comets. Arrowhead indicates MHBC. Scale bars: 10  $\mu\text{m}$ . Movie Link (Visetsouk et al., 2018):

<http://static-movie-usa.glencoesoftware.com/source/10.1242/687/7b1dd3677278dfeaa2099a8297961a7cca69552e/DEV167031.MovieS1.avi>

**Movie 3. Control MO EB3-GFP Tracks Timelapse.** Representative live confocal timelapse at the MHB of an embryo co-injected with memCherry, EB3-GFP mRNA, and Control MO. Timelapse data were acquired at 21-24 ss for 10 minutes at 1 frame per 4 seconds and cropped to 100 seconds. Video plays at 5 frames per second for 5 seconds and shows processed EB3-GFP comets and tracks. Images have been processed using the OTSU thresholding method and FIJI Trackmate plugin for particle



tracks. Arrowhead indicates MHBC. Scale bars: 10  $\mu$ m. Movie Link (Visetsouk et al., 2018):

[\[usa.glencoesoftware.com/source/10.1242/687/7b1dd3677278dfeaa2099a8297961a7cca69552e/DEV167031.MovieS2.avi\]\(http://static-movie-usa.glencoesoftware.com/source/10.1242/687/7b1dd3677278dfeaa2099a8297961a7cca69552e/DEV167031.MovieS2.avi\)](http://static-movie-</a></p></div><div data-bbox=)

**Movie 4. *wnt5b* MO EB3-GFP Raw Data Timelapse.** Representative live confocal timelapse at the MHB of an embryo co-injected with memCherry, EB3-GFP mRNA, and *wnt5b* MO. Timelapse data were acquired at 21-24 ss for 10 minutes at 1 frame per 4 seconds and cropped to 100 seconds. Video plays at 5 frames per second for 5 seconds and shows raw EB3-GFP comets. Arrowhead indicates MHBC. Scale bars: 10  $\mu$ m. Movie Link (Visetsouk et al., 2018):

[\[usa.glencoesoftware.com/source/10.1242/687/7b1dd3677278dfeaa2099a8297961a7cca69552e/DEV167031.MovieS3.avi\]\(http://static-movie-usa.glencoesoftware.com/source/10.1242/687/7b1dd3677278dfeaa2099a8297961a7cca69552e/DEV167031.MovieS3.avi\)](http://static-movie-</a></p></div><div data-bbox=)

**Movie 5. *wnt5b* MO EB3-GFP Tracks Timelapse.** Representative live confocal timelapse at the MHB of an embryo co-injected with memCherry, EB3-GFP mRNA, and *wnt5b* MO. Timelapse data were acquired at 21-24 ss for 10 minutes at 1 frame per 4 seconds and cropped to 100 seconds. Video plays at 5 frames per second for 5 seconds and shows processed EB3-GFP comets and tracks. Images have been processed using the OTSU thresholding method and FIJI Trackmate plugin for particle

tracks. Arrowhead indicates MHBC. Scale bars: 10  $\mu\text{m}$ . Movie Link (Visetsouk et al., 2018):

<http://static-movie->

[usa.glencoesoftware.com/source/10.1242/687/7b1dd3677278dfeaa2099a8297961a7cca69552e/DEV167031.MovieS4.avi](http://usa.glencoesoftware.com/source/10.1242/687/7b1dd3677278dfeaa2099a8297961a7cca69552e/DEV167031.MovieS4.avi)

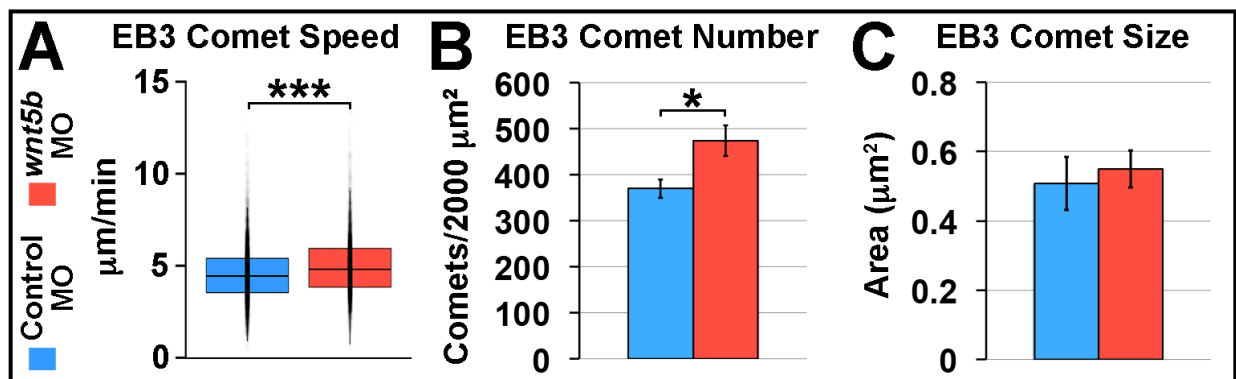


**Figure 30. *Wnt5b* regulates microtubule dynamics at the MHB.** (A-C) Quantification of Control versus *wnt5b* morphants for EB3-GFP comet speed in microns per minute (A), EB3-GFP comet number per 2000  $\mu\text{m}^2$  (B), and EB3-GFP comet size in  $\mu\text{m}^2$  (C). See also Movies 1, 2, 3, and 4. Boxplots indicate the 25th and 75th percentiles and the median. Three independent experiments are represented. EB3-GFP comet speed, Control MO, n=11; *wnt5b* MO, n=7. EB3-GFP comet number and comet size: Control MO, n=11; *wnt5b* MO, n=11. Welch t-tests were conducted to determine significance, \* indicates  $P < 0.05$ , \*\*\* indicates  $P < 0.005$ .

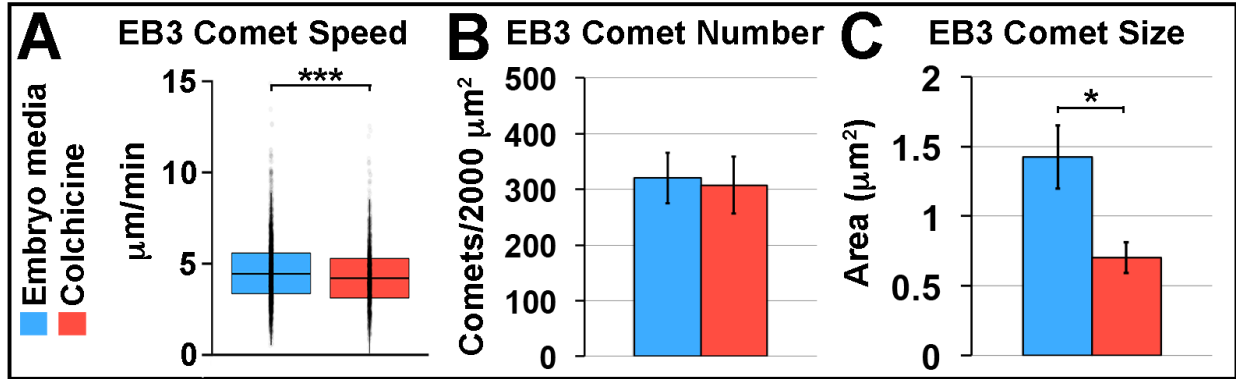


**Figure 31. Colchicine treatment affects microtubule dynamics at the MHBC.** (A-C) Quantification and comparison of 21-24 ss embryos injected with EB3-GFP mRNA and treated at 18 ss with either embryo media or Colchicine. Microtubule plus-end EB3-GFP comet speed in microns per minute (A), EB3-GFP comet number per 2000  $\mu\text{m}^2$  (B), and EB3-GFP comet size in  $\mu\text{m}^2$  (C). Boxplots indicate the 25th and 75th percentiles and the median. Three independent experiments are represented. Control embryo media, n=6; Colchicine, n=6. Welch t-tests were conducted to determine significance, \* indicated  $P < 0.05$ , \*\*\* indicates  $P < 0.005$ .

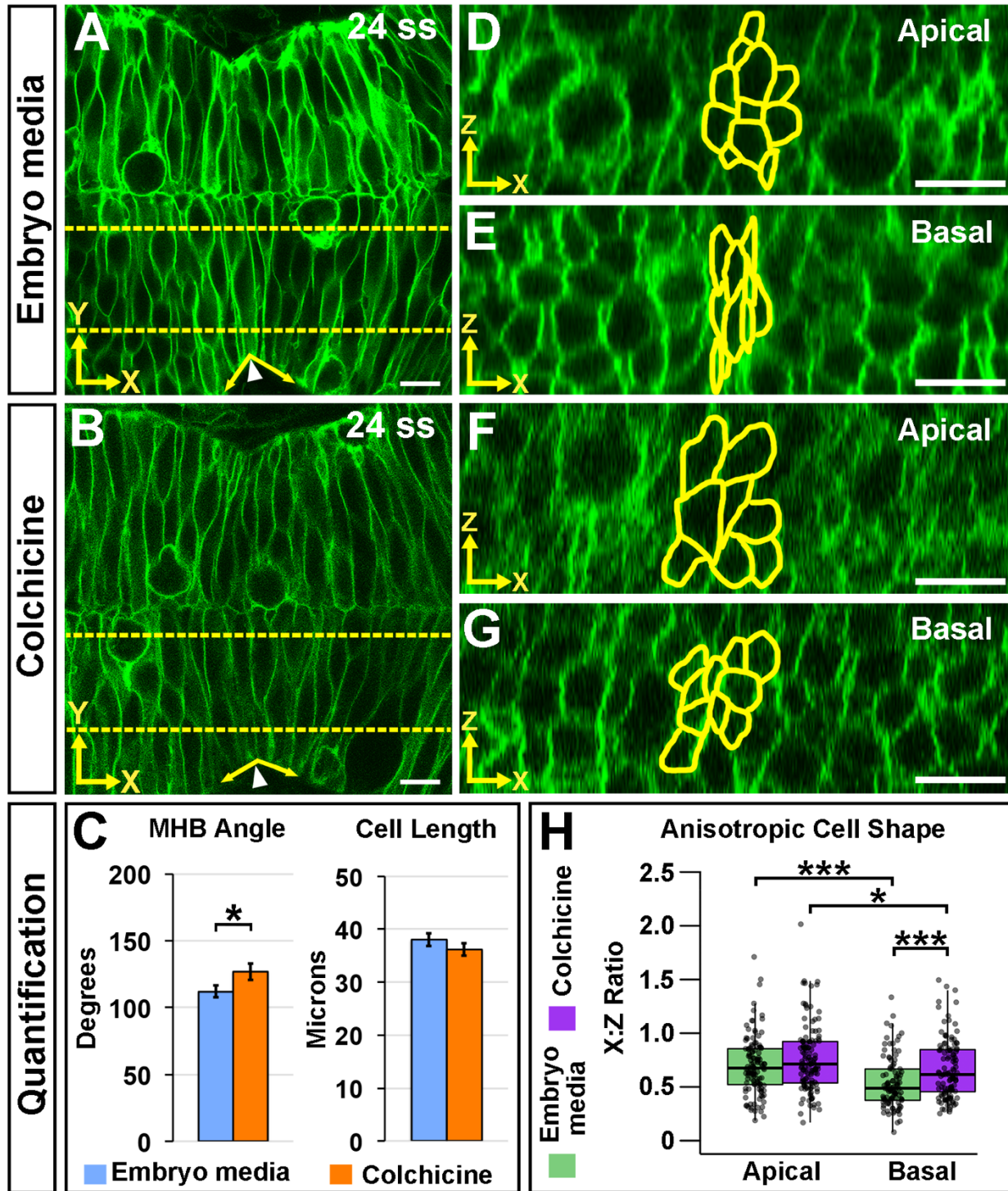


**Figure 32. Microtubule polymerization is required for basal anisotropic cell shape at the MHBC.** (A,B) Live confocal images of 24 ss memGFP injected wild-type embryos treated at 18 ss with Embryo media (A) or Colchicine (B). (C) Quantification of MHB

tissue angle and MHBC cell length. Data are represented as mean  $\pm$  SEM of three independent experiments. (D,E) Apical (D) and basal (E) digital slices of Embryo media treated embryos. (F,G) Apical (F) and basal (G) digital slices of Colchicine treated embryos. MHBC cells outlined in yellow. (H) Quantification of anisotropic cell shape using X:Z ratio. Boxplots indicate the 25th and 75th percentiles and the median. Three independent experiments are represented. Control embryo media, n=7; Colchicine, n=8. \* indicates  $P < 0.05$ , \*\*\* indicates  $P < 0.005$ . Arrowhead indicates MHBC. Scale bars: 10  $\mu\text{m}$ .

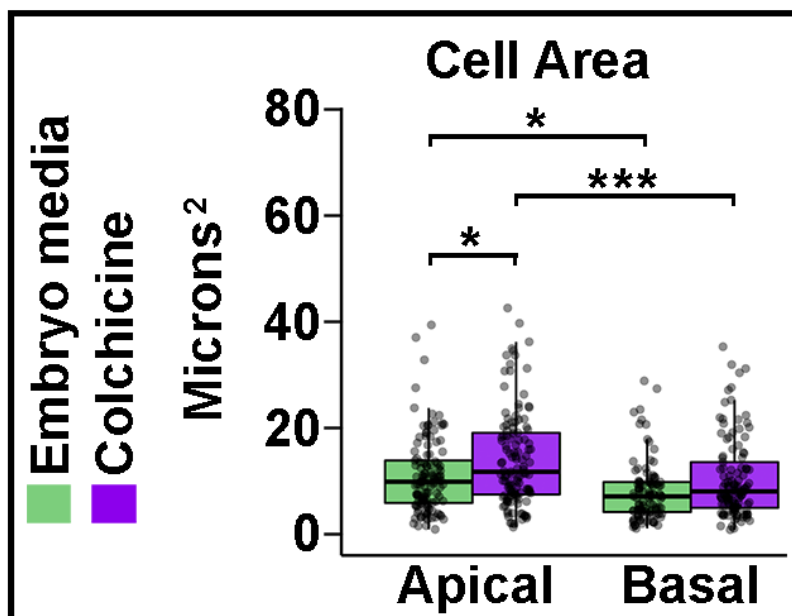


**Figure 33. Colchicine treatment does not affect basal MHBC cell area.**

Quantification of apical and basal cell area of 24 ss wild-type embryos injected with memGFP mRNA and treated at 18 ss with either embryo media or Colchicine. Boxplots indicate the 25th and 75th percentiles and the median. Three independent experiments

are represented. Control embryo media, n=7; Colchicine, n=8. \* indicates  $P < 0.05$ , \*\*\* indicates  $P < 0.005$ .

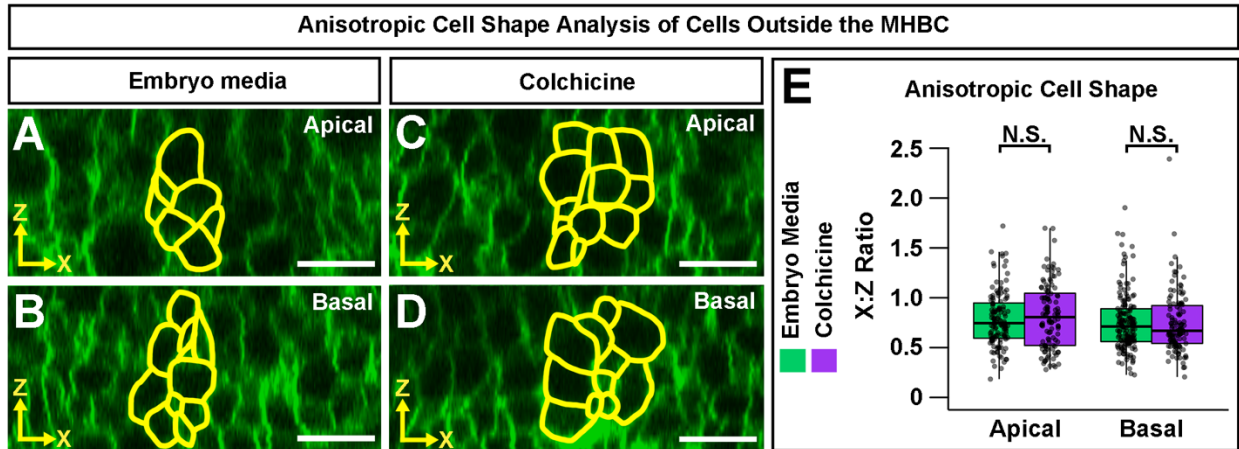


**Figure 34. Colchicine treatment does not affect cell shape outside the MHBC.** (A-D) Representative apical (A,C) and basal (B,D) digital slices of WT 24 ss embryos injected with memGFP and treated with either embryo media (A,B) or Colchicine (C,D). Cells that are 40 microns posterior to the MHBC are outlined in yellow. (E)

Quantification of X:Z ratio of cells outside the MHBC. Box plots indicate the 25th and 75th percentiles and the median. Three independent experiments are represented.

Embryo media, n=7; Colchicine, n=8. N.S. (not significant) indicates  $P > 0.05$ . Scale bars: 10  $\mu\text{m}$ .

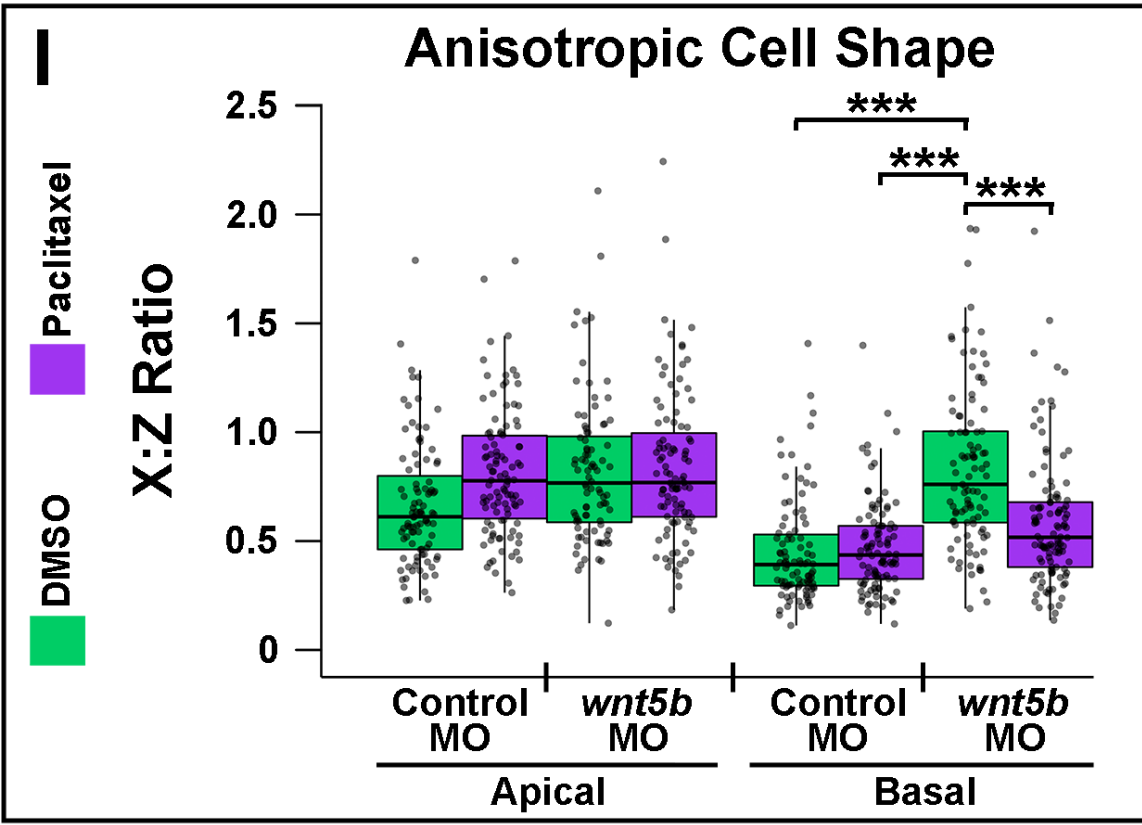
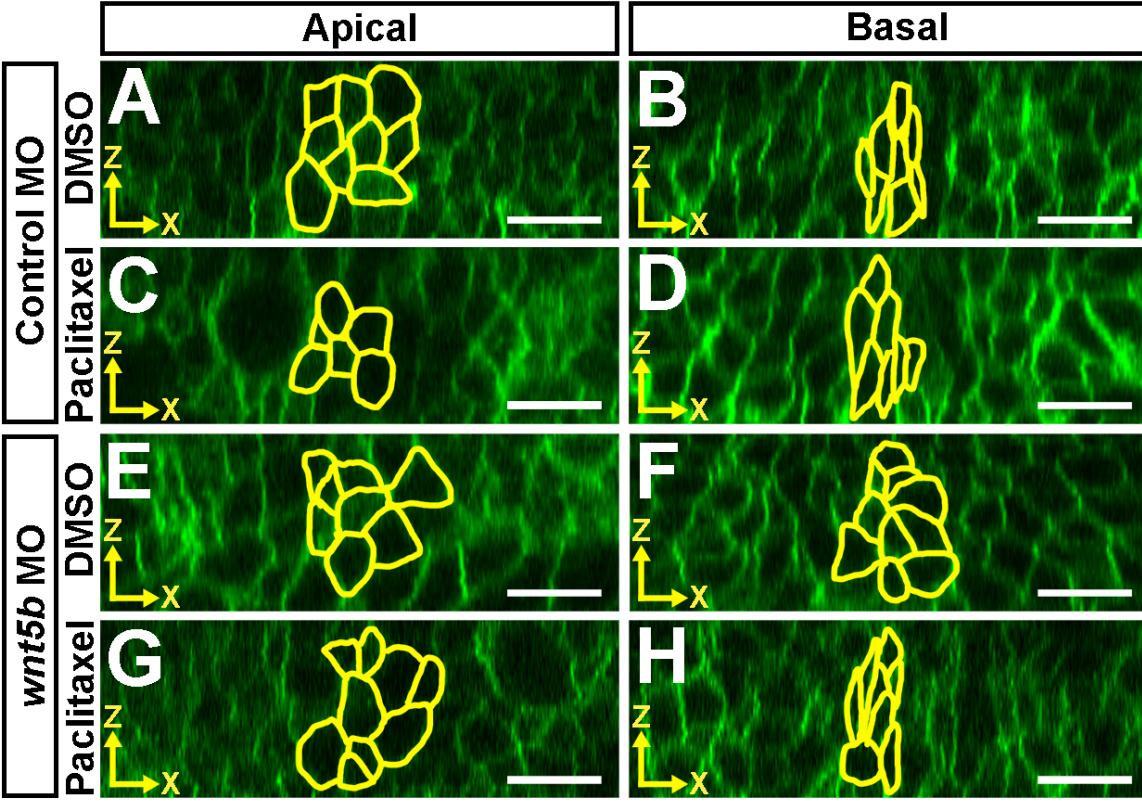




**Figure 35. Microtubule filament stability is required for Wnt5b-mediated basal anisotropic cell shape.** (A-H) Digital slices from Z-series images of wild-type embryos co-injected with memGFP and Control MO (A-D) or *wnt5b* MO (E-H). Embryos were treated at 18 ss with DMSO (A,B,E,F) or Paclitaxel (C,D,G,H) and imaged at 24 ss. MHBC cells are outlined in yellow in apical (A,C,E,G) and basal (B,D,F,H) digital slices. (I) Quantification of anisotropic cell shape using X:Z ratio. Apical measurements are compared post hoc to the Control MO DMSO Apical condition. Basal measurements are compared post hoc to the *wnt5b* MO DMSO Basal condition. Boxplots indicate the 25th and 75th percentiles and the median. Four independent experiments are represented. Control DMSO, n=7; Control Paclitaxel, n=9; *wnt5b* MO DMSO, n= 8; *wnt5b* MO Paclitaxel, n= 8. \*\*\* indicates  $P < 0.005$ . Scale bars: 10  $\mu\text{m}$ .

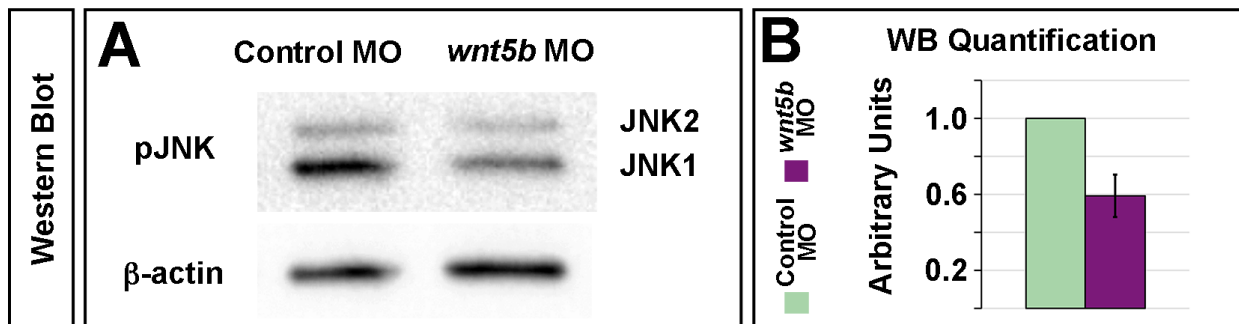


**Figure 36. JNK is regulated by *wnt5b*.** (A) Representative Western blot of phosphorylated JNK (pJNK) and  $\beta$ -actin levels from head tissue of Control and *wnt5b* morphants. (B) Quantification of four independent Western blot experiments, pJNK (JNK1 and JNK2) levels were normalized to  $\beta$ -actin. Data are represented as mean  $\pm$  SD.



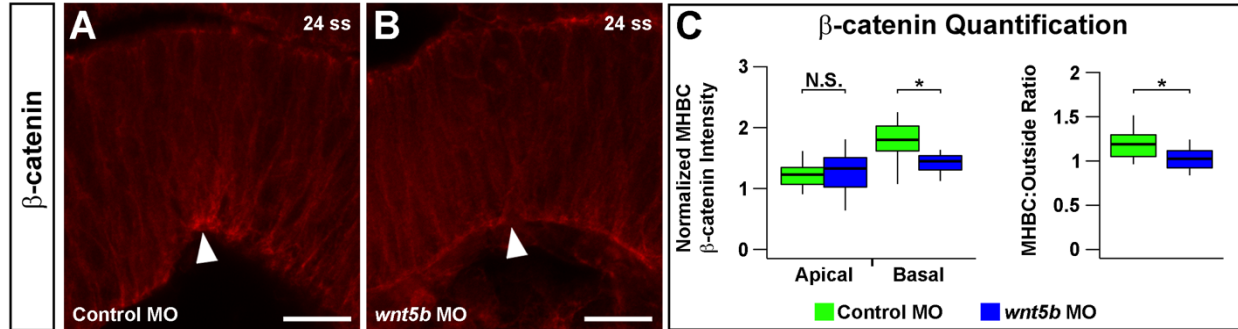


**Figure 37. *wnt5b* knockdown affects basal but not apical localization of  $\beta$ -catenin.**

(A,B) Average intensity projection of 10  $\mu$ m Z-series of 24 ss wild-type embryos co-injected with 3 pg/embryo *p53* MO and either 3 pg/embryo Control MO (A) or 3 pg/embryo *wnt5b* MO (B) and immunostained for  $\beta$ -catenin. (C) Quantification of the normalized apical and basal MHBC intensity and MHBC:Outside intensity ratio in Control versus *wnt5b* morphants. Box plots indicate the 25th and 75th percentiles and the median. Three independent experiments are represented. Control MO, n=8; *wnt5b* MO, n=8. N.S. (not significant) indicates  $P > 0.05$ , \* indicates  $P < 0.05$ . Scale bars: 10  $\mu$ m.

**Movie 6. DMSO EB3-GFP Raw Data Timelapse.** Representative live confocal timelapse at the MHB of an embryo co-injected with memCherry, EB3-GFP mRNA, and treated at 18 ss with DMSO. Timelapse data were acquired at 21-24 ss for 10 minutes at 1 frame per 4 seconds and cropped to 100 seconds. Video plays at 5 frames per second for 5 seconds and shows raw EB3-GFP comets. Arrowhead indicates MHBC. Scale bars: 10  $\mu$ m. Movie Link (Visetsouk et al., 2018):

<http://static-movie-usa.glencoesoftware.com/source/10.1242/687/7b1dd3677278dfeaa2099a8297961a7cca69552e/DEV167031.MovieS5.avi>

**Movie 7. DMSO EB3-GFP Tracks Timelapse.** Representative live confocal timelapse at the MHB of an embryo co-injected with memCherry, EB3-GFP mRNA, and treated at 18 ss with DMSO. Timelapse data were acquired at 21-24 ss for 10 minutes at 1 frame per 4 seconds and cropped to 100 seconds. Video plays at 5 frames per second for 5 seconds and shows processed EB3-GFP comets and tracks. Images have been processed using the OTSU thresholding method and FIJI Trackmate plugin for particle tracks. Arrowhead indicates MHBC. Scale bars: 10  $\mu$ m. Movie Link (Visetsouk et al., 2018):

[\[usa.glencoesoftware.com/source/10.1242/687/7b1dd3677278dfeaa2099a8297961a7cca69552e/DEV167031.MovieS6.avi\]\(http://static-movie-usa.glencoesoftware.com/source/10.1242/687/7b1dd3677278dfeaa2099a8297961a7cca69552e/DEV167031.MovieS6.avi\)](http://static-movie-</a></p></div><div data-bbox=)

**Movie 8. SP600125 EB3-GFP Raw Data Timelapse.** Representative live confocal timelapse at the MHB of an embryo co-injected with memCherry, EB3-GFP mRNA, and treated at 18 ss with SP600125. Timelapse data were acquired at 21-24 ss for 10 minutes at 1 frame per 4 seconds and cropped to 100 seconds. Video plays at 5 frames per second for 5 seconds and shows raw EB3-GFP comets. Arrowhead indicates MHBC. Scale bars: 10  $\mu$ m. Movie Link (Visetsouk et al., 2018):

[\[usa.glencoesoftware.com/source/10.1242/687/7b1dd3677278dfeaa2099a8297961a7cca69552e/DEV167031.MovieS7.avi\]\(http://static-movie-usa.glencoesoftware.com/source/10.1242/687/7b1dd3677278dfeaa2099a8297961a7cca69552e/DEV167031.MovieS7.avi\)](http://static-movie-</a></p></div><div data-bbox=)

**Movie 9. SP600125 EB3-GFP Tracks Timelapse.** Representative live confocal timelapse at the MHB of an embryo co-injected with memCherry, EB3-GFP mRNA, and treated at 18 ss with SP600125. Timelapse data were acquired at 21-24 ss for 10 minutes at 1 frame per 4 seconds and cropped to 100 seconds. Video plays at 5 frames per second for 5 seconds and shows processed EB3-GFP comets and tracks. Images have been processed using the OTSU thresholding method and FIJI Trackmate plugin for particle tracks. Arrowhead indicates MHBC. Scale bars: 10  $\mu\text{m}$ . Movie Link (Visetsouk et al., 2018):

<http://static-movie-usa.glencoesoftware.com/source/10.1242/687/7b1dd3677278dfeaa2099a8297961a7cca69552e/DEV167031.MovieS8.avi>

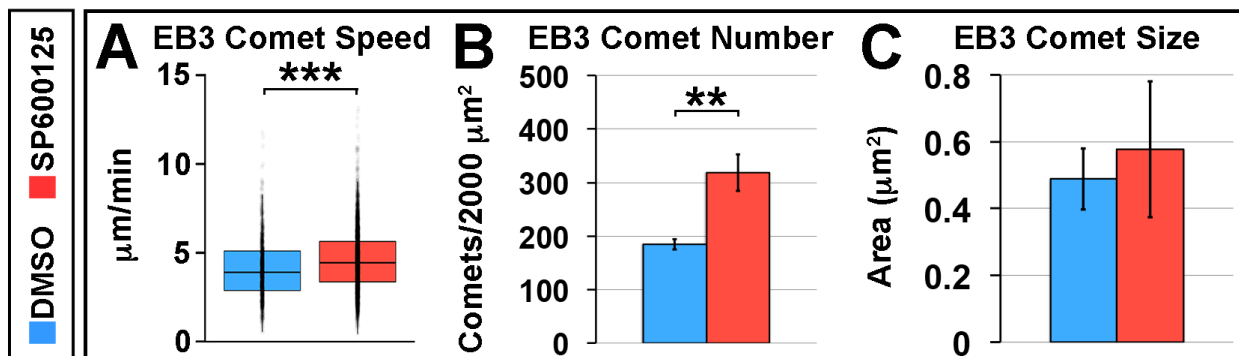


**Figure 38. JNK mediates microtubule dynamics at the MHBC.** (A-C) Quantification of EB3-GFP comet speed in microns per minute (A), EB3-GFP comet number per 2000  $\mu\text{m}^2$  (B), and EB3-GFP comet size in  $\mu\text{m}^2$  (C). Boxplots indicate the 25th and 75th percentiles and the median. Three independent experiments are represented. DMSO, n=6; SP600125, n=7. \*\* indicates P<0.01, \*\*\* indicates P<0.005.

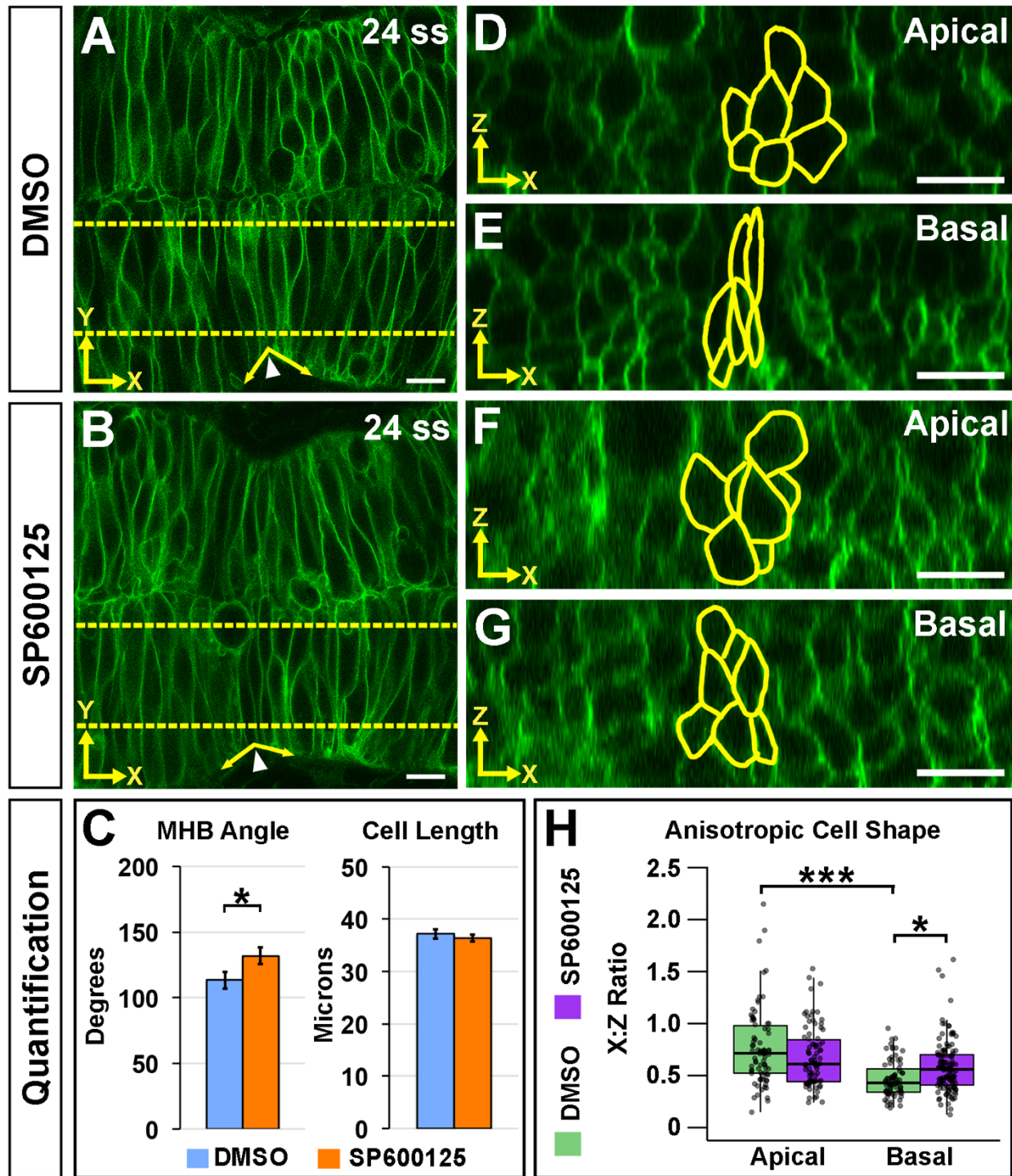


**Figure 39. JNK is required for basal anisotropic MHBC cell shape.** (A,B) Live confocal imaging of 24 ss embryos injected with memGFP and treated with DMSO (A) or SP600125 (B). (C) Quantification and comparison of MHB angle and length. Data

presented as mean  $\pm$  SEM of three independent experiments. (D,E) Apical (D) and basal (E) digital slices of DMSO treated embryos at 24 ss. (F,G) Apical (F) and basal (G) digital slices of SP600125 treated embryos at 24 ss. (H) Quantification of anisotropic cell shape using X:Z ratio in DMSO and SP600125 treated embryos. Boxplots indicate the 25th and 75th percentiles and the median. Three independent experiments are represented. DMSO, n=6; SP600125, n=6. \* indicates  $P < 0.05$ , \*\*\* indicates  $P < 0.005$ . Arrowhead indicates MHBC. Scale bars: 10  $\mu\text{m}$ .

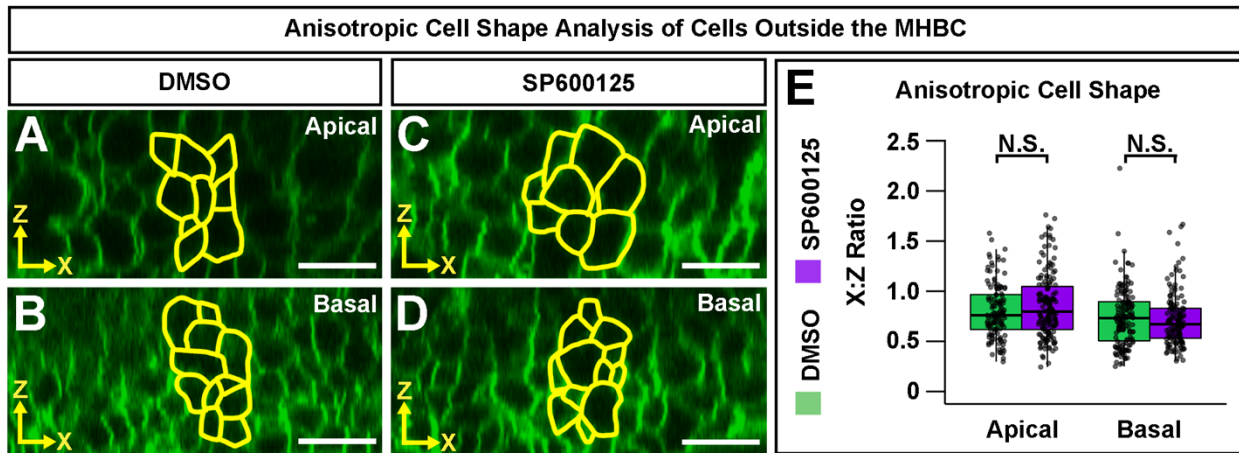


**Figure 40. JNK inhibition does not affect anisotropic cell shape outside the MHBC.** (A-D) Apical (A,C) and basal (B,D) digital slices of WT 24 ss embryos injected with memGFP and treated with either DMSO (E,G) or SP600125 (F,H). Cells that are 40 microns posterior to the MHBC are outlined in yellow. (K) Quantification of X:Z ratio of cells outside the MHBC. Box plots indicate the 25th and 75th percentiles and the median. Three independent experiments are represented. DMSO, n=6; SP600125, n=6. N.S. (not significant) indicates  $P > 0.05$ . Scale bars: 10  $\mu\text{m}$ .

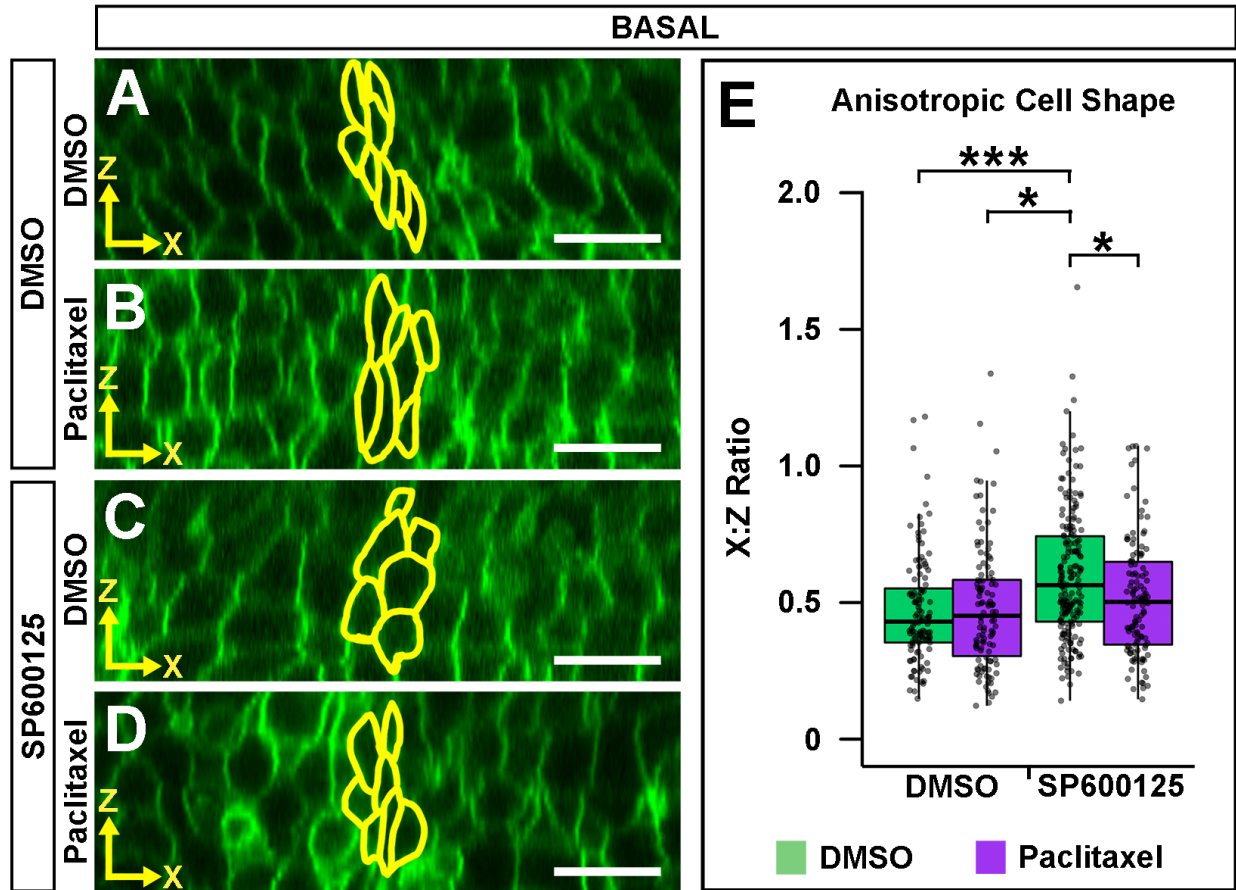


**Figure 41. Microtubule filament stability is required for JNK-mediated basal anisotropic cell shape.** (A-D) Digital slices from Z-series images of memGFP injected wild-type embryos treated at 16 ss with DMSO (A,B) or SP600125 (C,D). Embryos were then treated at 18 ss with DMSO (A,C) or Paclitaxel (B,D) and imaged at 24 ss. MHBC cells are outlined in yellow. (E) Quantification of anisotropic cell shape. All basal X:Z ratios are compared post hoc to the SP600125/DMSO. Boxplots indicate the 25th and 75th percentiles and the median. Four independent experiments are represented. DMSO/DMSO n=6; DMSO/Paclitaxel n=6; SP600125/DMSO n= 10; SP600125/Paclitaxel n= 7. \* indicate  $P < 0.05$ , \*\*\* indicates  $P < 0.005$ . Scale bars: 10  $\mu\text{m}$ .



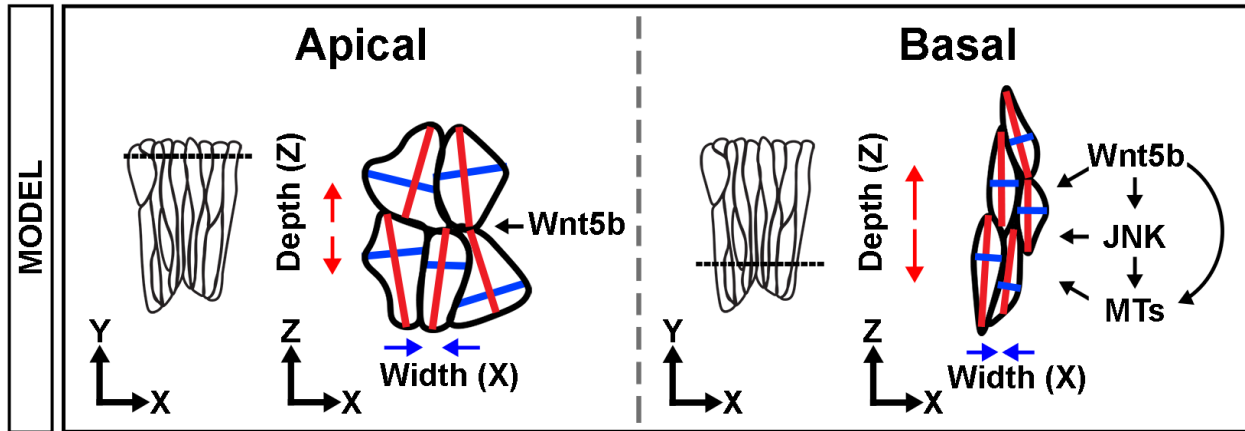


**Figure 42. Proposed mechanism for differential regulation of apical and basal anisotropic cell shape in MHBC cells.** Apically, MHBC cells are anisotropic, where cells are narrower in the anterior-posterior (X) direction and deeper in the dorsal-ventral (Z) direction. This cell shape is dependent on Wnt5b. Basally, Wnt5b, JNK, and microtubules all regulate anisotropic cell shape. Wnt5b and JNK regulation of basal MHBC cell shape is microtubule-dependent. Together, our model suggests that Wnt5b is likely to mediate JNK activation, and in turn affect microtubule stability and dynamics, to specifically regulate basal anisotropic cell shape during early MHB morphogenesis.

### **3.5 Discussion**

From these studies, we propose a mechanistic model for the differential regulation of apical versus basal MHBC anisotropic cell shape at 24 ss to form the basal MHB tissue fold (Figure 42). Apically, our data indicate that Wnt5b functions to maintain anisotropic cell shape in the width (X-axis) and depth (Z-axis) directions. However, we found a different role for Wnt5b, and other downstream factors, basally (Figure 42). On the basal side of the MHBC cells, Wnt5b, JNK, and microtubules are each required to decrease the X:Z ratio and to enhance changes in anisotropic cell shape. This enhancement is in turn required to fold the MHB epithelial tissue along the basal side in the anterior-posterior (X-axis) direction. These new data are consistent with our previous finding that narrowing of MHBC cells in the width (X-axis) direction is required for acute anterior-posterior fold formation. Here we propose that deepening of cells in the depth (Z-axis) direction may be required to restrict the overall tissue shape to generate the sharp MHB fold in two-dimensions. In contrast to the apical side of the cell, Wnt5b regulation of basal MHBC cell shape is microtubule-dependent. In addition, JNK modulates microtubule dynamics in a similar manner at the MHBC and JNK regulation of basal MHBC cell shape is also microtubule-dependent. Collectively, our data suggest a model where Wnt5b mediates JNK activity, which affects microtubule dynamics to specifically regulate basal anisotropic cell shape. We have shown that a single morphogen, Wnt5b, modulates both apical and basal anisotropic cell shape within the same cellular context, but through independent mechanisms where Wnt5b-mediated regulation of basal, but not apical, anisotropic cell shape is microtubule-dependent. Although we know that anisotropic cell shape, basally, at the MHBC is determined by



wnt5b-mediated microtubule stability, the exact mechanism for how Wnt5b specifically elicits this anisotropic cell shape is not yet known.

Microtubules have long been associated with regulating cell and tissue shape, such as neuroepithelial cell elongation (Burnside, 1971; Cearns et al., 2016; Jayachandran et al., 2016; Messier, 1969). Microtubules are also important for apical constriction in fly eye disc epithelium and salivary gland development (Booth et al., 2014; Fernandes et al., 2014), and in bottle cells during *Xenopus* gastrulation (Choi and Sokol, 2009; Lee and Harland, 2007). However, in bottle cells, microtubules were not found to regulate cell length, as they do in cells undergoing neurulation (Lee and Harland, 2007). Similarly, we found that microtubules did not regulate cell length in MHBC cells. This demonstrates that the role of microtubules in mediating different aspects of cell shape is cell context specific. When we perturbed microtubule polymerization with Colchicine, or when we stabilized microtubules using Paclitaxel in *wnt5b* knockdown embryos, basal, but not apical, MHBC cell shape was affected. Consistent with this, during these early stages of MHB morphogenesis, MHBC apical cell shape did not change. However, basal cell shape was more polarized and changed over time, suggesting that earlier stages of MHB folding differentially rely on microtubule-mediated basal cell shape changes.

One possible mechanism for how Wnt5b could modulate apical versus basal cell shape is by regulating apical- and basal-specifically localized proteins to polarize the cells. Shroom3, N-cadherin, and Vangl2 are all apically localized and are required for apical constriction (Morita et al., 2010; Ossipova et al., 2015a; Plageman et al., 2011), while basally localized integrins, focal adhesion kinase (FAK), and the basement membrane are required for basal constriction (Bogdanovic et al., 2012; Gutzman et al., 2018; Gutzman et

al., 2008). Although there have been numerous investigations of apically localized proteins in the context of planar cell polarity (PCP) and regulation of apical cell shape, there are limited studies describing the mechanisms by which basally localized proteins mediate basal cell shape. Here, we demonstrate that  $\beta$ -catenin, a Wnt signaling variant, is enriched basally and specifically at the MHBC, in a *wnt5b*-mediated manner. Based on these data, we propose that Wnt5b regulation of microtubule stability is likely to be required for its polarizing activity within the basal domain of the MHBC cells, which is in turn required for the MHB basal tissue fold (Gutzman et al., 2018).

During MHB basal tissue folding, we also found that Wnt5b modulates JNK activity, a known downstream target of non-canonical Wnt signaling (Komiya and Habas, 2008; Yamanaka et al., 2002; Yang, 2003). We also observed that JNK is necessary for proper basal, but not apical, cell shape and for microtubule dynamics. In addition, inhibition of glycogen synthase kinase 3 beta (GSK3 $\beta$ ), a kinase associated with canonical Wnt signaling, is also sufficient for Wnt5b-mediated tissue folding (Gutzman et al., 2018). This suggests a role for both canonical and non-canonical Wnt signaling in mediating MHB morphogenesis. In addition, both JNK signaling and GSK3 $\beta$  inhibition have been observed within the same cellular context to promote microtubule stability (Ciani and Salinas, 2007). Therefore, we postulate that the observed higher number and greater speed of EB3-GFP comets shown here with knockdown of *wnt5b* and with JNK inhibition, may be due to reduced microtubule stability within the MHBC region and be indicative of a compensatory response to the reduction of total microtubules. Together this leads us to hypothesize that Wnt5b regulation of JNK, and potentially GSK3 $\beta$ , mediate basal anisotropic cell shape through modulation of

microtubule-associated proteins (MAPs) such as microtubule-associated protein 1B (MAP1B), (Chang et al., 2003; Ciani and Salinas, 2007; Feltrin et al., 2012; Gutzman et al., 2018; Jayachandran et al., 2016).

JNK signaling is also a modulator of actomyosin activity. Studies have demonstrated a critical role for the actomyosin network in modulating apical and basal constriction (Gutzman et al., 2015; Martin et al., 2009; Nishimura et al., 2012). One obvious possibility is that Wnt5b affects basal cell shape via regulation of the actomyosin network. Interestingly, our studies did not reveal a direct link between Wnt5b signaling and the actomyosin network (Fig. 25). Upon re-analysis of our previously published data using the orthogonal slice method presented here, we found that non-muscle myosin IIB is required for basal anisotropic cell shape (Visetsouk and Gutzman, unpublished results) (Gutzman et al., 2015). These data confirm a role for the actomyosin network in mediating these cell shape changes, which appear to be Wnt5b-independent. However, we cannot exclude the possibility that Wnt5b-mediated microtubule stability is required to poise the cells to respond to mechanotransduction signals, which could be mediated through the extracellular matrix (Gutzman et al., 2008). Additional examination of potential crosstalk with other signaling pathways will be necessary to identify the specific functions of Wnt5b-mediated microtubule stability, which are likely to be multifactorial.

Since we know that Wnt signaling and microtubules are important for polarized PCP protein localization (Matis et al., 2014; Sepich et al., 2011) and planar polarization of actomyosin networks to regulate apical constriction (Nishimura et al., 2012), it is also possible that Wnt5b mediates trafficking of cargo basally within the X-Z plane of MHBC

cells to control basal MHB folding. Alternatively, microtubules may be required for trafficking of other protein complexes on the basal side of the cells to confer basal tissue folding. It is also possible that redistribution of basal cell membrane via endocytic pathways is important for basal tissue folding; however, it is not likely to be an early mechanism for mediating basal cell shape since we demonstrate that basal cell area is not changing at these early time points. The exact mechanisms for how Wnt5b differentially modulates apical versus basal cell shape remain unknown and will be the focus of future studies.

### **3.6 Contributions**

Mike R Visetsouk and Jennifer H. Gutzman made contributions to the design and performance of experiments, analysis of data, and wrote the manuscript. Elizabeth J Falat, Ryan J Garde, and Jennifer L. Wendlick made contributions to the performance of experiments and analysis of data. All authors collectively edited the final manuscript. This work was supported by UWM Research Growth Initiative to Jennifer H. Gutzman and a UWM AOP fellowship to Mike R Visetsouk.

## Chapter 4

### General Discussion

#### ***4.1 Summary of key findings and future directions.***

Utilizing zebrafish MHB formation as a model, we uncovered two molecular signals that mediate MHB cell shape critical for basal epithelial tissue folding. We found that calcium signaling and Wnt5b signaling are important for different aspects of MHBC cell shape. First, we demonstrated that calcium signaling regulates specifically apical-basal cell length at the MHBC via non-muscle myosin II (NMII) in a Calmodulin- and MLCK-dependent manner. We also revealed that Wnt5b mediates anisotropic cell shape, with cells narrower in the anterior-posterior direction and deeper in the dorsal-ventral direction during MHB basal tissue folding. Wnt5b mediates both apical and basal anisotropic cell shape, but only the basal shape was found to depend on microtubule stability. We showed that Wnt5b modulates JNK signaling and that JNK signaling mediates basal anisotropic cell shape in a microtubule-dependent manner.

In our calcium studies, we found that a calcium binding protein, Calmodulin, encoded by the gene *calmodulin 1a* that is spatially localized at the MHB, modulates phosphorylation of myosin regulatory light chain (MRLC), and regulates MHBC cell length via myosin light chain kinase (MLCK). Collectively, these data suggest a model where calcium signaling, through Calmodulin at the MHBC, activates MLCK to phosphorylate MRLC and regulate NMII function to mediate MHBC cell shortening.

In a previous study, we determined that non-muscle myosin IIA (NMIIA) is the NMII protein that mediates the length of cells at the MHBC, which is similar to the cell shape change that we observed with calcium signaling. Therefore, we hypothesize that calcium signaling specifically modulates NMIIA, but not non-muscle myosin IIB (NMIIB) during MHB basal tissue folding. Future experiments using co-immunoprecipitation of NMII isoforms could be designed to test this hypothesis. Myosin regulatory light chain (MRLC) binds to both the NMIIA and NMIIB and phosphorylation of MRLC (pMRLC) is indicative of NMII activation. Immunoprecipitation of either the NMIIA or NMIIB heavy chains will include bound pMRLC protein and would indicate relative abundance of pMRLC in each isoform that is activated. We could subsequently run a Western blot experiment and immunoblot for protein levels of pMRLC in MHB-specific tissue of 24 ss embryos treated with Thapsigargin or 2-APB to increase or decrease intracellular calcium levels, respectively. This experiment will indicate relative abundance of NMII activation via pMRLC, associated with either NMIIA or NMIIB with changes in intracellular calcium levels. We expect that an increase in intracellular calcium would result in more pMRLC protein associated with NMIIA compared to NMIIB.

We demonstrated that Calmodulin specifically regulates cell length via MLCK, and we know from our previous studies that NMIIA, but not NMIIB, is important for regulating cell length (Gutzman et al., 2015). Future experiments to test how MLCK and Calmodulin affect NMIIA and NMIIB activation could be conducted as described above using co-immunoprecipitation and evaluating associated pMRLC levels. These experiments could be conducted on MHB tissue extracted from 24 ss embryos that

have been injected with MLCK mRNA for over-expression or memGFP mRNA control. We could perform the same experiment with *calmodulin 1a* knockdown.

Our current data do not provide a mechanistic understanding for how NMIIA and NMIIB are differentially regulated *in vivo*. Differential localization of the two isoforms has been observed in cell culture and are important for regulating cell migration, actin organization and sarcomere formation in cardiomyocytes (Fenix et al., 2018), so we hypothesize that NMIIA and NMIIB are differentially localized within MHBC cells. To determine if NMIIA and NMIIB are differentially localized *in vivo* during MHB basal tissue folding, we could generate *myh9b* and *myh10* GFP and RFP knock-in transgenic zebrafish lines using the CRISPR/CAS 9 system. Live confocal imaging could be used to visualize GFP or RFP tagged protein localization at the MHB under different conditions. We could then examine localization of each isoform after intracellular calcium manipulation with Thapsigargin treatment and 2-APB treatment, after *calmodulin 1a* knockdown, or after MLCK overexpression. Location of each NMII isoform within the MHBC cell may indicate where actin contraction networks are positioned for each type of cell shape regulated by the specific NMII isoform. We would expect to see NMIIA localized along the lateral edges of neuroepithelial cells oriented in the apical-basal direction, in which cell shortening occurs. Further, we would expect to see NMIIB localized to the basal side of the cells, where basal constriction occurs.

This dissertation work also revealed a model in which Wnt5b modulates both apical and basal anisotropic cell shape, but only basally through JNK mediation of microtubule stability. Two important questions which we did not address in our Wnt5b studies are: 1. How does Wnt5b regulate apical anisotropic cell shape? 2. How do

microtubules specifically contribute to basal anisotropic cell shape during early MHB morphogenesis?

We know that GSK3 $\beta$  inhibition is important in basal epithelial tissue folding by mediating basal anterior-posterior cell width at the MHB (Gutzman et al., 2018). However, it is not known if GSK3 $\beta$  inhibition is also important in regulating anisotropic cell shape apically or basally. To determine if GSK3 $\beta$  is important for Wnt5b-mediated anisotropic cell shape, we could perform a rescue experiment of *wnt5b* knockdown using dominant-negative GSK3 $\beta$  and quantify anisotropic cell shape apically and basally as we have recently demonstrated. We show that  $\beta$ -catenin, which can accumulate when GSK3 $\beta$  is inhibited, is localized basally at the MHBC by Wnt signaling and may be a downstream effector molecule in directing basal anisotropic cell shape.

Since we found that microtubules are important for basal anisotropic cell shape at the MHBC, and we know that microtubules can function in intracellular trafficking (Rogers and Gelfand, 2000; Xie et al., 2018), next we could ask if microtubules are important for basal trafficking of  $\beta$ -catenin. This could be done using the microtubule depolymerizing drug, colchicine, and conducting immunohistochemistry for  $\beta$ -catenin protein localization as we recently demonstrated (See Appendix F). We would expect to see decreased basal localization of  $\beta$ -catenin with perturbation of microtubules. To determine if  $\beta$ -catenin plays a role in regulating apical and basal anisotropic cell shape in MHBC cells, without affecting early stages of development that require  $\beta$ -catenin, we could use photo-activatable morpholino mediated knockdown of  $\beta$ -catenin and photo-activate the morpholino at the onset of MHB morphogenesis (18 ss). We would then



analyze anisotropic cell shape as previously done and would expect to see a loss of basal, but not apical anisotropic cell shape.

It is possible that during MHB morphogenesis, microtubules may be modulating the intracellular trafficking of molecules basally to mediate the basal epithelial tissue fold. To test this hypothesis, we could track transport vesicles *in vivo* using transgenic zebrafish lines expressing EGFP fused to Rab5c, Rab11a, and Rab7 which are associated with early endosomes, recycling endosomes, and late endosomes, respectively (Clark et al., 2011). Using confocal live imaging of embryos after morpholino-mediated knockdown of *wnt5b*, we could acquire time-lapse images of the MHB and quantify the number, size, and localization of Rab endosome puncta at the MHBC. We would expect to see a decrease in the number of Rab endosome puncta basally, and not a change in the size of the puncta, as this would be indicative of reduced basal intracellular trafficking.

Microtubule filaments have tensile strength that provides protrusive force for cell shaping, as seen during *Drosophila* wing development and neuroepithelial cell elongation in zebrafish (Jayachandran et al., 2016; Singh et al., 2018). One possibility is that microtubules provide protrusive force for MHB basal epithelial tissue folding. Microtubule filaments may be oriented basally along the dorsal-ventral direction to stabilize cell depth, while cell contraction proceeds in the anterior-posterior direction via NMII activity. Our studies did not reveal a role for *Wnt5b* in regulating actin or myosin localization at the MHBC and did not reveal any changes in cell area, suggesting that anisotropic cell shape may require stabilization of one cell dimension during cell contractility. To test this hypothesis, we could conduct an immunohistochemistry

experiment. We could stain for  $\beta$ -tubulin to label total microtubules and stain for anti-detyrosinated tubulin (glu-tub) which labels stable microtubules (Jayachandran et al., 2016). We could then compare basal MHB tissue sections of *wnt5b* morphants to control morphants. We expect to see a greater abundance of both total and stable microtubule filaments (glu-tub) oriented in the dorsal-ventral direction compared to the anterior-posterior direction in control embryos, which might suggest more protrusive force and stability in the dorsal-ventral direction compared to the anterior-posterior direction.

Wnt signaling may activate calcium signaling; however, we did not find a role for calcium in regulating cell width, as was found for Wnt5b during MHB formation. Therefore, to rule out the possibility that Wnt5b activates calcium signaling, calcium transient events could be analyzed using the GCAMP6s-eGFP reporter with *wnt5b* MO knockdown or using a *wnt5b* mutant, *pipetail*. Here, we could quantify the frequency of calcium transient events found at the MHBC and outside of the MHBC and compare between each condition. We could normalize the baseline intensity of GFP signal at the MHBC to outside of the MHBC and compare this normalized value between each condition. We would expect to see no difference in Wnt5b-mediated intracellular calcium levels if Wnt5b does not activate calcium signaling. Complementary rescue experiments could be performed using Thapsigargin to increase intracellular calcium levels in *wnt5b* morpholino-mediated knockdown embryos, followed by live confocal imaging and quantification of anisotropic cell shape. Since we hypothesize that Wnt5b does not regulate cell shape via calcium signaling, we would not expect to see a rescue of anisotropic cell shape, either apically or basally.

Here, we have demonstrated how cell and tissue shaping can be controlled by two upstream signaling molecules using two different cytoskeletal networks. Several questions remain to be answered. What are other potential upstream regulators of cell shape during MHB basal epithelial tissue folding? Do microtubules behave similarly in other systems where anisotropic cell shape is generated? Addressing these additional questions will be an important next step in building a more comprehensive model for the molecular mechanisms that mediate basal tissue shaping during development.

## ***4.2 Mechanisms employed to control specific aspects of cell shape.***

### ***4.2.1 The role of molecular cues and molecular context in determining cell shape***

Similar molecular signals can control different types of cell shapes. For example, three distinctive roles have been shown for calcium in cell shaping within three distinctly different developmental processes. Calcium signaling during neural tube closure results in apical constriction and is mediated by the calcium-dependent intracellular protease, Calpain2 (Christodoulou and Skourides, 2015). During *Drosophila* egg chamber elongation, calcium signaling results in basal contraction and is Rho- and Rock-regulated (He et al., 2010). And our work demonstrates that during MHB morphogenesis, calcium is important for regulating cell length in the apical-basal direction and depends on the intracellular mediators, Calmodulin and MLCK (Sahu et al., 2017).

Wnt signaling has also been shown to mediate different cell shapes. Wnt regulates apical constriction during lung epithelium morphogenesis through  $\beta$ -catenin (Fumoto et al., 2017). Wnt5b signaling is suggested to be important for apical constriction during convergence and extension through regulation of planar cell polarity proteins, such as Vangl2, to control actomyosin activity (Lin et al., 2010; Ossipova et al., 2015b; Rochard et al., 2016; Sepich et al., 2011). However, within the context of MHB morphogenesis, Wnt5b regulates basal constriction which depends on GSK3 $\beta$  (Gutzman et al., 2018). In addition, our work now reveals a model in which Wnt5b mediates basal MHBC anisotropic cell shape through JNK signaling and microtubules.

Evidence also exists where similar cell shape changes are mediated by different types of molecular cues. For instance, the morphogenetic process of apical constriction can be induced by Wnt signaling during gastrulation in *C. elegans* and zebrafish (Lee et al., 2006; Lin et al., 2010; Sepich et al., 2011), calcium signaling during neural tube closure in *Xenopus* (Christodoulou and Skourides, 2015), BMP signaling during olfactory placode formation in chick (Jidigam et al., 2015), and Notch signaling during zebrafish lateral line development (Kozlovskaja-Gumbriene et al., 2017). Since different molecular cues can regulate a variety of cell shapes and cells have multi-faceted structures, having a diversity of independent regulatory mechanisms that can run in parallel within the same tissues and cells may be important for modulating the overall morphologies. For instance, Wnt signaling may regulate NMII function through the effector molecules RhoA and ROCK, meanwhile calcium regulates NMII function; however, via a different mechanism, Calmodulin and MLCK.

Our work demonstrates an example of how independent signaling pathways mediate different cell shapes but in the same cells. Calcium signaling modulates NMII protein to mediate apical-basal cell length, while Wnt5b signaling modulates JNK and microtubules to mediate anterior-posterior cell width and dorsal-ventral cell depth, basally, in the same MHBC cells. We found that Wnt5b signaling regulates apical anisotropic cell shape, but the mechanism is unclear and independent of the JNK and microtubule-mediated pathway.

Different signaling pathways share similar downstream effector molecules, with a common example being NMII. NMII can be activated by RhoA/ROCK or Calmodulin/MLCK, downstream of Wnt or Calcium signaling, respectively. Additionally, BMP signaling employs RhoA for mediating apical constriction through the actin cytoskeleton in chick placode invagination (Jidigam et al., 2015). In order to separate pathways that might converge or engage in cross-talk, cells may localize and restrict activation of signaling pathways and downstream effectors within a specific region or cellular domain, including apically or basally. This would allow different parts of the cell to respond independently to the different cues, through restricted localization or activation of the signaling components. For instance,  $\beta$ -integrin, a transmembrane adhesion receptor (Hynes, 2002), can be localized basally by NUMB and Ojoplano transmembrane protein and is important for basal contraction during optic cup morphogenesis (Bogdanovic et al., 2012; Nicolas-Perez et al., 2016; Sidhaye and Norden, 2017). Laminin, which can function in cell signaling through  $\beta$ -integrins (Hynes, 2002), is found to be important for basal accumulation of actomyosin and basal contraction during optic cup morphogenesis (Bryan et al., 2016; Sidhaye and Norden,

2017) and basal accumulation of actin as well as basal constriction during MHB formation (Gutzman et al., 2008). However, it is not known if laminin plays a signaling role during optic cup or MHB formation.

We have demonstrated that both cues and context are critical for differentially modulating cell shape. Molecular cues can modulate different cell shapes depending on the intracellular contexts that are important for determining which signaling pathways are activated. Examples also exist for different molecular cues that modulate similar cell shapes, which largely depend upon the intracellular context.

#### 4.2.2 Cytoskeletal networks in defining cell shape

One important morphogenetic mechanism for regulating cell shape is by localizing cytoskeletal filaments to a particular region of the cell, such as apical or basal, and orienting the cytoskeletal filaments along a particular cell direction, for instance, medial-lateral or anterior-posterior. As an example, localized recruitment of RhoGEF and ROCK have been shown to orient actin and activated myosin along the medial-lateral edges of cells during neural tube closure to promote polarized contractility (Nishimura et al., 2012). Although we know that calcium modulates NMII proteins to control apical-basal cell length, we do not know if there is a difference in localization of NMII protein or protein function. During *Drosophila* wing development, upstream cues from planar cell polarity signals orient microtubule filaments at adherens junctions and coordinate protrusive cytoskeletal forces from proximal to distal, causing cells to produce anisotropic cell shape (Singh et al., 2018). During MHB basal epithelial tissue folding, we now demonstrate that microtubules are enriched basally at the MHBC in a

Wnt5b-dependent manner. Although Wnt5b-mediated microtubules are critical for developing anisotropic basal cell shape, it is not known if microtubule filaments are oriented in a specific direction along the basal side.

Cytoskeletal function can be controlled by modulating protein abundance, or availability, of its constituent monomers. Stathmin, for instance, can bind and sequester tubulin dimers to reduce microtubule polymerization activity and promote catastrophe (Chauvin and Sobel, 2015; Etienne-Manneville, 2010). We show that Wnt5b signaling stabilizes or enhances the protein levels of  $\alpha$ - and  $\beta$ -tubulin at the MHB, but the mechanism for this remains unclear. Actin monomer availability may also be modulated in addition to actomyosin regulation through calcium signaling during MHB morphogenesis, but we have not examined this.

Cytoskeletal dynamics are often regulated by cytoskeletal binding proteins. For instance, microtubule associated proteins provide an additional level of microtubule regulation. We observed that Wnt5b mediates JNK activation at the MHB. We also revealed that JNK signaling is important for mediating MHBC basal anisotropic cell shape in a microtubule-dependent manner. JNK signaling has been shown to regulate downstream microtubule associated proteins (MAPS) like MAP1b that affect microtubule dynamics (Chang et al., 2003). Therefore, we hypothesize that Wnt5b activation of JNK signaling may regulate microtubules through MAPs. Actin polymerizing activity can be regulated by members of the Rho small protein GTPases including Rac1 and Cdc42, but it is not known if they play a role during MHB basal epithelial tissue folding. Actin-binding proteins that modulate actin polymerization,

depolymerization, or nucleation, such as profilin, cofilin, and formin, have not yet been examined during MHB morphogenesis.

The force generating mechanism of the actin cytoskeleton depends on the biochemical activation of NMII motor proteins via phosphorylation of MRLC. During MHB morphogenesis, calcium was now shown to signal to MLCK via Calmodulin to phosphorylate MRLC and induce cell shortening at the MHBC.

During basal epithelial tissue folding, we revealed the importance of the microtubule cytoskeleton in regulating anisotropic cell shape, basally and provide data showing that Wnt5b regulates stabilization and basal localization of microtubules. However, it remains unclear how stabilization is conferred or if microtubules are oriented along a specific direction on the basal side to control anisotropic cell shape. We further identified a role for Calmodulin and MLCK in differentially modulating apical-basal cell length during MHB morphogenesis through regulating NMII function. However, it is not clear how actin polymerization is regulated or if localization of NMII protein and protein function contribute to the underlying mechanisms for apical-basal cell length changes.

#### 4.2.3 Intracellular protein localization in determining shape

Proteins may be asymmetrically localized to different regions of a cell and could possibly drive cell domain specific shapes. For instance, asymmetrically localized cell membrane proteins, such as the apical adhesion complexes adherens junctions and tight junctions, can link to and localize the cytoskeleton. Examples include the protein



Celsr1, which controls medial-lateral actin accumulation and myosin dynamics apically, during neural tube closure (Nishimura et al., 2012). Nectin-2 and N-cadherin are cell adhesion proteins that link to F-actin networks to drive apical constriction (Morita et al., 2010). A family of tight junction proteins, Claudins, are required for normal apical accumulation of Vangl2, RhoA, and the phosphorylated form of myosin regulatory light chain to produce apical actomyosin-mediated constriction of cells during convergence and extension (Baumholtz et al., 2017).

In epithelial cells, cell adhesions can occur on the basal side. For example, basal cell adhesion to an extracellular matrix can be conferred by the focal adhesion complex (Burrige and Chrzanowska-Wodnicka, 1996). Several components make up the focal adhesion complex including  $\beta$ -integrins, vinculin, talin, paxillin, and  $\alpha$ -actinin, many of which have actin-binding domains that can function to stabilize actomyosin presence and modulate actomyosin dynamics within the basal domain (Burrige and Chrzanowska-Wodnicka, 1996). Basal localization of  $\beta$ -integrin was previously found to be dependent on a less-understood transmembrane protein, ojoplano (Bogdanovic et al., 2012; Martinez-Morales et al., 2009). Ojoplano inhibited basal  $\beta$ -integrin internalization by antagonizing NUMB-mediated endocytosis and is important for basal constriction during optic cup morphogenesis (Bogdanovic et al., 2012; Martinez-Morales et al., 2009).

$\beta$ -catenin, a known Wnt signaling molecule, binds and modulates E-cadherin-mediated cell adhesion and linkage to the actin cytoskeleton (Brembeck et al., 2006), but it is not clear if this function is important for mediating cell shape changes. Interestingly, in our studies, we observed that  $\beta$ -catenin is enriched basally, in a Wnt5b-

mediated manner. GSK3 $\beta$  inhibition, which is known to downregulate  $\beta$ -catenin protein levels, is sufficient to rescue the Wnt5b basal constriction defect (Gutzman et al., 2018). Therefore, we hypothesize that basal enrichment of  $\beta$ -catenin during MHB formation may function in mediating adhesion basally. However, it is not known if  $\beta$ -catenin is important for MHB basal tissue folding.

We have just begun to reveal the mechanisms underlying control of cell shape during basal tissue folding; however, many questions remain. What molecular contexts can independently coordinate apical versus basal cell shape changes? How does Wnt5b modulate microtubules? How does microtubule stability lead to changes in basal cell shape? Exploring these questions will be an important next step in the investigation of basal epithelial tissue folding.

### ***4.3 Differential cell shapes determine tissue structure.***

*In vivo* studies of morphogenesis have revealed several different tissue structures (Figures 2). The examples from these morphogenetic studies show that similar cell shaping mechanisms, such as cell constriction, are shared between different types of tissue shapes. However, the way that cell shapes are spatially arranged within the larger context of the tissue is important for determining overall tissue structure.

#### **4.3.1 Apical versus basal tissue structures**

Cell constriction apically versus basally is important for generating apical tissue structures versus basal tissue structures, respectively. The morphogenesis of the lens

placode in mouse (Muccioli et al., 2016) to form an apical tissue dome, salivary glands in *Drosophila* to form an apical tissue cone (Sanchez-Corrales et al., 2018), the neural tube in chick to form an apical tissue bend (Nishimura et al., 2012), and the ventral furrow in *Drosophila* to generate an apical tissue fold (Heer et al., 2017; Martin et al., 2009) all require apical constriction of cells. On the other hand, basal tissue shapes like the basal dome requires basal constriction. For example, during morphogenesis of the optic cup in zebrafish, cells are found to constrict basally (Bryan et al., 2016; Sidhaye and Norden, 2017). Morphogenesis of the MHB also requires basal constriction, but for the formation of a basal tissue fold (Gutzman et al., 2018; Gutzman et al., 2008; Gutzman et al., 2015; Sahu et al., 2017). Here we contribute data showing that during the course of zebrafish MHB basal tissue folding, MHBC cells become more anisotropic in shape basally relative to apically. Basal cones and basal bends have not yet been observed *in vivo*, but we hypothesize that these shapes would also require basal constriction.

#### 4.3.2 Radial versus axial tissue structures

Radial versus axial tissue structures require shape changes either radially from a center point or in a specific direction of the tissue. During lens placode invagination in mice, cells apically constrict isotropically and radially from the center of the tissue invagination to form a radial apical dome (Muccioli et al., 2016). In contrast, axial tissue shaping during neural tube formation in chick shows that apical constriction occurs in cells along the anterior-posterior axis of the neural plate tissue (Nishimura et al., 2012). Here, we provide new data demonstrating that axial tissue shaping requires cell shape

changes along a specific direction of the tissue. Digital slices of our confocal images, oriented in the anterior-posterior and dorsal-ventral plane, reveal cells that change shape linearly, but not radially, along the dorsal-ventral direction.

Interestingly, at the periphery of the lens placode in mice, the apical constriction of cells becomes anisotropic, where cell edges along the circumference of the placode are longer compared to perpendicular cell edges (Muccioli et al., 2016). We hypothesize that at the boundary between the central lens placode and the peripheral ectoderm is an example of a complex basal tissue fold that circumferentially, instead of axially or radially, delineates the lens from the surrounding ectoderm in mice embryos. It is important to mention that anisotropic cell shape is one mechanism for generating axial tissue shapes, but it is not the only possible means and can be mediated by other factors including induction by cell cortical junctions (Gomez-Galvez et al., 2018). However, the anisotropic cell shape within a tissue may be indicative of the presence of an axial tissue shape.

#### 4.3.3 Tissue bends versus tissue folds

Tissue bends versus tissue folds require the spatial arrangement of the cell contractions to occur either throughout the tissue in the case of a bend, or at the deepest point of the hinge in the case of a fold. During neural tube formation in chick, polarized recruitment of the actin-myosin contractility network in cells throughout the neural plate resulted in apical anisotropic constriction in the medial-lateral direction (Nishimura et al., 2012) and caused the overall neural plate to generate a tissue bend. Meanwhile in some instances of neural tube formation within the same model system or

in other species like *Xenopus*, only certain cells at the midline of the neural plate, called the medial hinge point cells, apically constrict and generate an apical tissue fold (Poznanski et al., 1997; Schroeder, 1970; Vijayraghavan and Davidson, 2017). Additionally, in *Xenopus*, some laterally positioned cells in the neural plate (Poznanski et al., 1997; Schroeder, 1970; Vijayraghavan and Davidson, 2017) apically constrict to promote apical tissue folding. The medial and lateral hinge point cells collectively fold the neural plate into their tubular tissue structure in *Xenopus*. One hypothesis for why the neural tube can form from tissue bends and tissue folds, both within the same model system and between species, is that the relative sizes and the mechanical strain both intrinsic and extrinsic to the neuroepithelium are different and require more or less work by actomyosin to generate the tissue structures. Together, these findings demonstrate that tissue bending requires cells throughout the neuroepithelium to constrict, while tissue folding requires constriction in a specific group of cells at the deepest hinge point of the neural plate. Here, we present new data to support a model in which specific basal shape changes are required at the hinge point of the MHB tissue fold.

The work of this dissertation reveals that anisotropic cell shape at the hinge point of the MHB is required for basal epithelial tissue folding. However, we demonstrate that greater anisotropic cell shape basally is critical for folding the tissue towards the basal side of the neural tube. We provide data suggesting that basal cell shaping during MHB basal tissue folding, occurs specifically along the dorsal-ventral tissue axis.

#### **4.4 Concluding remarks**

Uncovering the molecular mechanisms that control epithelial tissue morphogenesis during development is a necessary first step in understanding the pathogenesis of structural birth defects. Potential therapeutic targets or preventative measures can subsequently be determined from what we learn about these basic morphogenetic mechanisms. Progress in the field of regenerative medicine will benefit from our understanding of epithelial tissue morphogenesis. The limited regenerative capabilities of humans drive a need for us to build complex tissue and organ structures *in vitro*, which requires an understanding for which molecular cues and context will be important for shaping the cells and tissue models. *In vitro* tissue models may have a future in personalized transplant therapy, in modeling of human diseases, and in high-throughput testing for toxicological or therapeutic effects of different products.

## References

- Ashworth, R., Devogelaere, B., Fabes, J., Tunwell, R. E., Koh, K. R., De Smedt, H. and Patel, S.** (2007). Molecular and functional characterization of inositol trisphosphate receptors during early zebrafish development. *J Biol Chem* **282**, 13984-13993.
- Avagliano, L., Massa, V., George, T. M., Qureshy, S., Bulfamante, G. P. and Finnell, R. H.** (2018). Overview on neural tube defects: From development to physical characteristics. *Birth Defects Res.*
- Barreda, E. G. and Avila, J.** (2011). Tau regulates the subcellular localization of calmodulin. *Biochem Biophys Res Commun* **408**, 500-504.
- Basson, M. A. and Wingate, R. J.** (2013). Congenital hypoplasia of the cerebellum: developmental causes and behavioral consequences. *Front Neuroanat* **7**, 29.
- Baumholtz, A. I., Simard, A., Nikolopoulou, E., Oosenbrug, M., Collins, M. M., Piontek, A., Krause, G., Piontek, J., Greene, N. D. E. and Ryan, A. K.** (2017). Claudins are essential for cell shape changes and convergent extension movements during neural tube closure. *Dev Biol* **428**, 25-38.
- Berridge, M. J., Lipp, P. and Bootman, M. D.** (2000). The versatility and universality of calcium signalling. *Nat Rev Mol Cell Biol* **1**, 11-21.
- Bogdanovic, O., Delfino-Machin, M., Nicolas-Perez, M., Gavilan, M. P., Gago-Rodrigues, I., Fernandez-Minan, A., Lillo, C., Rios, R. M., Wittbrodt, J. and Martinez-Morales, J. R.** (2012). Numb/Numbl-Opo antagonism controls retinal epithelium morphogenesis by regulating integrin endocytosis. *Dev Cell* **23**, 782-795.
- Booth, A. J. R., Blanchard, G. B., Adams, R. J. and Roper, K.** (2014). A dynamic microtubule cytoskeleton directs medial actomyosin function during tube formation. *Dev Cell* **29**, 562-576.
- Bootman, M. D., Collins, T. J., Mackenzie, L., Roderick, H. L., Berridge, M. J. and Peppiatt, C. M.** (2002). 2-aminoethoxydiphenyl borate (2-APB) is a reliable blocker of store-operated Ca<sup>2+</sup> entry but an inconsistent inhibitor of InsP<sub>3</sub>-induced Ca<sup>2+</sup> release. *FASEB J* **16**, 1145-1150.
- Bovolenta, P. and Martinez-Morales, J. R.** (2018). Genetics of congenital eye malformations: insights from chick experimental embryology. *Hum Genet.*

- Brembeck, F. H., Rosario, M. and Birchmeier, W.** (2006). Balancing cell adhesion and Wnt signaling, the key role of beta-catenin. *Curr Opin Genet Dev* **16**, 51-59.
- Brues, A. M. and Cohen, A.** (1936). Effects of colchicine and related substances on cell division. *Biochem J* **30**, 1363-1368 1361.
- Bryan, C. D., Chien, C. B. and Kwan, K. M.** (2016). Loss of laminin alpha 1 results in multiple structural defects and divergent effects on adhesion during vertebrate optic cup morphogenesis. *Dev Biol* **416**, 324-337.
- Bulinski, J. C., Gruber, D., Faire, K., Prasad, P. and Chang, W.** (1999). GFP chimeras of E-MAP-115 (ensconsin) domains mimic behavior of the endogenous protein in vitro and in vivo. *Cell Struct Funct* **24**, 313-320.
- Burnside, B.** (1971). Microtubules and microfilaments in newt neuralation. *Dev Biol* **26**, 416-441.
- Burridge, K. and Chrzanowska-Wodnicka, M.** (1996). Focal adhesions, contractility, and signaling. *Annu Rev Cell Dev Biol* **12**, 463-518.
- Caceres, A., Bender, P., Snavely, L., Rebhun, L. I. and Steward, O.** (1983). Distribution and subcellular localization of calmodulin in adult and developing brain tissue. *Neuroscience* **10**, 449-461.
- Cearns, M. D., Escuin, S., Alexandre, P., Greene, N. D. and Copp, A. J.** (2016). Microtubules, polarity and vertebrate neural tube morphogenesis. *J Anat* **229**, 63-74.
- Chang, L., Jones, Y., Ellisman, M. H., Goldstein, L. S. B. and Karin, M.** (2003). JNK1 Is Required for Maintenance of Neuronal Microtubules and Controls Phosphorylation of Microtubule-Associated Proteins. *Dev Cell* **4**, 521-533.
- Chauvin, S. and Sobel, A.** (2015). Neuronal stathmins: a family of phosphoproteins cooperating for neuronal development, plasticity and regeneration. *Prog Neurobiol* **126**, 1-18.
- Cheeseman, C.** (1992). Role of intestinal basolateral membrane in absorption of nutrients. *Am J Physiol* **263**, R482-488.
- Choi, S. C. and Sokol, S. Y.** (2009). The involvement of lethal giant larvae and Wnt signaling in bottle cell formation in *Xenopus* embryos. *Dev Biol* **336**, 68-75.



- Christodoulou, N. and Skourides, P. A.** (2015). Cell-Autonomous Ca<sup>2+</sup> Flashes Elicit Pulsed Contractions of an Apical Actin Network to Drive Apical Constriction during Neural Tube Closure. *Cell Rep* **13**, 2189-2202.
- Ciani, L. and Salinas, P. C.** (2007). c-Jun N-terminal kinase (JNK) cooperates with Gsk3beta to regulate Dishevelled-mediated microtubule stability. *BMC Cell Biol* **8**, 27.
- Cirone, P., Lin, S., Griesbach, H. L., Zhang, Y., Slusarski, D. C. and Crews, C. M.** (2008). A role for planar cell polarity signaling in angiogenesis. *Angiogenesis* **11**, 347-360.
- Clark, B. S., Winter, M., Cohen, A. R. and Link, B. A.** (2011). Generation of Rab-based transgenic lines for in vivo studies of endosome biology in zebrafish. *Dev Dyn* **240**, 2452-2465.
- Crivici, A. and Ikura, M.** (1995). Molecular and structural basis of target recognition by calmodulin. *Annu Rev Biophys Biomol Struct* **24**, 85-116.
- Davidson, L. A. and Keller, R. E.** (1999). Neural tube closure in *Xenopus laevis* involves medial migration, directed protrusive activity, cell intercalation and convergent extension. *Development* **126**, 4547-4556.
- De Rienzo, G., Gutzman, J. H. and Sive, H.** (2012). Efficient shRNA-mediated inhibition of gene expression in zebrafish. *Zebrafish* **9**, 97-107.
- Dostal, V. and Libusova, L.** (2014). Microtubule drugs: action, selectivity, and resistance across the kingdoms of life. *Protoplasma* **251**, 991-1005.
- Du, L., Kim, J. J., Shen, J. and Dai, N.** (2016). Crosstalk between Inflammation and ROCK/MLCK Signaling Pathways in Gastrointestinal Disorders with Intestinal Hyperpermeability. *Gastroenterol Res Pract* **2016**, 7374197.
- Duncan, R. N., Panahi, S., Piotrowski, T. and Dorsky, R. I.** (2015). Identification of Wnt Genes Expressed in Neural Progenitor Zones during Zebrafish Brain Development. *PLoS One* **10**, e0145810.
- Elie-Caille, C., Severin, F., Helenius, J., Howard, J., Muller, D. J. and Hyman, A. A.** (2007). Straight GDP-tubulin protofilaments form in the presence of taxol. *Curr Biol* **17**, 1765-1770.
- Etienne-Manneville, S.** (2010). From signaling pathways to microtubule dynamics: the key players. *Curr Opin Cell Biol* **22**, 104-111.

- Feltrin, D., Fusco, L., Witte, H., Moretti, F., Martin, K., Letzelter, M., Fluri, E., Scheiffele, P. and Pertz, O.** (2012). Growth cone MKK7 mRNA targeting regulates MAP1b-dependent microtubule bundling to control neurite elongation. *PLoS Biol* **10**, e1001439.
- Fenix, A. M., Neininger, A. C., Taneja, N., Hyde, K., Visetsouk, M. R., Garde, R. J., Liu, B., Nixon, B. R., Manalo, A. E., Becker, J. R., et al.** (2018). Muscle-specific stress fibers give rise to sarcomeres in cardiomyocytes. *Elife* **7**.
- Fernandes, V. M., McCormack, K., Lewellyn, L. and Verheyen, E. M.** (2014). Integrins regulate apical constriction via microtubule stabilization in the *Drosophila* eye disc epithelium. *Cell Rep* **9**, 2043-2055.
- Freisinger, C. M., Fisher, R. A. and Slusarski, D. C.** (2010). Regulator of G protein signaling 3 modulates Wnt5b calcium dynamics and somite patterning. *PLoS Genet* **6**, e1001020.
- Friedberg, F. and Rhoads, A. R.** (2001). Evolutionary aspects of calmodulin. *IUBMB Life* **51**, 215-221.
- Friedberg, F. and Taliaferro, L.** (2005). Calmodulin genes in zebrafish (revisited). *Mol Biol Rep* **32**, 55-60.
- Fumoto, K., Takigawa-Imamura, H., Sumiyama, K., Kaneiwa, T. and Kikuchi, A.** (2017). Modulation of apical constriction by Wnt signaling is required for lung epithelial shape transition. *Development* **144**, 151-162.
- Ghawanmeh, A. A., Chong, K. F., Sarkar, S. M., Bakar, M. A., Othaman, R. and Khalid, R. M.** (2018). Colchicine prodrugs and codrugs: Chemistry and bioactivities. *Eur J Med Chem* **144**, 229-242.
- Gibbs, H. C., Chang-Gonzalez, A., Hwang, W., Yeh, A. T. and Lekven, A. C.** (2017). Midbrain-Hindbrain Boundary Morphogenesis: At the Intersection of Wnt and Fgf Signaling. *Front Neuroanat* **11**, 64.
- Gomez-Galvez, P., Vicente-Munuera, P., Tagua, A., Forja, C., Castro, A. M., Letran, M., Valencia-Exposito, A., Grima, C., Bermudez-Gallardo, M., Serrano-Perez-Higueras, O., et al.** (2018). Scutoids are a geometrical solution to three-dimensional packing of epithelia. *Nat Commun* **9**, 2960.
- Gottschalk, C. W. and Mylle, M.** (1959). Micropuncture study of the mammalian urinary concentrating mechanism: evidence for the countercurrent hypothesis. *Am J Physiol* **196**, 927-936.

- Graeden, E. and Sive, H.** (2009). Live imaging of the zebrafish embryonic brain by confocal microscopy. *J Vis Exp*.
- Gutzman, J. H., Graeden, E., Brachmann, I., Yamazoe, S., Chen, J. K. and Sive, H.** (2018). Basal constriction during midbrain-hindbrain boundary morphogenesis is mediated by Wnt5b and focal adhesion kinase. *Biol Open* **7**.
- Gutzman, J. H., Graeden, E. G., Lowery, L. A., Holley, H. S. and Sive, H.** (2008). Formation of the zebrafish midbrain-hindbrain boundary constriction requires laminin-dependent basal constriction. *Mech Dev* **125**, 974-983.
- Gutzman, J. H., Sahu, S. U. and Kwas, C.** (2015). Non-muscle myosin IIA and IIB differentially regulate cell shape changes during zebrafish brain morphogenesis. *Dev Biol* **397**, 103-115.
- Gutzman, J. H. and Sive, H.** (2010). Epithelial relaxation mediated by the myosin phosphatase regulator Mypt1 is required for brain ventricle lumen expansion and hindbrain morphogenesis. *Development* **137**, 795-804.
- Hammerschmidt, M., Pelegri, F., Mullins, M. C., Kane, D. A., Brand, M., van Eeden, F. J., Furutani-Seiki, M., Granato, M., Haffter, P., Heisenberg, C. P., et al.** (1996). Mutations affecting morphogenesis during gastrulation and tail formation in the zebrafish, *Danio rerio*. *Development* **123**, 143-151.
- Hanna, S. and El-Sibai, M.** (2013). Signaling networks of Rho GTPases in cell motility. *Cell Signal* **25**, 1955-1961.
- He, L., Wang, X., Tang, H. L. and Montell, D. J.** (2010). Tissue elongation requires oscillating contractions of a basal actomyosin network. *Nat Cell Biol* **12**, 1133-1142.
- He, Y., Cai, C., Sun, S., Wang, X., Li, W. and Li, H.** (2016). Effect of JNK inhibitor SP600125 on hair cell regeneration in zebrafish (*Danio rerio*) larvae. *Oncotarget* **7**, 51640-51650.
- Heer, N. C., Miller, P. W., Chanet, S., Stoop, N., Dunkel, J. and Martin, A. C.** (2017). Actomyosin-based tissue folding requires a multicellular myosin gradient. *Development* **144**, 1876-1886.
- Holz, O., Apel, D., Steinmetz, P., Lange, E., Hopfenmuller, S., Ohler, K., Sudhop, S. and Hassel, M.** (2017). Bud detachment in hydra requires activation of fibroblast growth factor receptor and a Rho-ROCK-myosin II signaling pathway to ensure formation of a basal constriction. *Dev Dyn* **246**, 502-516.

- Holzapfel, G., Wehland, J. and Weber, K.** (1983). Calcium control of actin-myosin based contraction in triton models of mouse 3T3 fibroblasts is mediated by the myosin light chain kinase (MLCK)-calmodulin complex. *Exp Cell Res* **148**, 117-126.
- Hoyert, D. L., Mathews, T. J., Menacker, F., Strobino, D. M. and Guyer, B.** (2006). Annual summary of vital statistics: 2004. *Pediatrics* **117**, 168-183.
- Hynes, R. O.** (2002). Integrins: bidirectional, allosteric signaling machines. *Cell* **110**, 673-687.
- Ito, M., Nakano, T., Erdodi, F. and Hartshorne, D. J.** (2004). Myosin phosphatase: structure, regulation and function. *Mol Cell Biochem* **259**, 197-209.
- Jayachandran, P., Olmo, V. N., Sanchez, S. P., McFarland, R. J., Vital, E., Werner, J. M., Hong, E., Sanchez-Alberola, N., Molodstov, A. and Brewster, R. M.** (2016). Microtubule-associated protein 1b is required for shaping the neural tube. *Neural Dev* **11**, 1.
- Jidigam, V. K., Srinivasan, R. C., Patthey, C. and Gunhaga, L.** (2015). Apical constriction and epithelial invagination are regulated by BMP activity. *Biol Open* **4**, 1782-1791.
- Katsuda, S., Okada, Y. and Nakanishi, I.** (1987). Dimethyl sulfoxide induces microtubule formation in cultured arterial smooth muscle cells. *Cell Biol Int Rep* **11**, 103-110.
- Kim, H. Y. and Davidson, L. A.** (2011). Punctuated actin contractions during convergent extension and their permissive regulation by the non-canonical Wnt-signaling pathway. *J Cell Sci* **124**, 635-646.
- Kimmel, C. B., Ballard, W. W., Kimmel, S. R., Ullmann, B. and Schilling, T. F.** (1995). Stages of embryonic development of the zebrafish. *Dev Dyn* **203**, 253-310.
- Kobayashi, H., Saragai, S., Naito, A., Ichio, K., Kawauchi, D. and Murakami, F.** (2015). Calm1 signaling pathway is essential for the migration of mouse precerebellar neurons. *Development* **142**, 375-384.
- Komiya, Y. and Habas, R.** (2008). Wnt signal transduction pathways. *Organogenesis* **4**, 68-75.

- Kovacs, M., Toth, J., Hetenyi, C., Malnasi-Csizmadia, A. and Sellers, J. R.** (2004). Mechanism of blebbistatin inhibition of myosin II. *J Biol Chem* **279**, 35557-35563.
- Kozlovskaja-Gumbriene, A., Yi, R., Alexander, R., Aman, A., Jiskra, R., Nagelberg, D., Knaut, H., McClain, M. and Piotrowski, T.** (2017). Proliferation-independent regulation of organ size by Fgf/Notch signaling. *Elife* **6**.
- Kreiling, J. A., Balantac, Z. L., Crawford, A. R., Ren, Y., Toure, J., Zchut, S., Kochilas, L. and Creton, R.** (2008). Suppression of the endoplasmic reticulum calcium pump during zebrafish gastrulation affects left-right asymmetry of the heart and brain. *Mech Dev* **125**, 396-410.
- Lagunowich, L. A., Stein, A. P. and Reuhl, K. R.** (1994). N-cadherin in normal and abnormal brain development. *Neurotoxicology* **15**, 123-132.
- Lang, R. A., Herman, K., Reynolds, A. B., Hildebrand, J. D. and Plageman, T. F., Jr.** (2014). p120-catenin-dependent junctional recruitment of Shroom3 is required for apical constriction during lens pit morphogenesis. *Development* **141**, 3177-3187.
- Lee, J. Y. and Harland, R. M.** (2007). Actomyosin contractility and microtubules drive apical constriction in *Xenopus* bottle cells. *Dev Biol* **311**, 40-52.
- Lee, J. Y., Marston, D. J., Walston, T., Hardin, J., Halberstadt, A. and Goldstein, B.** (2006). Wnt/Frizzled signaling controls *C. elegans* gastrulation by activating actomyosin contractility. *Curr Biol* **16**, 1986-1997.
- Lee, M. H., Korja, P., Qu, J. and Andreadis, S. T.** (2009). JNK phosphorylates beta-catenin and regulates adherens junctions. *FASEB J* **23**, 3874-3883.
- Lele, Z., Bakkers, J. and Hammerschmidt, M.** (2001). Morpholino phenocopies of the swirl, snailhouse, somitabun, minifin, silberblick, and pipetail mutations. *Genesis* **30**, 190-194.
- Liao, G., Tao, Q., Kofron, M., Chen, J. S., Schloemer, A., Davis, R. J., Hsieh, J. C., Wylie, C., Heasman, J. and Kuan, C. Y.** (2006). Jun NH2-terminal kinase (JNK) prevents nuclear beta-catenin accumulation and regulates axis formation in *Xenopus* embryos. *Proc Natl Acad Sci U S A* **103**, 16313-16318.
- Lin, S., Baye, L. M., Westfall, T. A. and Slusarski, D. C.** (2010). Wnt5b-Ryk pathway provides directional signals to regulate gastrulation movement. *J Cell Biol* **190**, 263-278.

- Lopez-Escobar, B., Caro-Vega, J. M., Vijayraghavan, D. S., Plageman, T. F., Sanchez-Alcazar, J. A., Moreno, R. C., Savery, D., Marquez-Rivas, J., Davidson, L. A. and Ybot-Gonzalez, P.** (2018). The non-canonical Wnt-PCP pathway shapes the mouse caudal neural plate. *Development* **145**.
- Lowery, L. A., De Rienzo, G., Gutzman, J. H. and Sive, H.** (2009). Characterization and classification of zebrafish brain morphology mutants. *Anat Rec (Hoboken)* **292**, 94-106.
- Lowery, L. A. and Sive, H.** (2005). Initial formation of zebrafish brain ventricles occurs independently of circulation and requires the *nagie oko* and *snakehead/atp1a1a.1* gene products. *Development* **132**, 2057-2067.
- (2009). Totally tubular: the mystery behind function and origin of the brain ventricular system. *Bioessays* **31**, 446-458.
- Martin, A. C., Kaschube, M. and Wieschaus, E. F.** (2009). Pulsed contractions of an actin-myosin network drive apical constriction. *Nature* **457**, 495-499.
- Martinez-Morales, J. R., Rembold, M., Greger, K., Simpson, J. C., Brown, K. E., Quiring, R., Pepperkok, R., Martin-Bermudo, M. D., Himmelbauer, H. and Wittbrodt, J.** (2009). *ojoplano*-mediated basal constriction is essential for optic cup morphogenesis. *Development* **136**, 2165-2175.
- Matis, M., Russler-Germain, D. A., Hu, Q., Tomlin, C. J. and Axelrod, J. D.** (2014). Microtubules provide directional information for core PCP function. *Elife* **3**, e02893.
- Merks, A. M., Swinarski, M., Meyer, A. M., Muller, N. V., Ozcan, I., Donat, S., Burger, A., Gilbert, S., Mosimann, C., Abdelilah-Seyfried, S., et al.** (2018). Planar cell polarity signalling coordinates heart tube remodelling through tissue-scale polarisation of actomyosin activity. *Nat Commun* **9**, 2161.
- Messier, P. E.** (1969). Effects of beta-mercaptoethanol on the fine structure of the neural plate cells of the chick embryo. *J Embryol Exp Morphol* **21**, 309-329.
- Morita, H., Nandadasa, S., Yamamoto, T. S., Terasaka-lioka, C., Wylie, C. and Ueno, N.** (2010). Nectin-2 and N-cadherin interact through extracellular domains and induce apical accumulation of F-actin in apical constriction of *Xenopus* neural tube morphogenesis. *Development* **137**, 1315-1325.

- Muccioli, M., Qaisi, D., Herman, K. and Plageman, T. F., Jr.** (2016). Lens placode planar cell polarity is dependent on Cdc42-mediated junctional contraction inhibition. *Dev Biol* **412**, 32-43.
- Munjal, A. and Lecuit, T.** (2014). Actomyosin networks and tissue morphogenesis. *Development* **141**, 1789-1793.
- Ng, A. N., de Jong-Curtain, T. A., Mawdsley, D. J., White, S. J., Shin, J., Appel, B., Dong, P. D., Stainier, D. Y. and Heath, J. K.** (2005). Formation of the digestive system in zebrafish: III. Intestinal epithelium morphogenesis. *Dev Biol* **286**, 114-135.
- Nicolas-Perez, M., Kuchling, F., Letelier, J., Polvillo, R., Wittbrodt, J. and Martinez-Morales, J. R.** (2016). Analysis of cellular behavior and cytoskeletal dynamics reveal a constriction mechanism driving optic cup morphogenesis. *Elife* **5**.
- Nishimura, T., Honda, H. and Takeichi, M.** (2012). Planar cell polarity links axes of spatial dynamics in neural-tube closure. *Cell* **149**, 1084-1097.
- Norden, C., Young, S., Link, B. A. and Harris, W. A.** (2009). Actomyosin is the main driver of interkinetic nuclear migration in the retina. *Cell* **138**, 1195-1208.
- Orrenius, S., McCabe, M. J., Jr. and Nicotera, P.** (1992). Ca(2+)-dependent mechanisms of cytotoxicity and programmed cell death. *Toxicol Lett* **64-65 Spec No**, 357-364.
- Ossipova, O., Chuykin, I., Chu, C. W. and Sokol, S. Y.** (2015a). Vangl2 cooperates with Rab11 and Myosin V to regulate apical constriction during vertebrate gastrulation. *Development* **142**, 99-107.
- Ossipova, O., Kim, K. and Sokol, S. Y.** (2015b). Planar polarization of Vangl2 in the vertebrate neural plate is controlled by Wnt and Myosin II signaling. *Biol Open* **4**, 722-730.
- Parisi, M. and Glass, I.** (1993). Joubert Syndrome. In *GeneReviews((R))* (ed. M. P. Adam, H. H. Ardinger, R. A. Pagon, S. E. Wallace, L. J. H. Bean, K. Stephens & A. Amemiya). Seattle (WA).
- Plageman, T. F., Jr., Chauhan, B. K., Yang, C., Jaudon, F., Shang, X., Zheng, Y., Lou, M., Debant, A., Hildebrand, J. D. and Lang, R. A.** (2011). A Trio-RhoA-Shroom3 pathway is required for apical constriction and epithelial invagination. *Development* **138**, 5177-5188.

- Plageman, T. F., Jr., Chung, M. I., Lou, M., Smith, A. N., Hildebrand, J. D., Wallingford, J. B. and Lang, R. A.** (2010). Pax6-dependent Shroom3 expression regulates apical constriction during lens placode invagination. *Development* **137**, 405-415.
- Poznanski, A., Minsuk, S., Stathopoulos, D. and Keller, R.** (1997). Epithelial cell wedging and neural trough formation are induced planarly in *Xenopus*, without persistent vertical interactions with mesoderm. *Dev Biol* **189**, 256-269.
- Quarmby, L. M. and Lohret, T. A.** (1999). Microtubule severing. *Cell Motil Cytoskeleton* **43**, 1-9.
- Ravelli, R. B., Gigant, B., Curmi, P. A., Jourdain, I., Lachkar, S., Sobel, A. and Knossow, M.** (2004). Insight into tubulin regulation from a complex with colchicine and a stathmin-like domain. *Nature* **428**, 198-202.
- Rinschen, M. M., Limbutara, K., Knepper, M. A., Payne, D. M. and Pisitkun, T.** (2018). From Molecules to Mechanisms: Functional Proteomics and Its Application to Renal Tubule Physiology. *Physiol Rev* **98**, 2571-2606.
- Robinson, J. and Engelborghs, Y.** (1982). Tubulin polymerization in dimethyl sulfoxide. *J Biol Chem* **257**, 5367-5371.
- Robu, M. E., Larson, J. D., Nasevicius, A., Beiraghi, S., Brenner, C., Farber, S. A. and Ekker, S. C.** (2007). p53 activation by knockdown technologies. *PLoS Genet* **3**, e78.
- Rochard, L., Monica, S. D., Ling, I. T., Kong, Y., Roberson, S., Harland, R., Halpern, M. and Liao, E. C.** (2016). Roles of Wnt pathway genes *wls*, *wnt9a*, *wnt5b*, *frzb* and *gpc4* in regulating convergent-extension during zebrafish palate morphogenesis. *Development* **143**, 2541-2547.
- Rogers, S. L. and Gelfand, V. I.** (2000). Membrane trafficking, organelle transport, and the cytoskeleton. *Curr Opin Cell Biol* **12**, 57-62.
- Romero, D. M., Bahi-Buisson, N. and Francis, F.** (2018). Genetics and mechanisms leading to human cortical malformations. *Semin Cell Dev Biol* **76**, 33-75.
- Rossi, A., Kontarakis, Z., Gerri, C., Nolte, H., Holper, S., Kruger, M. and Stainier, D. Y.** (2015). Genetic compensation induced by deleterious mutations but not gene knockdowns. *Nature* **524**, 230-233.

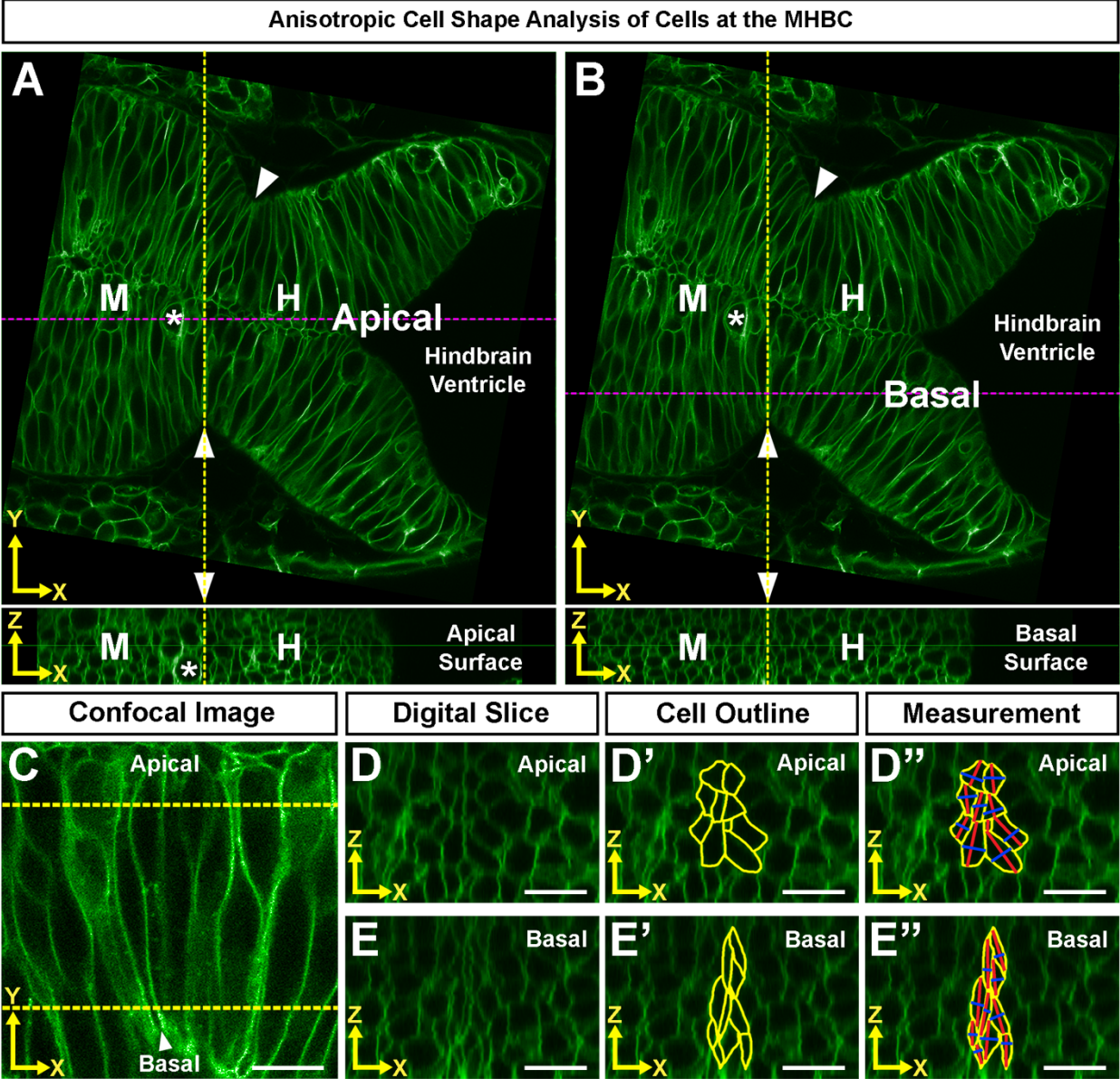


- Sahu, S. U.** (2015). Role of Non-Muscle Myosin II and Calcium in Zebrafish Midbrain-Hindbrain Boundary Morphogenesis. Masters thesis, University of Wisconsin-Milwaukee, Milwaukee, WI. Paper **836**.
- Sahu, S. U., Visetsouk, M. R., Garde, R. J., Hennes, L., Kwas, C. and Gutzman, J. H.** (2017). Calcium signals drive cell shape changes during zebrafish midbrain-hindbrain boundary formation. *Mol Biol Cell* **28**, 875-882.
- Sanchez-Corrales, Y. E., Blanchard, G. B. and Roper, K.** (2018). Radially patterned cell behaviours during tube budding from an epithelium. *Elife* **7**.
- Schambony, A. and Wedlich, D.** (2007). Wnt-5A/Ror2 regulate expression of XPAPC through an alternative noncanonical signaling pathway. *Dev Cell* **12**, 779-792.
- Schroeder, T. E.** (1970). Neurulation in *Xenopus laevis*. An analysis and model based upon light and electron microscopy. *J Embryol Exp Morphol* **23**, 427-462.
- Sepich, D. S., Usmani, M., Pawlicki, S. and Solnica-Krezel, L.** (2011). Wnt/PCP signaling controls intracellular position of MTOCs during gastrulation convergence and extension movements. *Development* **138**, 543-552.
- Sheetz, M. P.** (1996). Microtubule motor complexes moving membranous organelles. *Cell Struct Funct* **21**, 369-373.
- Shyer, A. E., Tallinen, T., Nerurkar, N. L., Wei, Z., Gil, E. S., Kaplan, D. L., Tabin, C. J. and Mahadevan, L.** (2013). Villification: how the gut gets its villi. *Science* **342**, 212-218.
- Sidhaye, J. and Norden, C.** (2017). Concerted action of neuroepithelial basal shrinkage and active epithelial migration ensures efficient optic cup morphogenesis. *Elife* **6**.
- Singh, A., Saha, T., Begemann, I., Ricker, A., Nusse, H., Thorn-Seshold, O., Klingauf, J., Galic, M. and Matis, M.** (2018). Polarized microtubule dynamics directs cell mechanics and coordinates forces during epithelial morphogenesis. *Nat Cell Biol* **20**, 1126-1133.
- Slusarski, D. C. and Pelegri, F.** (2007). Calcium signaling in vertebrate embryonic patterning and morphogenesis. *Dev Biol* **307**, 1-13.
- Somlyo, A. P. and Somlyo, A. V.** (2003). Ca<sup>2+</sup> sensitivity of smooth muscle and nonmuscle myosin II: modulated by G proteins, kinases, and myosin phosphatase. *Physiol Rev* **83**, 1325-1358.

- Suzuki, M., Morita, H. and Ueno, N.** (2012). Molecular mechanisms of cell shape changes that contribute to vertebrate neural tube closure. *Dev Growth Differ* **54**, 266-276.
- Suzuki, M., Sato, M., Koyama, H., Hara, Y., Hayashi, K., Yasue, N., Imamura, H., Fujimori, T., Nagai, T., Campbell, R. E., et al.** (2017). Distinct intracellular Ca(2+) dynamics regulate apical constriction and differentially contribute to neural tube closure. *Development* **144**, 1307-1316.
- Szikora, S., Foldi, I., Toth, K., Migh, E., Vig, A., Bugyi, B., Maleth, J., Hegyi, P., Kaltenecker, P., Sanchez-Soriano, N., et al.** (2017). The formin DAAM is required for coordination of the actin and microtubule cytoskeleton in axonal growth cones. *J Cell Sci* **130**, 2506-2519.
- Thisse, B., Heyer, V., Lux, A., Alunni, V., Degrave, A., Seilliez, I., Kirchner, J., Parkhill, J. P. and Thisse, C.** (2004). Spatial and temporal expression of the zebrafish genome by large-scale in situ hybridization screening. *Methods Cell Biol* **77**, 505-519.
- Thisse, B., Pflumio, S., Fürthauer, M., Loppin, B., Heyer, V., Degrave, A., Woehl, R., Lux, A., Steffan, T., Charbonnier, X.Q. and Thisse, C.** (2001). Expression of the zebrafish genome during embryogenesis. *ZFIN Direct Data Submission*. (<http://zfin.org>).
- Thisse, C., Thisse, B.** (2005). High Throughput Expression Analysis of ZF-Models Consortium Clones. *ZFIN Direct Data Submission*.
- Thompson, J. C.** (1969). Gastrin and gastric secretion. *Annu Rev Med* **20**, 291-314.
- Thut, C. J., Rountree, R. B., Hwa, M. and Kingsley, D. M.** (2001). A large-scale in situ screen provides molecular evidence for the induction of eye anterior segment structures by the developing lens. *Dev Biol* **231**, 63-76.
- Tidow, H. and Nissen, P.** (2013). Structural diversity of calmodulin binding to its target sites. *FEBS J* **280**, 5551-5565.
- Van Aelst, L. and Symons, M.** (2002). Role of Rho family GTPases in epithelial morphogenesis. *Genes Dev* **16**, 1032-1054.
- Vicente-Manzanares, M., Ma, X., Adelstein, R. S. and Horwitz, A. R.** (2009). Non-muscle myosin II takes centre stage in cell adhesion and migration. *Nat Rev Mol Cell Biol* **10**, 778-790.

- Vijayraghavan, D. S. and Davidson, L. A.** (2017). Mechanics of neurulation: From classical to current perspectives on the physical mechanics that shape, fold, and form the neural tube. *Birth Defects Res* **109**, 153-168.
- Visetsouk, M. R., Falat, E. J., Garde, R. J., Wendlick, J. L. and Gutzman, J. H.** (2018). Basal epithelial tissue folding is mediated by differential regulation of microtubules. *Development* **145**.
- Walton, K. D., Freddo, A. M., Wang, S. and Gumucio, D. L.** (2016). Generation of intestinal surface: an absorbing tale. *Development* **143**, 2261-2272.
- Webb, S. E. and Miller, A. L.** (2003). Calcium signalling during embryonic development. *Nat Rev Mol Cell Biol* **4**, 539-551.
- (2007). Ca<sup>2+</sup> signalling and early embryonic patterning during zebrafish development. *Clin Exp Pharmacol Physiol* **34**, 897-904.
- Westerfield, M.** (2007). *The Zebrafish Book. A Guide for the Laboratory Use of Zebrafish (Danio rerio)* (5th edn). Eugene: University of Oregon Press.
- Xie, Y., Miao, H. and Blankenship, J. T.** (2018). Membrane trafficking in morphogenesis and planar polarity. *Traffic*.
- Yamanaka, H., Moriguchi, T., Masuyama, N., Kusakabe, M., Hanafusa, H., Takada, R., Takada, S. and Nishida, E.** (2002). JNK functions in the non-canonical Wnt pathway to regulate convergent extension movements in vertebrates. *EMBO Rep* **3**, 69-75.
- Yang, Y.** (2003). Wnts and wing: Wnt signaling in vertebrate limb development and musculoskeletal morphogenesis. *Birth Defects Res C Embryo Today* **69**, 305-317.
- Young, T., Poobalan, Y., Tan, E. K., Tao, S., Ong, S., Wehner, P., Schwenty-Lara, J., Lim, C. Y., Sadasivam, A., Lovatt, M., et al.** (2014). The PDZ domain protein Mcc is a novel effector of non-canonical Wnt signaling during convergence and extension in zebrafish. *Development* **141**, 3505-3516.
- Zhang, J., Webb, S. E., Ma, L. H., Chan, C. M. and Miller, A. L.** (2011). Necessary role for intracellular Ca<sup>2+</sup> transients in initiating the apical-basolateral thinning of enveloping layer cells during the early blastula period of zebrafish development. *Dev Growth Differ* **53**, 679-696.

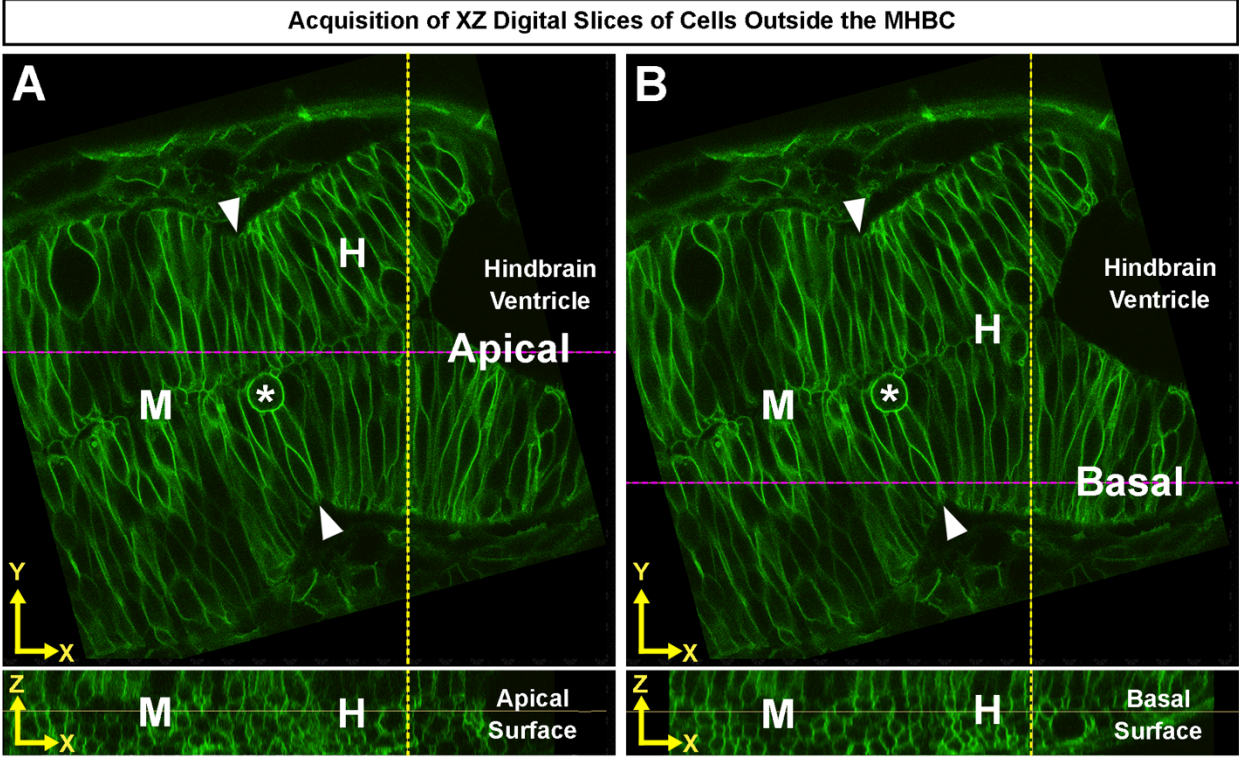
**APPENDIX A: Z-series processing of live confocal images to project data in the X-Z plane and to quantify anisotropic cell shape at the MHBC.**



(A,B) NIS Elements Software Digital Slices View Module of Apical (A) and Basal (B) slices in a Wild-Type (WT) embryo. M, midbrain. H, hindbrain. Arrowhead indicates MHBC. Dotted yellow line indicates position of MHBC in X-Y and X-Z plane views. Dotted purple line indicates position where digital orthogonal slices were acquired from

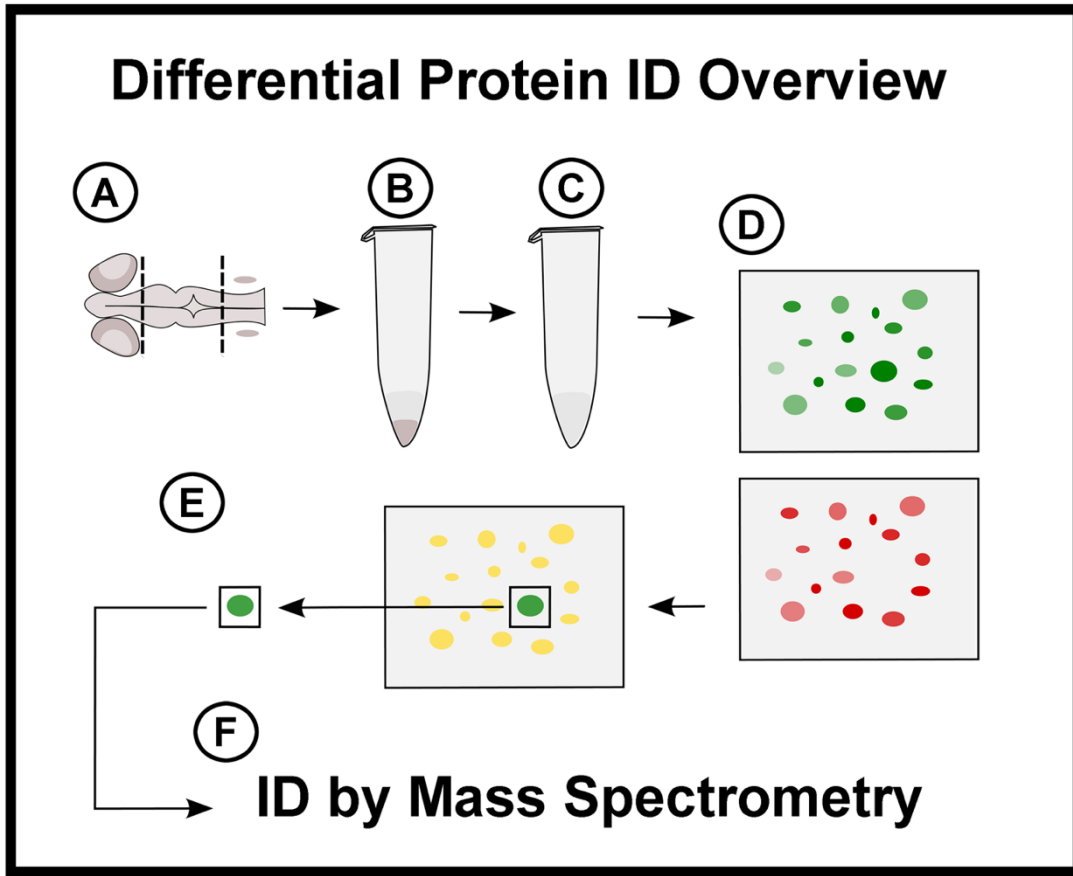
the X-Y image. \* indicates proliferative cell. (C) Live confocal imaging of 24 ss wild-type embryo injected with memGFP mRNA. Yellow dotted lines indicate position of apical and basal digital slices. (D,D'') Digital slice of Z-series at the apical end of the cell. (E') Apical MHBC cells outlined in yellow. (D'') Representative measurements of cell width (X) (red lines), and cell depth (Z) (blue lines). (E,E'') Digital slice of Z-series at the basal end of the cell. (F') Basal MHBC cells outlined in yellow. (E'') Representative measurements of cell width (X) and cell depth (Z). Arrowhead indicates MHBC. Anterior is to the left in all images. Scale bars: 10  $\mu\text{m}$ .

**APPENDIX B: Z-series processing of live confocal images to project data in the X-Z plane and to quantify anisotropic cell shape in cells outside of MHBC.**



(A,B) Z-series processing of live confocal images to quantify anisotropic cell shape in cells outside of the MHBC, 40 microns posterior. NIS Elements Software Digital Slices View Module of Apical (A) and Basal (B) slices in a 24 ss WT embryo. M, midbrain. H, hindbrain. Arrowhead indicates MHBC. Dotted yellow line indicates position of cells that are 40 microns posterior to the MHBC in X-Y and X-Z plane views. Dotted purple line indicates position where digital orthogonal slices were acquired from the X-Y image. \* indicates proliferative cell.

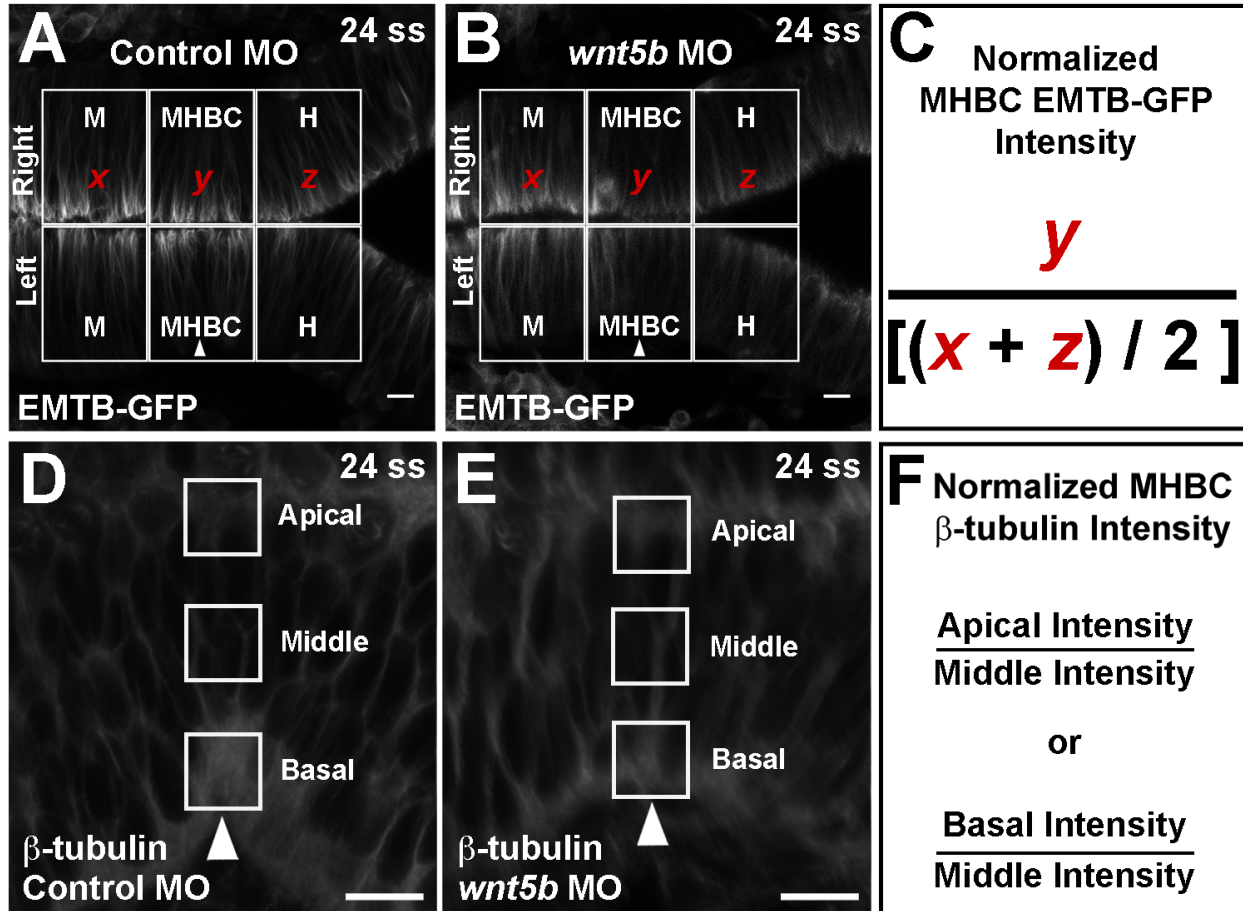
## APPENDIX C: Differential Two-Dimensional SDS-PAGE and Mass Spectrometry Pipeline.



Illustrated pipeline for analyzing differential protein. For analysis of differential proteins upon knockdown of *wnt5b*, we conducted the following: (A-C) We dissected MHB tissue as previously described and extracted total protein content. (D) We then conducted isoelectric focusing and SDS-PAGE to separate total protein by charge and size. We then stained gels for total protein using Sypro-Ruby protein gel stain and imaged. Gel images were then false-colored and overlaid to determine differences in protein spots. Differential spots of interest were then excised and sent for mass spectrometric analysis to determine proteins.



**APPENDIX D: Quantification of microtubules using live imaging of EMTB-GFP and  $\beta$ -tubulin immunohistochemistry.**

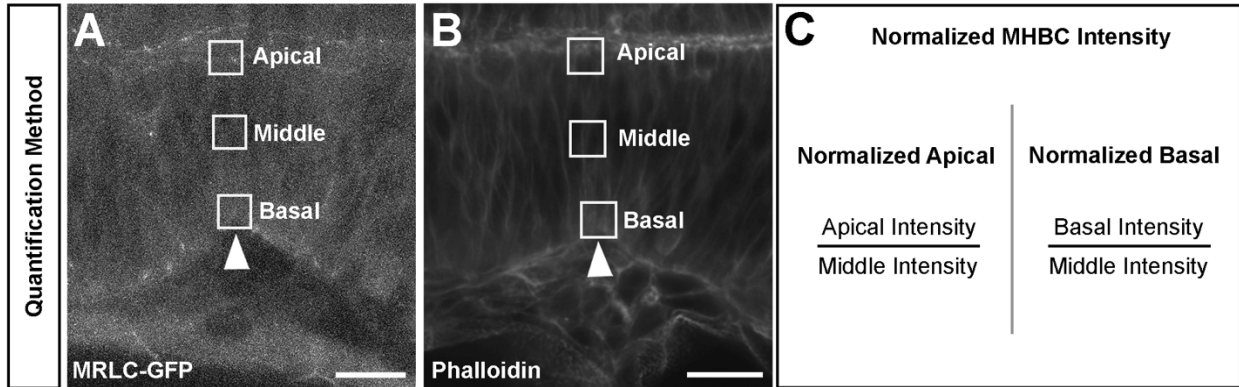


(A,B) Representative images of a 10  $\mu$ m Z-series average intensity projection. Boxed area indicates regions where average EMTB-GFP intensity was quantified. Intensity at the midbrain was averaged with the intensity at the hindbrain. The intensity measured at the MHBC was divided by the averaged intensity of the midbrain and hindbrain, for each embryo side. Left and Right. M, midbrain. MHB, midbrain-hindbrain boundary. H, hindbrain. (C) Formula for normalizing MHBC average intensity per side of neural tube. This normalization was used for comparison of MHBC intensity across embryos and experiments. First, midbrain and hindbrain intensity is averaged. MHBC intensity is then



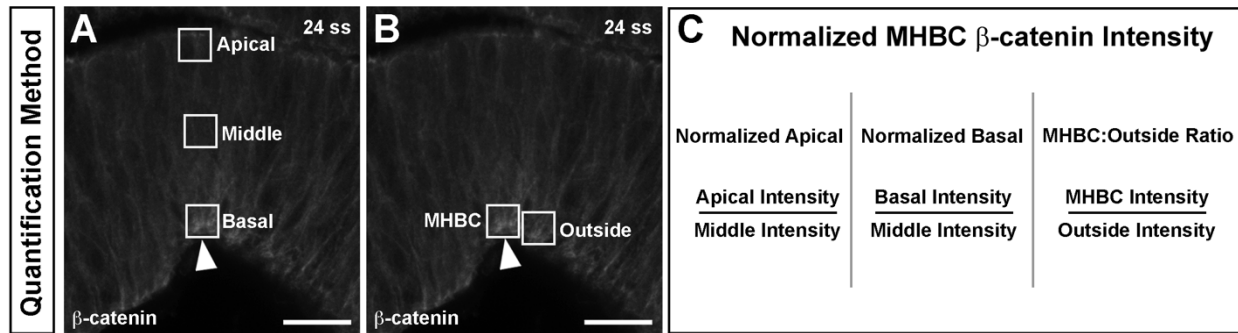
divided by the averaged midbrain-hindbrain intensity. Final comparisons are made between Control and *wnt5b* MO injected embryos. (D,E) Representative images of a 10  $\mu\text{m}$  Z-series average intensity projection of  $\beta$ -tubulin immunostaining. Boxed areas indicate where  $\beta$ -tubulin average intensity was quantified for apical, middle, and basal regions of the MHBC within a single embryo. The average intensity at either the apical MHBC region or the basal MHBC region is divided by the average intensity at the middle MHBC region in the same embryo to acquire apical or basal MHBC  $\beta$ -tubulin intensity, respectively. (F) Formula for normalizing MHBC apical or basal average intensity. This normalization was used for comparison of basal MHBC intensity across embryos and for comparisons between Control MO and *wnt5b* MO injected embryos. Scale bars: 10  $\mu\text{m}$ .

**APPENDIX E: Quantification of NMII using MRLC-GFP and actin using phalloidin staining.**



To assess the potential role of *wnt5b* in mediating the actomyosin network at the MHBC, we examined MRLC localization using live imaging of GFP-tagged myosin regulatory light chain (MRLC-GFP) and examined actin localization using fixed tissue imaging of AlexaFluor-488 phalloidin-stained embryos. (A,B) Representative confocal image of MRLC-GFP mRNA injected embryo (A) or phalloidin stained embryo (B) showing 10  $\mu\text{m}$  average intensity projections at 24 ss. Boxed areas indicate where average intensity of either MRLC-GFP or phalloidin was quantified for apical, middle, and basal regions of the MHBC cells. (C) Formula is shown for normalizing apical or basal MHBC average intensity. Briefly, either apical or basal MHBC average intensity is divided by the average intensity of the middle MHBC region within the same embryo, for each embryo. This normalization was used for comparison of apical or basal MHBC intensity across embryos and experiments.

## APPENDIX F: Quantification of $\beta$ -catenin immunohistochemistry.



(A,B) Average intensity projections of a 10  $\mu$ m Z-series of 24 ss embryos immunostained for  $\beta$ -catenin. Boxed areas indicate where average intensity was quantified for apical, middle, and basal regions of the MHBC and the outside basal region posterior to the MHBC. (C) Formula for normalizing MHBC apical and basal average intensity. Apical or basal MHBC average intensity is divided by the average intensity of the middle MHBC region within the same embryo. MHBC:Outside ratios are acquired by dividing the basal MHBC intensity by the average intensity directly adjacent and posterior to the MHBC region. Control and *wnt5b* MO injected embryos were compared for each normalized intensity.

## Curriculum Vitae

# Mike Roger Visetsouk

---

### EDUCATION

- 2013 – Current      **Ph.D., Cellular and Molecular Biology**  
University of Wisconsin-Milwaukee  
Expected May 2019
- 2009 – 2012        **B.S., Biological Sciences**  
Marquette University
- 

### RESEARCH EXPERIENCE

- 2013 – present     **Investigation of molecular mechanisms that mediate basal tissue folding in vertebrate brain development.**  
Graduate Advisor: Dr. Jennifer Gutzman  
Biological Sciences – Cellular and Molecular Biology  
Department of Biological Sciences, University of Wisconsin-Milwaukee
- 2011-2012         **Molecular investigation of amphipathic helix-based protein complex assembly in flagella formation.**  
Undergraduate Research Advisor: Dr. Pinfen Yang  
Biological Sciences – Cellular and Molecular Biology  
Department of Biological Sciences, Marquette University
- 2011-2012         **Functional analysis of potential *mir-244* targets in developmental timing during *C. elegans* development.**  
Undergraduate Research Advisor: Dr. Allison Abbott  
Biological Sciences – Developmental Biology  
Department of Biological Sciences, Marquette University
- 

### AWARDS AND HONORS

- 2018                 R1 Advanced Opportunity Program Fellowship, Graduate Research Fellowship Program; University of Wisconsin-Milwaukee

2018	Asian Faculty and Staff Association Student Award, Asian Faculty and Staff Association; University of Wisconsin-Milwaukee
2018	James J. Magnino Award, Department of Biological Sciences; University of Wisconsin-Milwaukee
2017	James D. Anthony Memorial Scholarship Award, Department of Biological Sciences; University of Wisconsin-Milwaukee
2015 - 2017	Advanced Opportunity Program Fellowship, Graduate Research Fellowship Program; University of Wisconsin-Milwaukee
2013 - 2017	Chancellor Award, Graduate School; University of Wisconsin-Milwaukee
2015, 2016	Ruth Walker Grant-in-aid Award, Department of Biological Sciences; University of Wisconsin-Milwaukee
2015	Best Graduate Poster Award, Midwest Regional Zebrafish Conference; St. Louis, Missouri.
2015	Best Graduate Poster Award, Biological Sciences Research Symposium; University of Wisconsin-Milwaukee

---

## **TEACHING EXPERIENCE**

2013 – present	Graduate Teaching Assistant Biological Sciences 203 – Anatomy & Physiology II Lab University of Wisconsin-Milwaukee Description: Primary laboratory instructor for ~24 students each class. 3hrs/week. Development and coordination of lab lecture, exercises, assignments and exams.
2014 – 2017	Graduate Teaching Assistant Biological Sciences 372 – Animal Physiology and Neurobiology Lab University of Wisconsin-Milwaukee Description: Axillary laboratory instructor for ~8 students each class. 3hrs/week. Handled set up, testing of laboratory exercises, and grading.
2014	Graduate Teaching Assistant Biological Sciences 370 – Animal Physiology University of Wisconsin-Milwaukee Description: Handled student questions and grading.

---

## **PROFESSIONAL AFFILIATIONS**

2017	Student Member, American Society for Cell Biology
------	---

---

---

## **PUBLICATIONS**

**Visetsouk MR\***, Falat LJ, Garde RJ, Wendlick J, Gutzman JH. Basal epithelial tissue folding is mediated by differential regulation of microtubules. *Development*. 2018 Nov 19;145. \*Recommended by F1000Prime

Sahu SU\*, **Visetsouk MR\***, Garde R, Hennes L, Kwas C, Gutzman JH. Calcium signals drive cell shape changes during zebrafish midbrain-hindbrain boundary formation. *Molecular Biology of the Cell*. 2017 Apr 1;28(7):875-882. \*These authors contributed equally to this work.

Liu Y, **Visetsouk M<sup>#</sup>**, Mynlieff M, Qin H, Lehtreck KF, Yang P. H<sup>+</sup>- and Na<sup>+</sup>- elicited swift changes of the microtubule cytoskeleton in the biflagellated green alga *Chlamydomonas*. *eLife*. 2017 Sep 6; 6:e26002. <sup>#</sup>indicates work performed as an undergraduate.

Fenix, AM, Neiningner, AC, Taneja, N, Hyde, K, **Visetsouk, MR**, Garde, RJ, Liu, B, Nixon, BR, Manalo, AE, Becker, JR, Crawley, SW, Bader, DM, Tyska, MJ, Liu, Q, Gutzman, JH, Burnette, DT. Muscle-specific stress fibers give rise to sarcomeres in cardiomyocytes. *eLife* 2018 Dec 13; 7:e42144

---

---

## **NON-PEER REVIEWED MANUSCRIPTS**

Fenix AM, Taneja N, Neiningner AC, **Visetsouk MR**, Nixon BR, Manalo AE, Becker JR, Crawley SW, Bader DM, Tyska MJ, Gutzman JH, Burnette D. Muscle specific stress fibers give rise to sarcomeres and are mechanistically distinct from stress fibers in non-muscle cells. bioRxiv 235424.

---

---

## **ORAL PRESENTATIONS**

2018 **Visetsouk MR**, Falat E, Garde RJ, Wendlick J, Gutzman JH. Shaping the early vertebrate brain: From cell shape to tissue fold. Talk at the Biological Sciences Departmental Colloquium; University of Wisconsin-Milwaukee.

2018 **Visetsouk MR**, Gutzman JH. Shaping the early vertebrate brain: From molecules to tissue shape. Three-Minute Thesis talk at the UWM Research Foundation; University of Wisconsin-Milwaukee.

2016 **Visetsouk MR**, Falat E, Garde R, Wendlick J, Kwas C, Gutzman JH. Wnt5b regulation of cytoskeletal activity to promote cell width

changes during MHB morphogenesis. Talk at the Biological Sciences Research Symposium; University of Wisconsin-Milwaukee.

- 2016 **Visetsouk MR**, Kwas C, Gutzman JH. Wnt5b Regulation of Brain Morphogenesis. Talk at Neuroscience Mini-Symposium, University of Wisconsin-Milwaukee; Milwaukee, WI

---

### **PEER-REVIEWED ABSTRACTS**

- 2018 Falat EJ\*, **Visetsouk MR**, Wendlick J, Gutzman JH. The role of the basement membrane in mediating basal tissue folding. Abstract 274 at the International Zebrafish Conference; Madison, WI.
- 2017 **Visetsouk MR**, Falat E, Garde R, Wendlick J, Kwas C, Gutzman JH. Wnt5b regulates basal constriction during neuroepithelial tissue folding. Abstract P2604 at the annual conference of the American Society for Cell Biology; Philadelphia, PA.
- 2017 Fenix AM\*, Taneja N, **Visetsouk MR**, Nixon BR, Manalo A, Becker JR, Crawley SW, Bader D, Tyska MJ, Gutzman JH, Burnette D. Evolutionarily Conserved Mechanisms Drive Sarcomere Assembly in Cardiomyocytes. Abstract E55 at the annual conference of the American Society for Cell Biology; Philadelphia, PA.
- 2016 **Visetsouk MR**, Garde R, Falat E, Sahu SU, Kwas C, Gutzman JH. Regulation of Cell Shape Changes During Brain Morphogenesis. Abstract Z6071B at The Allied Genetics Conference; 12th International Conference on Zebrafish Development and Genetics; Orlando, FL.
- 2015 **Visetsouk MR**, Kwas C, Gutzman JH. Wnt5b Regulation of Brain Morphogenesis. Abstract P63 at Midwest Regional Zebrafish Conference; St. Louis, MO

---

### **ADDITIONAL ACTIVITIES**

- 2019 Search Committee, Multicultural Student Success Coordinator Position in the African-American and Southeast Asian-American Offices, University of Wisconsin – Milwaukee

2019 Panelist, Southeast Asian Youth Education and Career Conference, Milwaukee Area Technical College

2018 – 2019 Panelist, Asian-American Graduate Student Panel, University of Wisconsin – Milwaukee

2015 – 2018 Mentor, Undergraduate Students, University of Wisconsin – Milwaukee

2017 – 2018 Evaluator, Anatomy and Physiology II Laboratory Fetal Pig RFP Committee, University of Wisconsin – Milwaukee

2017 – 2018 Presenter – 2 Talks, Neuroscience Mini-Symposium, University of Wisconsin-Milwaukee

2014 – 2018 Presenter – 4 Posters, Biological Sciences Research Symposium, University of Wisconsin-Milwaukee

2017 Presenter – Poster, pre-SFN Neuroscience Symposium, University of Wisconsin – Milwaukee

2016 – 2017 Presenter – 2 Talks, UW-Zebrafish Meeting; University of Wisconsin-Madison

2016 Presenter – Poster, Graduate Student Research Symposium; University of Wisconsin-Milwaukee

2014 Treasurer, Graduate Student Organization of the Biological Sciences, University of Wisconsin – Milwaukee

---